

University of Nebraska - Lincoln

DigitalCommons@University of Nebraska - Lincoln

Theses, Dissertations, and Student Research from
Electrical & Computer Engineering

Electrical & Computer Engineering, Department of

Summer 7-2010

A Comparison of Induction Motor Starting Methods Being Powered by a Diesel-Generator Set

Adam John Wigington

University of Nebraska at Lincoln, ajwigington@gmail.com

Follow this and additional works at: <http://digitalcommons.unl.edu/elecengtheses>



Part of the [Controls and Control Theory Commons](#), and the [Power and Energy Commons](#)

Wigington, Adam John, "A Comparison of Induction Motor Starting Methods Being Powered by a Diesel-Generator Set" (2010).
Theses, Dissertations, and Student Research from Electrical & Computer Engineering. 8.
<http://digitalcommons.unl.edu/elecengtheses/8>

This Article is brought to you for free and open access by the Electrical & Computer Engineering, Department of at DigitalCommons@University of Nebraska - Lincoln. It has been accepted for inclusion in Theses, Dissertations, and Student Research from Electrical & Computer Engineering by an authorized administrator of DigitalCommons@University of Nebraska - Lincoln.

A COMPARISON OF INDUCTION MOTOR STARTING METHODS
BEING POWERED BY A DIESEL-GENERATOR SET

by

Adam Wigington

A THESIS

Presented to the Faculty of
The Graduate College at the University of Nebraska
In Partial Fulfillment of Requirements
For the Degree of Master of Science

Major: Electrical Engineering

Under the Supervision of Professor Sohrab Asgarpoor

Lincoln, Nebraska

July, 2010

A COMPARISON OF INDUCTION MOTOR STARTING METHODS
BEING POWERED BY A DIESEL-GENERATOR SET

Adam Wigington, M.S.

University of Nebraska, 2010

Adviser: Sohrab Asgarpoor

Starting induction motors on isolated or weak systems is a highly dynamic process that can cause motor and load damage as well as electrical network fluctuations. Mechanical damage is associated with the high starting current drawn by a ramping induction motor. In order to compensate the load increase, the voltage of the electrical system decreases. Different starting methods can be applied to the electrical system to reduce these and other starting method issues. The purpose of this thesis is to build accurate and usable simulation models that can aid the designer in making the choice of an appropriate motor starting method. The specific case addressed is the situation where a diesel-generator set is used as the electrical supplied source to the induction motor. The most commonly used starting methods equivalent models are simulated and compared to each other. The main contributions of this thesis is that motor dynamic impedance is continuously calculated and fed back to the generator model to simulate the coupling of the electrical system. The comparative analysis given by the simulations has shown reasonably similar characteristics to other comparative studies. The diesel-generator and induction motor simulations have shown good results, and can adequately demonstrate the dynamics for testing and comparing the starting methods. Further work is suggested to refine the equivalent impedance presented in this thesis.

I. Table of Contents

I. TABLE OF CONTENTS	3
II. LIST OF TABLES	5
III. LIST OF FIGURES	6
IV. ACKNOWLEDGEMENTS	9
V. INTRODUCTION.....	10
VI. LITERATURE REVIEW.....	11
1. LITERATURE REVIEW	11
1.1. <i>Full Voltage Techniques</i>	16
1.1.1. <i>Direct-On-Line (DOL)</i>	16
1.1.2. <i>Shunt Capacitors</i>	17
1.2. <i>Electromechanical Reduced Voltage Techniques</i>	18
1.2.1. <i>Star-Delta</i>	18
1.2.2. <i>Autotransformer</i>	19
1.2.3. <i>Primary Resistor or Reactor</i>	20
1.3. <i>Soft-Starter Techniques</i>	20
1.4. <i>Models and Simulation Techniques</i>	22
1.5. <i>Comparative Analyses</i>	24
2. SCOPE OF THIS WORK.....	26
3. PLAN OF DEVELOPMENT.....	27
VII. SYSTEM MODELS.....	29
1. SYSTEM OVERVIEW.....	29
2. SYNCHRONOUS GENERATOR	31
2.1. <i>State Variable Model</i>	32
3. SQUIRREL CAGE INDUCTION MOTOR.....	39
3.1. <i>State Variable Model</i>	40
3.2. <i>Modeling the Magnetic Core Saturation</i>	47
4. DIESEL ENGINE AND SPEED GOVERNOR.....	50
5. EXCITATION SYSTEM	52
5.1. <i>Reference Voltage Setpoint</i>	53
5.2. <i>Power System Stabilizer</i>	54
6. MECHANICAL LOAD	55
7. ELECTRICAL SYSTEM	57
7.1. <i>Calculating Equivalent Impedance</i>	58
7.2. <i>Equivalent Impedance Feedback to the Generator</i>	60
7.3. <i>Cable Impedance</i>	61
VIII. MOTOR STARTER SIMULATION AND RESULTS.....	64
1. STARTING METHODS IMPLEMENTATION.....	64
1.1. <i>Direct-On-Line (DOL) Start</i>	64
1.2. <i>Shunt Capacitance</i>	65
1.3. <i>Star-Delta</i>	65
1.4. <i>Autotransformer</i>	66
1.5. <i>Primary Resistance and Reactance</i>	67

1.	STUDIED CASES.....	69
2.	200 HP SIMULATION RESULTS.....	70
1.6.	200 HP Genset Source Results.....	72
1.6.1.	Direct-On-Line (DOL) Start.....	72
1.6.2.	Shunt Capacitor Start.....	73
1.6.3.	Star-Delta Start.....	74
1.6.4.	Autotransformer Start.....	75
1.6.5.	Primary Resistance Start.....	76
1.6.6.	Primary Reactance Start.....	77
1.7.	200 HP Performance Summary.....	78
2.	500 HP SIMULATION RESULTS.....	85
2.1.	500 HP Genset Source Results.....	87
2.1.1.	Direct-On-Line (DOL) Start.....	87
2.1.2.	Shunt Capacitor Start.....	88
2.1.3.	Star-Delta Start.....	89
2.1.4.	Autotransformer Start.....	90
2.1.5.	Primary Resistance Start.....	91
2.1.6.	Primary Reactance Start.....	92
2.2.	500 HP Motor Performance Summary.....	93
IX.	SUMMARY AND CONCLUSION.....	99
V.	BIBLIOGRAPHY.....	102
APPENDIX A:	REFERENCE FRAME TRANSFORMATIONS.....	107
APPENDIX B:	ADDITIONAL ENGINE MODELS.....	109
1.	SIMPLE GENSET MODEL.....	109
2.	STEAM ENGINE AND GOVERNOR.....	109
2.1.	Electro-Hydraulic Speed-Governing Model.....	111
2.2.	General Model for Steam Turbine Speed-Governor.....	112
APPENDIX C:	NEMA LETTER CODES.....	114
APPENDIX D:	MODEL PARAMETERS.....	116
APPENDIX E:	SIMULATION SETTINGS.....	118
APPENDIX F:	LINEAR PIECEWISE CONVERSION CODE.....	119

II. List of Tables

1. General Synchronous Generator DQ Models Table	32
2. Comparative Analysis Metric Descriptions	69
3. Starter Metrics for 200 HP Induction Motor Results.....	84
4. Starter Metrics for 500 HP Induction Motor Results.....	98
5. NEMA Letter Code Typical Characteristics (NEMA Standards Publication Condensed MG 1-2007)	114
6. NEMA Code Letter Locked-Rotor kVA (NEMA, 2009).....	115
7. 200 HP Induction Motor Simulation Parameter Values	116
8. 500 HP Induction Motor Simulation Parameter Values	116
9. Mechanical Load Parameters	117
10. The Simulink Setting Parameters	118

III. List of Figures

1. Generic Speed-Torque of a Motor and Associated Load	15
2. System Model Overview	30
3. Relationship between the abc and dq0 general state variable quantities	33
4. Synchronous Generator dq Equivalent Circuit Diagram	35
5. Simulation Flow for the Synchronous Generator Model.....	38
6. Simulink Electromagnetic Torque Calculation (Equation VII-7).....	38
7. Squirrel Cage Induction Motor dq Equivalent Circuit Diagram.....	42
8. Block Diagram of the Induction Motor Stator Flux Linkage per Second Calculations	44
9. Block Diagram of the Induction Motor Rotor Flux Linkage per Second Calculations	45
10. Simulink Block of the Induction Motor Stator Current Calculations	45
11. Simulink Block of the Induction Motor Rotor Current Calculation.....	46
12. Simulink Block of the Motor Rotational Speed Calculation	47
13. No Load Saturation Curve of Stator Current and Terminal Voltage	48
14. Simulink Block to Calculate Mutual Magnetic Flux Linkage with Saturation	49
15. Block Diagram of the Overall Induction Motor	49
16. General Model of the Diesel Engine and Governor Controller	51
17. Functional Block Model of the AC8B Alternator-Rectifier Excitation System.....	52
18. Simulink Block of the Automatic Voltage Regulator.....	53
19. The Volts per Hertz Curve of the Reference Voltage Regulator	54
20. Power System Stabilizer (PSS1A).....	54
21. Speed-Torque Curve of Equation (VII-22).....	56
22. Speed-Torque Curve of Equation (VII-23).....	56
23. Simulink Infinite Source Test System Overview	57
24. Simulink Genset System Overview	58
25. Equivalent Circuit of the Generator and Apparent Impedance.....	60
26. Line Equivalent dq0 Reference Frame Calculation of the Voltage Drop Across the Line	63
27. DOL Start Scheme	64
28. Shunt Capacitor Start Scheme	65

29. Wye-Delta Start Scheme.....	66
30. Autotransformer Start Scheme.....	67
31. Primary Impedance Start Scheme.....	68
32. Genset and Constant DOL Starter Results for the 200 HP Motor	72
33. Genset Shunt Capacitor Starter Results for the 200 HP Motor	73
34. Genset Star-Delta Starter Results for the 200 HP Motor.....	74
35. Genset Autotransformer Starter Results for the 200 HP Motor.....	75
36. Genset Primary Resistance Starter Results for the 200 HP Motor	76
37. Genset Primary Reactance Starter Results for the 200 HP Motor	77
38. Comparison of All Genset Source Results for Inrush Current, Generator Voltage, and Generator Frequency for the 200 HP Motor	80
39. Comparison of All Genset Source Results for Motor Speed, Generator Real and Reactive Powers for the 200 HP Motor	81
40. Comparison of All Genset Source Results for Load Mechanical Torque, Inrush Torques, and Generator Torques for the 200 HP Motor.....	82
41. Genset and Constant DOL Starter Results for the 500 HP Motor	87
42. Genset Shunt Capacitor Starter Results for the 500 HP Motor	88
43. Genset Star-Delta Starter Results for the 500 HP Motor.....	89
44. Genset Autotransformer Starter Results for the 500 HP Motor.....	90
45. Genset Primary Resistance Starter Results for the 500 HP Motor	91
46. Genset Primary Reactance Starter Results for the 500 HP Motor.....	92
47. Comparison of All Genset Source Results for Inrush Current, Generator Voltage, and Generator Frequency for the 500 HP Motor.....	95
48. Comparison of All Genset Source Results for Motor Speed, Generator Real and Reactive Power for the 500 HP Motor.....	96
49. Comparison of All Genset Source Results for Load Torques, Motor Inrush Torques, and Generator Torques for the 500 HP Motor	97
50. The Simplified Diesel-Generator Set Model	109
51. Linear Approximate Functional Block Model of the Tandem Compound Steam Turbine Engine with Double Reheat	110

52. Simulink Block of the Tandem Compound Steam Turbine Engine with Double Reheat	111
53. Electro-Hydraulic Speed-Governor Model for a Steam Turbine.....	111
54. Simulink Block of the Electro-Hydraulic (GE) Speed-Governor and Steam Turbine	112
55. Functional Block Model of a General Speed-Governor	112
56. Simulink Block of General Speed-Governor and Steam Turbine	113

IV. Acknowledgements

I am very thankful to have the support and guidance of Dr. Marcelo Algrain, and, of course, my advisor Dr. Sohrab Asgarpoor. Dr. Algrain's hard work has made this thesis and my graduate education possible. Throughout this work Dr. Algrain's insightful recommendations over the last few years have time and time again added a fresh perspective when I was frustrated with various technical challenges. I am immensely fortunate to have Dr. Asgarpoor as my advisor. His personal attention to my work and to me throughout my time at the University of Nebraska-Lincoln has been invaluable to me. His recommendations have added considerably to this thesis, and his patience and firmness at times have kept me on course. I will miss our face-to-face talks, but look forward to our future discussions.

I would also like to thank Caterpillar Inc. as an organization, which has supported me both financially and professionally. In particular, I would like to recognize Magdalena Dilimot. She has provided the technical information and expertise for a solid foundation that this thesis has built upon.

Thank you to Dr. Jerry Hudgins and Dr. John Boye for their support and comments to improve the content of this thesis. The administrative support at the Electrical Engineering department at the University of Nebraska-Lincoln is much appreciated. I would also like to thank Nathan Schemm and Dr. Sina Balkir whose work for a previous project allowed me to make an easier transition into the work for this thesis. Last of all, I would like to thank my family and friends, including those above, that have leant me a hand and support, and despite my best efforts continued to tolerate me.

V. Introduction

In this thesis the combined dynamic models for an induction motor load and a diesel generator set source are developed, and used to simulate different motor starting methods. Induction motor starting is a highly dynamic process that can have many adverse effects on the entire power system. Two of the prominent issues are the effects caused by high inrush currents on the mechanical system of the load, and the response of the generation source to the load step, of which voltage dip is of most concern. To address these issues, different starting methodologies have been developed to mitigate damaging effects. It is not economically practical to test each of these methods on a physical system because of possible equipment damage, electrical system vulnerability, and other problems. Through simulation of these systems it is possible to compare the various starting methods in an economical, secure and yet effective manner.

First, a thorough literature detailing the problems associated with motor starting is given and the common starting methods are described. Different metrics are identified in this review, which are then used in the comparative analysis. The second section covers the construction of models including the components necessary for simulating the system dynamics. The well-accepted starting methods are simulated on both a constant and diesel-generator sources. The results and metrics are analyzed to draw conclusions. Also in the conclusion section, future work and limitations of the method as applied are addressed.

VI. Literature Review

1. Literature Review

Induction motor starting poses many challenging problems to the machine, in the form of wear and tear, and to maintaining a stable supply of power. Engineers and technicians must take these considerations into account when deciding on a starting methodology. The dynamic characteristics desired during the starting process are often conflicting, and tradeoffs must be made based on system characteristics. These characteristics include the system robustness, efficiency, equipment cost, and machine lifetime. Many different methods have been developed to address particular induction motor starting problems associated with motor size and the stability of the connected network. Induction motors makeup a large part of the load in power systems and in industrial applications in particular. The three-phase AC squirrel cage induction motors are the preferred motor type due to their economical cost and robustness (Kjellberg & Kling, 2003), (Trzynadlowski, 2001), (Gobbi, Sa'diah, & Siang, 2003), (Chapman, 2005). They make up approximately 85% of industrial motors (Gobbi, Sa'diah, & Siang, 2003). Wound-rotor motors have an advantage during startup; because of their slip rings resistance can be added to the rotor circuit. However, wound-rotor motors are more expensive and more difficult to maintain.

Many reports have been published discussing the parameters that need to be taken into account during startup that can be used to judge the characteristic features of starting methods for a particular application (Kay, Paes, Seggewiss, & Ellis, 1999), (Larabee, Pellegrino, & Flick, 2005), (IEEE Std 399-1997, 1998), (Pillay, Nour, Yang, Datu Harun,

& Haw, 2009), and (McElveen, Toney, Autom, & Mountain, 2001). The common factors when considering the choice of starting method are:

Inrush Current – This is the initial current seen by the motor during the starting operations. The inrush current directly relates to mechanical stress of the bearings and belts on the motor load (Cohen, 1995). The resistive or copper losses are proportional to the square of current, I^2R , and therefore affect the efficiency. The power lost is dissipated as heat, causing thermal stress to the machine and affecting its upkeep cost and overall lifetime.

Voltage Dip – The allowable amount of voltage dip is usually dependent on the size of the network and the load torque characteristics. The latter is due to the fact that the torque is approximately proportional to the square of the voltage. According to (IEEE Std 399-1997, 1998), the allowable voltage dip range can vary between 80% and 95% of the rated value. The minimum voltage dip for NEMA type B motors is approximately 80%, given a static prime mover torque, so as to achieve the 150% of rated torque required to accelerate the rotor during starting (NEMA, 2009). Tables describing general use and the locked-rotor starting kVA are given Appendix C. In power systems a common voltage dip limit is 94% of rated voltage. Shunt capacitors and other reactive power compensators are often used to improve voltage response.

Frequency Dip – To maintain system stability it is important to retain as close to the fundamental frequency of the system as possible. The frequency dip is usually not considered as important as the voltage dip.

Acceleration Time – The time it takes to approximately reach the rated speed of the motor. It is often indicative of other parameters such as torque and current. Faster acceleration time is desired, but often means that high-rated current and other undesirable affects occur. However, a longer acceleration can mean that the applied torque is too low and that a still significant current is applied over a longer span of time resulting in a still too high amount of thermal stress to the motor.

Torque – The speed-torque curve is used to represent the required torques of the motor for different speeds. During startup the initial locked rotor starting torque must be met to overcome the potential energy at stand still, and the accelerating torque must be exceeded to maintain acceleration or the motor will stall (IEEE Std 399-1997, 1998), (Larabee, Pellegrino, & Flick, 2005), and (Kay, Paes, Seggewiss, & Ellis, 1999). Figure 1 shows a generic speed-torque characteristic of a motor; at zero speed is the locked rotor torque, the acceleration torque is the torque required at any time up to the maximum torque. The starting torque is inversely proportional to the square of the terminal voltage, while the inrush current is inversely proportional to the terminal voltage. Care must be taken to balance the reduction of the inrush current and the starting torque.

Reactive Power and Starting Power Factor – It is important to take into account the high reactive power consumed by the motor. In such a case, the rating of the upstream equipment may need to be rated higher than the steady-state condition (Kay, Paes, Seggewiss, & Ellis, 1999). The reactive power during startup is closely related to the voltage dip. Typical values of the power factor are about 0.20 for motors under 1000 HP (IEEE Std 399-1997, 1998). The locked rotor kVA per HP is defined for each NEMA code letter, see Appendix C, which can help determine the expected starting reactive power corresponding with the starting power factor (Chapman, 2005).

Robustness – The ability of the starting method to perform consistently, time after time or upon emergency.

Cost – The expense of the starting equipment and installation process. Interoperability is also an important consideration.

Many of these considerations are related, and tradeoffs between them are made to choose the starting method and size the generator-set. Sizing the generator set is a practical engineering problem that boasts a particular expertise and special software tools.

It should be noted that the impact of the startup process dynamics on the fatigue of the induction motor is generally much less than the impact on the motor's mechanical load (Kjellberg & Kling, 2003), (Cohen, 1995), (McElveen, Toney, Autom, & Mountain, 2001). The thermal stress must be taken into consideration when determining induction

motor rotor bar fatigue and motor expected lifetime (Cabanas, et al., 2003). This work focuses on the system dynamics and is not a long-term reliability analysis.

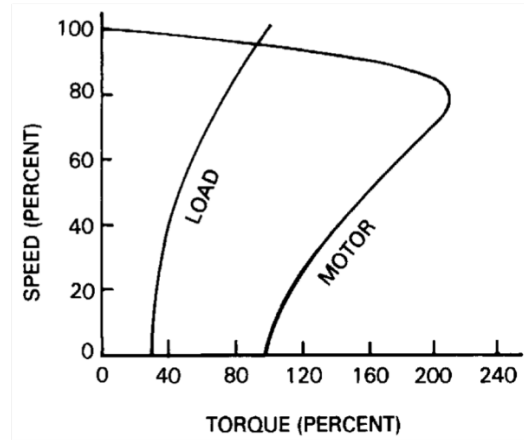


Figure 1: Generic Speed-Torque of a Motor and Associated Load
 Reproduced from IEEE Standard 399-1997, Figure 9-3, p. 239

Taking into consideration the technology of the starting equipment, the starting methods can be divided into electronic drives and those that are not, i.e. conventional electrical network equipment. Other categorizations focus on the voltage manipulation as applied to the terminals. It is typical to separate the methods into the variations of the following categories: full voltage, reduced voltage, incremental voltage, soft-starter, and variable frequency drives (Patil & Porate, 2009), (Larabee, Pellegrino, & Flick, 2005), (McElveen, Toney, Autom, & Mountain, 2001), (Pillay, Nour, Yang, Datu Harun, & Haw, 2009), (Kjellberg & Kling, 2003), and (Bellarmine, Suri, Robinette, & Dreadin, 1994). In this thesis the methods have been divided into the following functional categories based on their physical characteristics and function: full voltage, electromechanical reduced voltage, and soft-starters. Variable Frequency Drives (VFD) are considered beyond the scope of this thesis because they completely decouple the electrical system. Another starting technique (not included in this thesis) is to control the

applied torque of the attached prime mover, such as the fluid coupling method. Other methods not discussed below include single-phase starting of a three-phase motor that can be found in work by (Badr, Alolah, & Abdel-Halim, 1995). The reader is also referred to (Ansari & Deshpande, 2009) for a review the problems associated with unbalanced voltage starting.

1.1. Full Voltage Techniques

These methods include the direct-on-line method and conventional circuit introductions that connect the full terminal voltage to the motor stator.

1.1.1. Direct-On-Line (DOL)

DOL is the traditional and simplest method of motor starting, and most other methods are baselined against it. It is also often called across the line start. This method is the direct connection of the terminal voltage to the motor stator with no additional components, and also for this reason is most economical in terms of installation cost and ease of use. It is also one of most reliable and robust methods. Of all the starting methods it produces the highest inrush current, usually six to eight times the rated current, and the highest starting torque; and due to the high starting torque it has the shortest acceleration time (apart from the shunt capacitor start) (Larabee, Pellegrino, & Flick, 2005) and (Pillay, Nour, Yang, Datu Harun, & Haw, 2009). The DOL method is most commonly used for small motors relative to the size of the generation and system, due to the fact that the startup of a small motor will only have a low impact on the system, and in particular the voltage drop (Cohen, 1995), (Kay, Paes, Seggewiss, & Ellis, 1999), and (Pillay, Nour, Yang, Datu Harun, & Haw, 2009). Other drawbacks include the mechanical stress put on

the motor's load and the low startup efficiency due to the high reactive power consumed at startup. This approach is typically not suitable for large motors.

1.1.2. Shunt Capacitors

Connecting a capacitor in parallel to the motor can help compensate the reactive demand from the motor during startup by supplying a leading current and thus improve the power factor while still achieving high starting torque because of the full voltage. This provides some relief to the supply source. The shunt capacitance may be left connected if they are properly rated so as to provide power factor correction; or removed as the motor approaches rated speed. In reference (Larabee, Pellegrino, & Flick, 2005) the authors state that the shunt capacitance that is left connected should never be sized larger than the motor's magnetizing current. Capacitor starting may be used in conjunction with other starting methods. Work done by (Li, Zhao, Yang, & Zhang, 2009) presents a method with a startup capacitor array using a dynamic controller, which allows for capacitor switching so that the reactive support power can be varied. Shunt capacitor starting is analyzed and compared to other starting methods in references (Patil & Porate, 2009), (Li, Zhao, Yang, & Zhang, 2009), (Lewis & Woodbury, 1978), (Stout, 1978), (Williams & Griffith, 1978), and (Liu, Jiang, Hu, & Zhou, 1997). In general, capacitor starting is used for relatively large motors that need fast starting or improved efficiency during startup. In the system tested by (Stout, 1978) it was found that capacitor starting could reduce up to half the maximum voltage dip as compared to the DOL start and still maintain other adequate starting characteristics. Capacitor starting is a reliable and robust method for motor starting on weak electrical system (Kay, Paes, Seggewiss, & Ellis, 1999).

1.2. Electromechanical Reduced Voltage Techniques

The electromechanical reduced voltage methods can be implemented through conventional circuitry, such as resistors and transformers. During these reduced voltage startup methods, the thermal capability due to the increased time to reach rated speed must be taken into consideration. Transient current surges are produced from open circuit transitions, but with closed circuit transitions these switching transients are avoided.

1.2.1. Star-Delta

The star-delta (wye-delta) starting method controls whether the lead connections from the motor are configured in a star or delta electrical connection. The initial connection should be in the star pattern that results in a reduction of the line voltage by a factor of $1/\sqrt{3}$ (57.7%) to the motor and the current is reduced to 1/3 of the current at full voltage, but the starting torque is also reduced 1/3 to 1/5 of the DOL starting torque (Kjellberg & Kling, 2003). The motor must be delta connected at rated voltage. The transition from star to delta transition usually occurs once nominal speed is reached, but is sometimes performed as low as 50% of nominal speed (McElveen, Toney, Autom, & Mountain, 2001). The star-delta method is usually only applied to low to medium voltage motors (Larabee, Pellegrino, & Flick, 2005) and (McElveen, Toney, Autom, & Mountain, 2001). The operation of the star-delta method is simple and rugged, and is relatively cheap compared to other reduced voltage methods with only additional contactors added to the cost (Pillay, Nour, Yang, Datu Harun, & Haw, 2009). However, the system cannot be modified once installed without considerable rework. Closed-circuit transitions can be performed to avoid open-circuit current surges.

1.2.2. Autotransformer

An autotransformer uses tap changes to reduce the low voltage as needed on the low side connected to the motor terminal. Therefore, the current can be reduced during startup; however the torque is also reduced as the square of the voltage and needs to be taken into consideration to ensure enough torque is supplied during acceleration. The authors in (Larabee, Pellegrino, & Flick, 2005) claim that 10% of the full load torque margin should be supplied at all points on the speed-torque characteristic curve. As the motor speeds up, the line is switched to the full voltage. Common taps range from 50-80% of the rated voltage (Williams & Griffith, 1978), (Pillay, Nour, Yang, Datu Harun, & Haw, 2009), (Larabee, Pellegrino, & Flick, 2005), and (IEEE Std 399-1997, 1998). IEEE Standard 399-1997 provides a table describing the currents at the typical 50%, 65%, and 80% of full voltage as 25%, 42%, and 64% of the current realized at full voltage during startup, respectively. A practical advantage of the autotransformer is the ability to provide different tap changes so that a wide range of applications, which vary in their starting torque and inrush current needs, can be performed. The star-delta starter is electrically equivalent to an autotransformer tapped at 57.7%. However, autotransformers have a higher cost than other conventional electromechanical starting methods (Pillay, Nour, Yang, Datu Harun, & Haw, 2009). Autotransformer starting is simulated and compared to other methods in (Patil & Porate, 2009).

1.2.3. Primary Resistor or Reactor

A switchable primary series resistor or reactor bank can be added at the motor terminals to limit the current or limit change in the current, respectively. The resistor bank will cause a drop in voltage across it reducing the current. The heat dissipated from the resistor also needs to be taken into consideration. Series resistor starting is usually only performed for small motors (Larabee, Pellegrino, & Flick, 2005). When using a series reactor bank, it will oppose the inrush current initially and reduce the terminal voltage proportionally. The most advantageous characteristic of the series reactor starting is that the voltage increases over time as a function of the rate of change of the current without additional control. The added reactance will also further increase the starting reactive power and thus lower the starting efficiency. Switching transients will also occur if it is connected in an open-circuit.

1.3. Soft-Starter Techniques

A soft-starter is any solid-state electronic circuit based device that manipulates the supply voltage prior to connecting to the motor terminals. Many different topologies for soft-starters exist, and many of them are presented in the literature (Charles & Bhuvameswari, 2009), (Solveson, Mirafzal, & Demerdash, 2006), (Li & Liu, 2009), (Rajaji, Kumar, & Vasudevan, 2008), (Youxin, Zezhong, Yalan, Peigang, & Wanquan, 2007). The standard soft-starter consists of thyristors or SCRs that manipulate the source signal via control of the thyristor firing angles (Chapman, 2005). The soft-starter can be based on controlling different starting characteristics, including current, torque, and

voltage, and can be easily adjusted based on the different loadings. Two basic types of soft-starters are the voltage ramping and current limiting types.

The voltage ramping soft-starter is able to gradually increase the voltage from a preset level, as low as 0V, to the rated voltage; the result being a very smooth startup. The current profile generally follows the voltage profile for voltage ramping soft-starters. One of the drawbacks of the ramping soft-starter is increased harmonics, which produce extra heating (McElveen, Toney, Autom, & Mountain, 2001).

The current limiting soft-starter senses the current at the motor so that the fire angle can be controlled in a manner that the voltage is regulated to maintain the desired current. Of course, the tradeoff of lower current equating to lower torque still applies. Typical values of the current limit are 175% to 500% of the rated current of the motor (Larabee, Pellegrino, & Flick, 2005).

The soft-starter adds significant flexibility in operation (e.g. acceleration time and winding heat) and interoperability, due to the fact that it is more sensitive to the mechanical load characteristics (Kjellberg & Kling, 2003). This also results in lower maintenance cost and increased lifetime of the mechanical load, and can result in improved energy efficiency. However, the tradeoff is the increased operational complexity, and soft-starters are generally expensive devices (McElveen, Toney, Autom, & Mountain, 2001). Limitations include harmonics produced by the electronics and the installation distance from the motor. They are common in higher power applications due to their operation flexibility and improved lifetime of equipment (Patil & Porate, 2009).

As an example of a more recent soft-starter control designs, (Youxin, Zezhong, Yalan, Peigang, & Wanquan, 2007) simulate a voltage ramping soft-starter using fuzzy

logic to control a controller reactor in Matlab/Simulink. The results are compared to the DOL method. The research performed by (Rajaji, Kumar, & Vasudevan, 2008) implements an artificial neural network trained fuzzy logic inference soft-starter in Matlab/Simulink. It combines the speed and torque to determine the firing angle to maintain steady ramping of the motor speed. (Li & Liu, 2009) built a fuzzy logic based soft-starter that controls the motor current based on the sensed current magnitude and rate of change. (Solveson, Mirafzal, & Demerdash, 2006) use Matlab to simulate dynamic modeling of different soft-starting firing angle mappings and compare the starting time, torque profiles, and thermal stress. The method is verified against the DOL starting method. The authors in reference (Charles & Bhuvameswari, 2009) apply a shunt reactor with a soft-starter using Matlab/Simulink to simulate. The shunt reactor helps protect the connected system from the voltage dip.

1.4. Models and Simulation Techniques

The works presented in references (IEEE Std 399-1997, 1998) and (Williams & Griffith, 1978) provide a general method to calculate characteristics of a motor's speed-torque curve and accelerating time. The equations presented in the standard are based on the steady-state equivalent network model. While these calculations are helpful and straightforward, a more detailed (Williams & Griffith, 1978) simulation based on more dynamic models will provide better accuracy and more information and insights into how the system behaves.

The models used for the electric machines have varied between the dynamic dq0 or abc flux based models, and the per-phase equivalent circuit steady state model that

expresses the rotor resistance based on the motor's slip. The slip, s , is the difference between the electrical signal synchronous speed, ω_e , and the rotor speed, ω_r , normalized on the synchronous speed:

$$s = \frac{\omega_e - \omega_r}{\omega_e} \quad (\text{VI-1})$$

However, most of the recent works, perhaps due to improvements in computation speed and available software programs, have used the dynamic models. In (Mirošević, Maljkovic, & Miškovic, 2009), (Ong, 1998), (Hadidi, Mazhari, & Kazemi, 2007), (Ozpineci & Tolbert, 2003) for example, the SimPowerSys toolbox of Matlab/Simulink provides various models using the dynamic flux-based representations (TransÉnergie Technologies Inc, 2003).

The importance of saturation and skin effects in modeling induction motors has been simulated and discussed in (Seman, Saitz, & Arkkio, 2004), (Okoro, Weidemann, & Oswald, 2006), (Jabr & Kar, 2007), (Erdogan, Henao, & Grisel, 2004), (Ong, 1998), and (Krause, Wasynczuk, & Sudhoff, 2002). As a general rule it depends on the type of application and size of the generator and induction motor and the modeling principle. The modeling approaches that are most commonly used are either based on dynamic change of the inductances (Erdogan, Henao, & Grisel, 2004), (Jabr & Kar, 2007), (Seman, Saitz, & Arkkio, 2004) or mapping of the fluxes (IEEE Std 399-1997, 1998), (Ong, 1998), (Krause, Wasynczuk, & Sudhoff, 2002).

The switching transients are often of concern for starting methods, and in particular those that perform many online transitions within the startup process. However, modern methods such as closed transitions and other power electronics and transient protection equipment can largely negate the switching transients.

Software programs that have been developed to test induction motor include Electric Transient Analyzer Program's (ETAP) Motor Starting Analysis library (Patil & Porate, 2009); the EDSA Paladin DesignBase® Software (EDSA Corporation, Inc., 2009) and a software tool written in Turbo Pascal for Gulf Power (Bellarmine, Suri, Robinette, & Dreadin, 1994). But most of the literature has either developed unique software or been implemented using Matlab/Simulink. Matlab/Simulink was used to develop all the models in a comprehensive work by (Ong, 1998) and has been used in references (Youxin, Zezhong, Yalan, Peigang, & Wanquan, 2007), (Charles & Bhuvameswari, 2009), (Li, Zhao, Yang, & Zhang, 2009), (Hadidi, Mazhari, & Kazemi, 2007), (Ozpineci & Tolbert, 2003), (Ansari & Deshpande, 2009), while the SimPower System Toolbox for Simulink has been used in references (Youxin, Zezhong, Yalan, Peigang, & Wanquan, 2007), (Charles & Bhuvameswari, 2009), (Ansari & Deshpande, 2009). SimPower Systems Toolbox is a Simulink toolbox specifically used for power systems and includes dynamic electric machine models (TransÉnergie Technologies Inc., 2003).

1.5. Comparative Analyses

From practical and engineering perspectives, selection of starting method for induction motors is discussed in (Kay, Paes, Seggewiss, & Ellis, 1999), (Larabee, Pellegrino, & Flick, 2005), (Williams & Griffith, 1978), (Kjellberg & Kling, 2003), (Cohen, 1995), (Pillay, Nour, Yang, Datu Harun, & Haw, 2009), (Lewis & Woodbury, 1978), (McElveen, Toney, Autom, & Mountain, 2001), and (IEEE Std 399-1997, 1998), primarily focusing on impacts of specific applications. The Soft-Starter Handbook from

ABB (Kjellberg & Kling, 2003) provides practical aspects based (Ozpineci & Tolbert, 2003) on the type of mechanical load.

Comparative simulation analyses for multiple starting methods have been performed in (Medrea & Demean, 2008), (Hadidi, Mazhari, & Kazemi, 2007), (Patil & Porate, 2009). Research by (Medrea & Demean, 2008) compare the DOL, star-delta, autotransformer, and soft-starter methods using the ESDA Paladin Designbase® software. The network is modeled as an ideal grid, connected through a transformer and a bus. The authors of reference (Hadidi, Mazhari, & Kazemi, 2007) perform their analysis using the dynamic dq0 model for a comparison of the DOL, star-delta, and soft-starter (constant ramping) with and without a static VAR compensator. The simulation is performed for connection to a much larger generator through a transformer and transmission network, and it does not model the engine, exciter, or voltage regulator. The authors of reference (Patil & Porate, 2009) used the ETAP software's Dynamic Motor Acceleration, which uses dynamic models and the starters that are provided in the program library. The simulated network is a grid, which is connected through a cable to a 3 HP induction motor. The DOL and autotransformer methods are compared in three scenarios: without line impedance, with line impedance, and with line impedance and reactive compensation.

Most of the works previously mentioned in the discussion of the starting methods performed simulated analysis and compared to the DOL starting method. These methods for the most part are simulated with ideal sinusoid sources. The works that have focused on weak or isolated systems include (Tuinman, Piers, & De Weerd, 1998), (Mirošević, Maljkovic, & Miškovic, 2005), (Mirošević, Maljkovic, & Miškovic, 2009). In reference

(Tuinman, Piers, & De Weerd, 1998) the authors model a synchronous generator and induction motor coupled together based on the stator flux in the dq0 reference frame. They also model the Automatic Voltage Regulator (AVR) and exciter. However, only the DOL is simulated and the equations would need to be modified in detail for each of the other starting methods. The engine is not modeled. Diesel generator set dynamics connected to induction motors have been researched in (Mirosevic, Maljkovic, & Milkovic, 2005), (Mirosevic, Maljkovic, & Milkovic, 2007), (Mirosevic, Maljkovic, & Milkovic, 2009). They use the dynamic dq0 models to simulate both the synchronous generator and induction motor using the program package *MatrixX*. They have studied only DOL starting in their work: DOL starting and validation (Mirosevic, Maljkovic, & Milkovic, 2009), the impact of DOL starting on torsional dynamics (Mirosevic, Maljkovic, & Milkovic, 2007), and the DOL starting of a second induction motor (Mirosevic, Maljkovic, & Milkovic, 2005).

2. Scope of This Work

The purpose of this work is to develop an accurate simulation for comparing starting methods of an isolated synchronous generator and squirrel cage induction motor system, while considering engine dynamics. This work is to provide a comprehensive approach to simulate the starting methods and dynamic machine models for this type of system. Previous work has used constant voltage sources or only DOL starting methodology for base lining. To facilitate usability in a generator set and motor system, this work proposes a method that keeps the parameters of the network separate from the synchronous generator by measuring the equivalent impedance and supplying it as feedback to the

synchronous generator model. The simulation program is performed in Matlab/Simulink as it has become a widely used and accepted platform. Matlab/Simulink allows for easily testing different simulation step times and solution algorithms (TransÉnergie Technologies Inc., 2003). However, the main contribution of this thesis is the use of the equivalent load impedance used in the simulation to closely simulate the response. It also allows the models to be connected within the simulation environment through a cut-and-paste technique. However, further work could be done to improve the linkage between the components. Only general conclusions are drawn in this thesis; recommendations and judgments are not appropriate in this work.

According to how the models have been built, the main limitation of this work is that it is not scalable to looped systems and can only be used on a single generator source. The simulated starters also have ideal characteristics, whereas further detailed models could be developed if a higher level of fidelity were to be sought.

3. Plan of Development

The first phase is the research and development of the electric machine models. The electric machine models are then tested on ideal networks. The synchronous generator model, which included the automatic voltage regulator with the excitation system, is tested with static loads. The induction motor model is tested on an ideal three-phase voltage source. Once the synchronous generator works with parameters for rated power of 1 MW, two different induction motor models with a rated power of 200 HP and 500 HP are simulated to compare the starting methods.

Once the electric machine models are developed, the other components of the system necessary for accurate dynamic modeling of the isolated system are built. The necessary components include the engine model, speed governor and mechanical load. A power system stabilizer is also built.

The secondary components are tested next. The engine block is originally tested with the synchronous generator still connected to the static RL load. The diesel engine model and the generator voltage regulator were validated against actual data.

Next, the block that controls the connection of the electrical system is built and tested to connect the synchronous generator with a reasonably small induction motor with the DOL starting method. The next step is to develop each of the other starting methods one by one and test them with the 200 HP motor connected to a constant source. Once verified on the constant source the starters are connected to the diesel-generator set. The same process was performed for the 500 HP motor. Once the results for both the 200 HP and 500 HP motor are obtained the results are compared and some general conclusions are drawn.

VII. System Models

1. System Overview

The overview of the system modeled in this thesis is shown in Figure 2. The main components of the system are the engine model, synchronous generator, and induction motor. The engine model mechanical load makes up the mechanical system and the generator and motor the electrical system. The applied torque to the rotor of the motor is an external input. Another important system element that will affect the dynamic response is the excitation system of the synchronous generator that consists of the automatic voltage regulator (AVR) and the power system stabilizer (PSS). The excitation system controls the applied field voltage to the synchronous generator based on the engines output, which in this case will be the rotating frequency. Also, included is the engines speed-governor that is used to maintain a consistent speed based on different system characteristics (applied power and electrical frequency). In this system, the conductor impedance connecting the generator and motor is considered negligible, and the breaker closing is treated as ideal. These two aspects should be addressed in future work.

One of the important aspects to the model is the components are easily interchangeable. This is accomplished by continuously calculating the induction motor model stator effective impedance seen by the generator. The dynamic effective load impedance is used as feedback to the generator model.

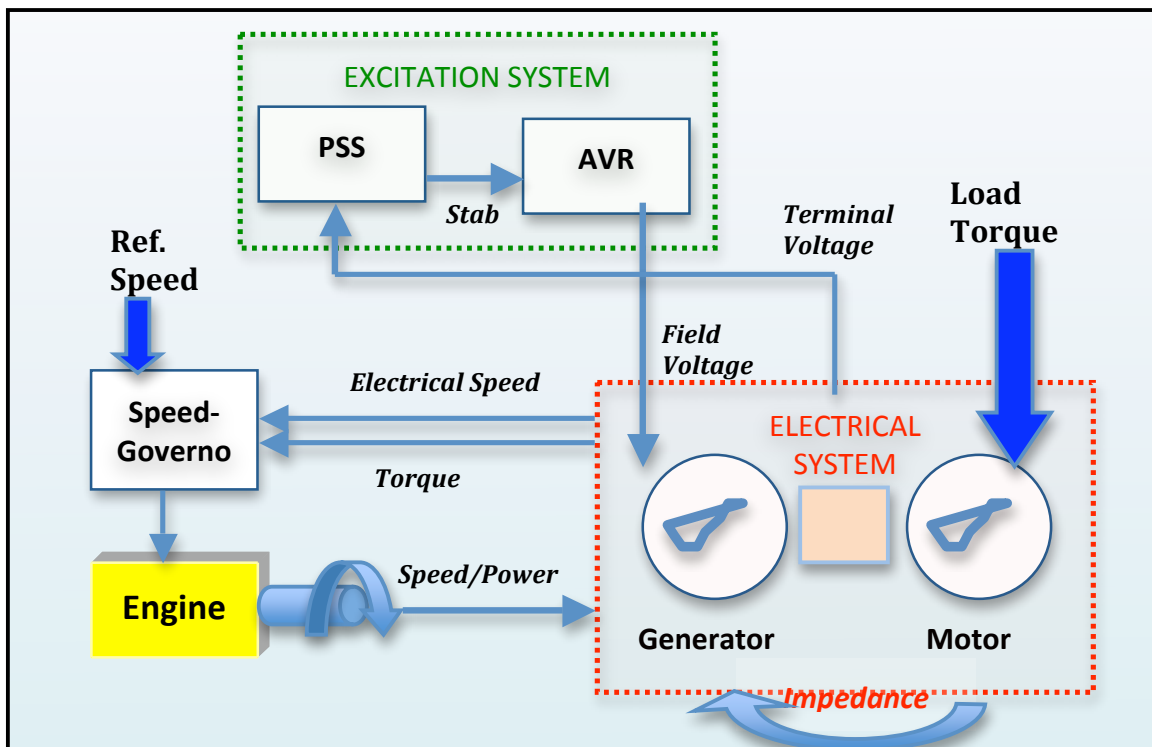


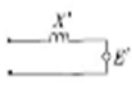
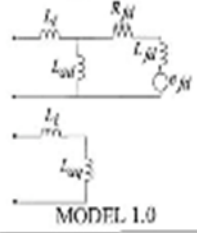
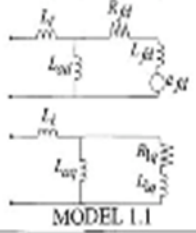
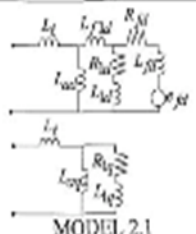
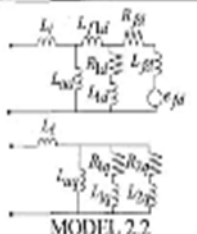
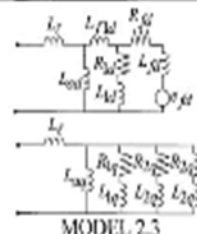
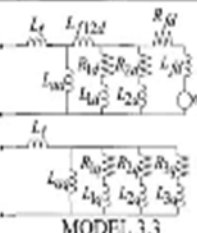
Figure 2: System Model Overview

2. Synchronous Generator

Electric power, with only a few exceptions, is generated using synchronous machines. To reduce air resistance and other mechanical losses most synchronous generators that run on fossil fuels are salient and low pole pair machines. These characteristics are the principles kept in mind when choosing the model and parameters of the synchronous machine.

IEEE Standard 1110-2002 provides the basic practices for synchronous generator modeling (IEEE Std 1110-2002, 2003). The key concept of modeling synchronous machines for stability studies has been to change the variables into a simplified and intuitive reference frame. Table 1 classifies several models developed in IEEE Standard 1110-2002 for representing a synchronous generator, depending on their degree of complexity and structural design. In this thesis, Model 2.1 is selected to represent asynchronous machine. The model includes the field winding on the direct axis and one damper winding on both the direct and quadrature axis. This is the most common type associated with salient-pole machines and is recommended in IEEE Standard 1110-2002.

Table 1: General Synchronous Generator DQ Models Table

Table 1—Selection of generator models of varying degrees of complexity				
CONSTANT ROTOR FLUX LINKAGES	THEVENIN EQUIVALENT 			
Q-AXIS → D-AXIS ↓	NO EQUIVALENT DAMPER CIRCUIT	ONE EQUIVALENT DAMPER CIRCUIT	TWO EQUIVALENT DAMPER CIRCUITS	THREE EQUIVALENT DAMPER CIRCUITS
FIELD CIRCUIT ONLY	 MODEL 1.0	 MODEL 1.1	NOT CONSIDERED	NOT CONSIDERED
FIELD CIRCUIT + ONE EQUIVALENT DAMPER CIRCUIT	NOT CONSIDERED	 MODEL 2.1	 MODEL 2.2	 MODEL 2.3
FIELD CIRCUIT + TWO EQUIVALENT DAMPER CIRCUITS	NOT CONSIDERED	NOT CONSIDERED	NOT CONSIDERED	 MODEL 3.3

Reproduced from IEEE Standard 1110-2002 Table 1 p. 15

2.1. State Variable Model

The synchronous generator model is usually simulated after a transformation from the AC three-phase frame to direct and quadrature axes that simplify the flux-based calculations. The dq0 transformation in the arbitrary reference frame is the generalization of earlier work starting with Park's Transformation (Park, 1929) and was introduced by Krause and Thomas (Krause & Thomas, 1965). For the dq0 transformation the direct (d)

axis is centered on the magnetic peak, and the quadrature (q) axis is electrically orthogonal, 90° , from the direct axis. This transformation simplifies the relationship between the fluxes and currents, and this spatial relationship is shown in Figure 3, where f is any of the state-space variables. The dq0 transformation and its inverse transformation (dq0 to abc reference frame) are provided in Appendix A.

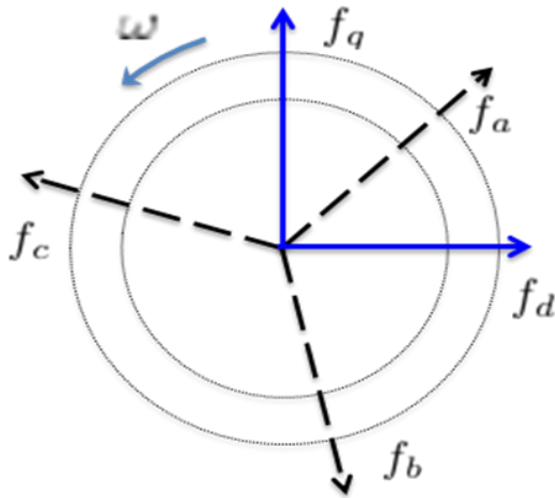


Figure 3: Relationship between the abc and dq0 general state variable quantities

The equivalent circuit diagram for the d and q axes, which represent the impact of the orthogonal fluxes (multiplied by the speed) as voltage sources, is shown in Figure 4. The field winding branch is included on the d-axis since it is directly applied. The damper windings, one on each of the direct and quadrature axes, must also be included. The symbol to denote their parameters is k . All parameters are referred to the stator, thus to denote the rotor parameters referred to the stator a prime ' symbol is used.

The stator parameters are:

v_d d-axis stator voltage

v_q q-axis stator voltage

i_d	d-axis stator current
i_q	q-axis stator current
λ_d	d-axis flux linkage
λ_q	q-axis flux linkage
R_s	Stator resistance
L_{ls}	Stator leakage inductance

The rotor parameters referred to the stator are:

v_{fd}'	d-axis field voltage (often denoted with e , for excitation, instead of v)
v_{kd}'	d-axis damper winding voltage
v_{kq}'	q-axis damper winding voltage
i_{fd}'	d-axis field current
i_{kd}'	d-axis damper winding current
i_{kq}'	q-axis damper winding current
λ_{fd}'	d-axis field flux linkage
λ_{kd}'	d-axis damper winding flux linkage
λ_{kq}'	q-axis damper winding flux linkage
R_{fd}'	d-axis field resistance
R_{kd}'	d-axis damper winding resistance
R_{kq}'	q-axis damper winding resistance
L_{lfd}'	d-axis field leakage inductance
L_{lkd}'	d-axis damper winding leakage inductance
L_{lkq}'	q-axis damper winding leakage inductance

The mutual magnetizing parameters are:

i_{md}	d-axis stator to rotor mutual current
i_{mq}	q-axis stator to rotor mutual current
λ_{md}	d-axis stator to rotor mutual flux linkage
λ_{mq}	q-axis stator to rotor mutual flux linkage
L_{md}	d-axis stator to rotor mutual inductance
L_{mq}	q-axis stator to rotor mutual inductance

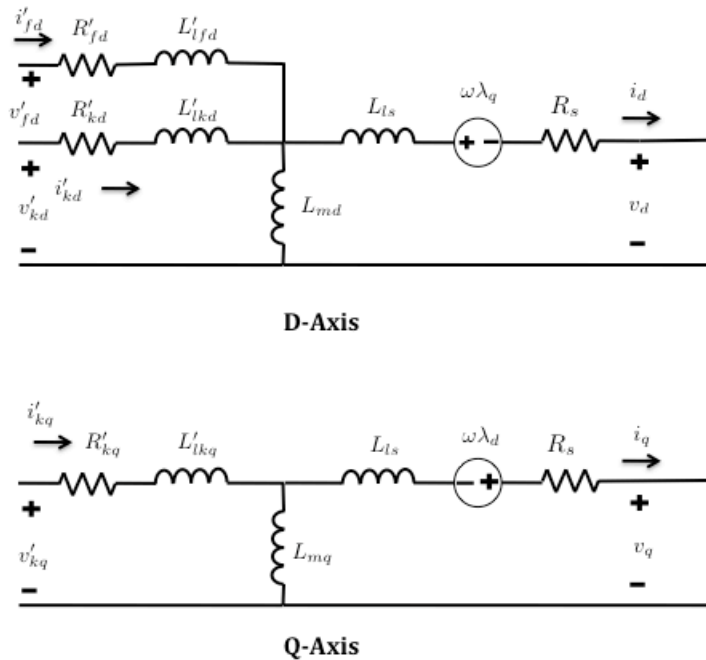


Figure 4: Synchronous Generator dq Equivalent Circuit Diagram

The zero sequence in the equations is ignored because only a balanced system is considered in this thesis, in other words the abc phases are equal magnitude and equidistant in electrical degrees. Upon transformation to the dq0 reference frame the

voltage loop equations can be written as (Krause, Wasynczuk, & Sudhoff, 2002), (Ong, 1998):

$$\begin{aligned}
 v_q &= -R_s i_q + \omega_e \lambda_d + \frac{d}{dt} \lambda_q \\
 v_d &= -R_s i_d - \omega_e \lambda_q + \frac{d}{dt} \lambda_d \\
 v'_{fd} &= R'_{fd} i'_{fd} + \frac{d}{dt} \lambda'_{fd} \\
 v'_{kd} &= R'_{kd} i'_{kd} + \frac{d}{dt} \lambda'_{kd} \\
 v'_{kq} &= R'_{kq} i'_{kq} + \frac{d}{dt} \lambda'_{kq}
 \end{aligned} \tag{VII-1}$$

(V).

The input stator electrical speed, ω_e , is calculated from the mechanical speed, ω_{eng} , from the engine corrected for the pole pairs, N_p , $\omega = N_p \omega_{eng}$

Letting,

$$\begin{aligned}
 L_q &= L_{ls} + L_{mq} \\
 L_d &= L_{ls} + L_{md} \\
 L'_{fd} &= L'_{lfd} + L_{md} \\
 L'_{kd} &= L'_{lkd} + L_{md} \\
 L'_{kq} &= L'_{lkq} + L_{mq}
 \end{aligned} \tag{H),}$$

(VII-2)

then the associated flux linkage equations are (Krause, Wasynczuk, & Sudhoff, 2002), (Ong, 1998):

$$\begin{aligned}
 \lambda_q &= -L_q i_q + L_{mq} i'_{kq} \\
 \lambda_d &= -L_d i_d + L_{md} i'_{fd} + L_{md} i'_{kd} \\
 \lambda'_{fd} &= -L_{md} i_d + L'_{fd} i'_{fd} + L_{md} i'_{kd} \\
 \lambda'_{kd} &= -L_{md} i_d + L_{md} i'_{fd} + L'_{kd} i'_{kd} \\
 \lambda'_{kq} &= -L_{mq} i_q + L'_{kq} i'_{kq}
 \end{aligned} \tag{VII-3}$$

(Wb-turns).

The equivalent matrix form is:

$$\begin{bmatrix} \lambda_q \\ \lambda_d \\ \lambda'_{fd} \\ \lambda'_{kd} \\ \lambda'_{kq} \end{bmatrix} = \begin{bmatrix} -L_q & 0 & 0 & 0 & L_{mq} \\ 0 & -L_d & L_{md} & L_{md} & 0 \\ 0 & -L_{md} & L'_{fd} & L_{md} & 0 \\ 0 & -L_{md} & L_{md} & L'_{kd} & 0 \\ -L_{mq} & 0 & 0 & 0 & L'_{kq} \end{bmatrix} \begin{bmatrix} i_q \\ i_d \\ i'_{fd} \\ i'_{kd} \\ i'_{kq} \end{bmatrix} \quad (\text{VII-4})$$

(Wb-turns).

In the simulation, the voltage loop equations (VII-1) are manipulated to solve the time derivatives of the flux linkages. Thereby, the simulation can be performed straightforward through integration of the state variables. This also means that the time step must be sufficiently small to ensure a high degree of accuracy for dynamic performance. The simulation is performed in matrix form through the equation:

$$\begin{bmatrix} \frac{d}{dt} \lambda_q \\ \frac{d}{dt} \lambda_d \\ \frac{d}{dt} \lambda'_{fd} \\ \frac{d}{dt} \lambda'_{kd} \\ \frac{d}{dt} \lambda'_{kq} \end{bmatrix} = \begin{bmatrix} v_q \\ v_d \\ v'_{fd} \\ 0 \\ 0 \end{bmatrix} - \begin{bmatrix} -R_s & 0 & 0 & 0 & 0 \\ 0 & -R_s & 0 & 0 & 0 \\ 0 & 0 & R_{fd} & 0 & 0 \\ 0 & 0 & 0 & R_{kd} & 0 \\ 0 & 0 & 0 & 0 & R_{kq} \end{bmatrix} \begin{bmatrix} i_q \\ i_d \\ i'_{fd} \\ i'_{kd} \\ i'_{kq} \end{bmatrix} \quad (\text{VII-5})$$

$$- \omega_r \begin{bmatrix} 0 & -L_d & L_{md} & L_{md} & 0 \\ L_q & 0 & 0 & 0 & -L_{mq} \\ 0 & 0 & 0 & 0 & 0 \\ 0 & 0 & 0 & 0 & 0 \\ 0 & 0 & 0 & 0 & 0 \end{bmatrix} \begin{bmatrix} i_q \\ i_d \\ i'_{fd} \\ i'_{kd} \\ i'_{kq} \end{bmatrix} \quad (\text{V}).$$

Equation (VII-5) is implemented in the simulation to derive the flux linkage derivatives. The flux linkages derivatives can be integrated to produce the flux linkages. Then, they are converted to the currents using Equation (VII-4) with the inverted inductance matrix.

$$\begin{bmatrix} i_q \\ i_d \\ i'_{fd} \\ i'_{kd} \\ i'_{kq} \end{bmatrix} = \begin{bmatrix} -L_q & 0 & 0 & 0 & L_{mq} \\ 0 & -L_d & L_{md} & L_{md} & 0 \\ 0 & -L_{md} & L'_{fd} & L_{md} & 0 \\ 0 & -L_{md} & L_{md} & L'_{kd} & 0 \\ -L_{mq} & 0 & 0 & 0 & L'_{kq} \end{bmatrix}^{-1} \begin{bmatrix} \lambda_q \\ \lambda_d \\ \lambda'_{fd} \\ \lambda'_{kd} \\ \lambda'_{kq} \end{bmatrix} \quad (\text{VII-6})$$

(A).

The block diagram that shows the simulation flow using Equations (VII-5, VII-6) is given in Figure 5. The electromagnetic torque, represented as T_{em} , can be calculated in the dq0 reference frame using the equation (IEEE Std 1110-2002, 2003):

$$T_{em} = \frac{3}{2} N_P (\lambda_d i_q - \lambda_q i_d) \quad (\text{N-m}). \quad (\text{VII-7})$$

The electromagnetic torque calculated Simulink block is shown in Figure 6.

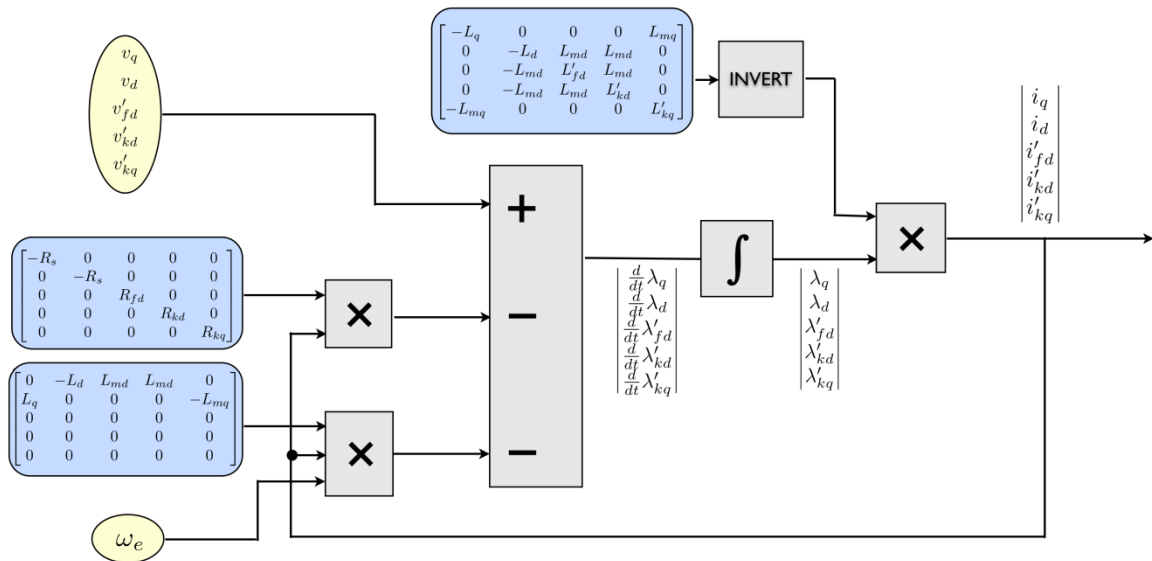


Figure 5: Simulation Flow for the Synchronous Generator Model

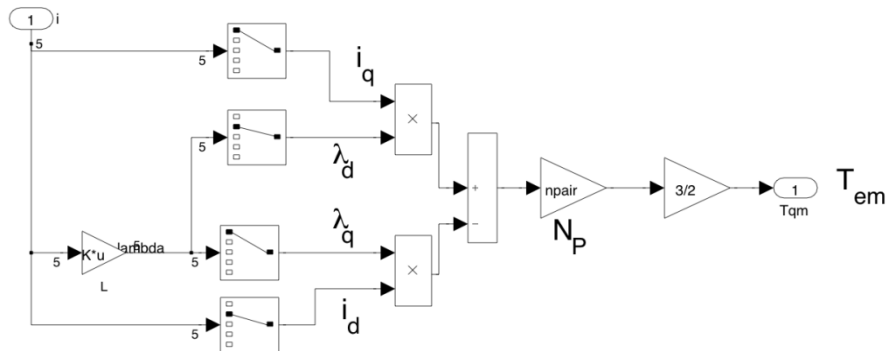


Figure 6: Simulink Electromagnetic Torque Calculation (Equation VII-7)

3. Squirrel Cage Induction Motor

Three-phase AC induction motors are extensively used for industrial applications such as pumps and mills. The reason for their popularity is because of their low cost, as compared to synchronous motors. They are more robust, rugged for varying operating conditions and require less maintenance (Krause, Wasynczuk, & Sudhoff, 2002), (Ong, 1998). However, the drawbacks of induction motors include the high starting currents and the increased variability and difficulty of control. The induction motor is considered a dynamic load because its response varies as the system operating state changes. This is a challenge that is receiving increased attention in power system studies.

The fundamental aspect of induction motors is that they do not have a field circuit; instead a current is induced in the rotor by the magnetic field from electrical signals applied to the stator. The induced current in the rotor creates another magnetic field. These two magnetic fields induce a torque on the rotor. There are two common types of induction motors; the squirrel cage and wound rotor. The squirrel cage design consists of shorted bars along the body. The currents are induced in these bars creating another magnetic field that lags behind the stator magnetic field producing a rotating torque. As the name implies, the wound-rotor induction motor consists of wires wrapped around the rotor and which induces the current. They can include externally accessible brushes so as to add resistance. Therefore, the wound-rotor has the ability to change the effective resistance and manipulate starting speeds.

3.1. State Variable Model

Similar to the synchronous generator model, the induction motor model is usually simulated after a transformation from the AC three-phase frame to DC phases that simplify the calculations in the terms of the flux. The transformation and the inverse transformation (dq0 to abc) are provided in Appendix A. The reference frames can be used interchangeably. But, when sharing parameters care must be taken to ensure they are in the same frame of reference.

The squirrel cage induction motor equivalent circuit model in the dq0 reference frame is shown in Figure 7. It is similar to the synchronous model with the noticeable exceptions that the field winding is missing and the orthogonal fluxes are treated as voltage sources. The diagram shows the currents in the proper direction for motor operation. In the squirrel cage induction motor the rotor bars are shorted out, which means that the rotor voltages are zero. All parameters are referred to the stator, the parameters that are modified are denoted with the prime symbol '. The induction motor stator parameters are:

v_{ds}	d-axis stator voltage
v_{qs}	q-axis stator voltage
i_{ds}	d-axis stator current
i_{qs}	q-axis stator current
λ_{ds}	d-axis flux linkage
λ_{qs}	q-axis flux linkage
R_s	Stator resistance
L_{ls}	Stator leakage inductance

The induction motor rotor parameters are:

v_{dr}' d-axis rotor voltage

v_{qr}' q-axis rotor voltage

i_{dr}' d-axis rotor current

i_{qr}' q-axis rotor current

λ_{dr}' d-axis rotor flux linkage

λ_{qr}' q-axis rotor flux linkage

R_r' Rotor resistance

L_{lr}' Rotor leakage inductance

The induction motor mutual parameters are:

i_{md} d-axis stator to rotor mutual current

i_{mq} q-axis stator to rotor mutual current

λ_{md} d-axis stator to rotor mutual flux linkage

λ_{mq} q-axis stator to rotor mutual flux linkage

L_m Stator to rotor mutual inductance

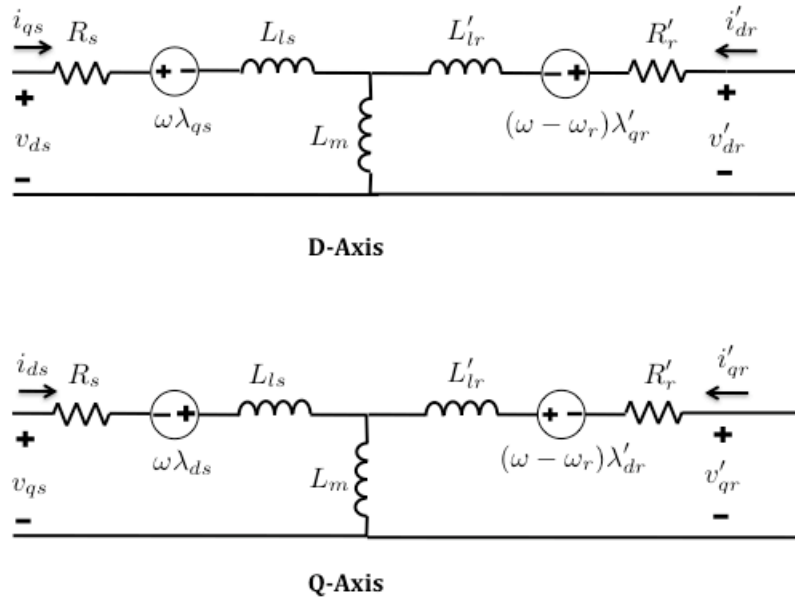


Figure 7: Squirrel Cage Induction Motor dq Equivalent Circuit Diagram

The voltage loop equations of the equivalent circuit produce the following equations:

$$\begin{aligned}
 v_{qs} &= R_s i_{qs} + \omega \lambda_{ds} + \frac{d}{dt} \lambda_{qs} \\
 v_{ds} &= R_s i_{ds} - \omega \lambda_{qs} + \frac{d}{dt} \lambda_{ds} \\
 v'_{qr} &= 0 = R'_r i'_{qr} + (\omega - \omega_r) \lambda'_{dr} + \frac{d}{dt} \lambda'_{qr} \\
 v'_{dr} &= 0 = R'_r i'_{dr} - (\omega - \omega_r) \lambda'_{qr} + \frac{d}{dt} \lambda'_{dr}
 \end{aligned} \tag{VII-8}$$

where ω_r is the induction motor rotating speed and ω is the general rotating reference frame speed (stationary, synchronous, or rotor). For the squirrel cage induction motor the rotor voltages are zero since the rotor bars are short-circuited. The corresponding current-flux relationships are:

$$\begin{aligned}
 \lambda_{qs} &= L_{ls} i_{qs} + L_m i_{qs} + L_m i'_{qr} \\
 \lambda_{ds} &= L_{ls} i_{ds} + L_m i_{ds} + L_m i'_{dr} \\
 \lambda'_{qr} &= L_{lr} i'_{qr} + L_m i_{qs} + L_m i'_{qr} \\
 \lambda'_{dr} &= L_{lr} i'_{dr} + L_m i_{ds} + L_m i'_{dr}
 \end{aligned} \tag{VII-9}$$

(Wb-turns),

and the mutual flux linkages are:

$$\begin{aligned}\lambda_{mq} &= L_m (i_{qs} + i'_{qr}) \\ \lambda_{md} &= L_m (i_{ds} + i'_{dr})\end{aligned}\quad (\text{Wb-turns}), \quad (\text{VII-10})$$

Using the Equations (VII-9, VII-10) the currents can be calculated in terms of flux linkages:

$$\begin{aligned}i_{qs} &= \frac{\lambda_{qs} - \lambda_{mq}}{L_{ls}} \\ i_{ds} &= \frac{\lambda_{ds} - \lambda_{md}}{L_{ls}} \\ i'_{qr} &= \frac{\lambda'_{qr} - \lambda_{mq}}{L_{lr}} \\ i'_{dr} &= \frac{\lambda'_{dr} - \lambda_{md}}{L_{lr}}\end{aligned}\quad (\text{A}), \quad (\text{VII-11})$$

These Equations (VII-11) can be plugged into the voltage loop Equations (VII-8) to produce a straightforward calculation of the flux linkage derivatives that are used in the simulation:

$$\begin{aligned}\lambda_{qs} &= \int (v_{qs} - \omega \lambda_{ds} - \frac{R_s}{L_{ls}} (\lambda_{qs} - \lambda_{mq})) dt \\ \lambda_{ds} &= \int (v_{ds} + \omega \lambda_{qs} - \frac{R_s}{L_{ls}} (\lambda_{ds} - \lambda_{md})) dt \\ \lambda'_{qr} &= \int (- (\omega - \omega_{rm}) \lambda'_{dr} - \frac{R'_r}{L'_{lr}} (\lambda'_{qr} - \lambda_{mq})) dt \\ \lambda'_{dr} &= \int ((\omega - \omega_{rm}) \lambda'_{qr} - \frac{R'_r}{L'_{lr}} (\lambda'_{dr} - \lambda_{md})) dt\end{aligned}\quad (\text{VII-12})$$

(Wb-turns).

The actual implementation is performed by the flux linkage per second, denoted ψ . This is because it has been found to have better computational performance in testing. The only difference is the multiplication of the flux linkages with the fundamental frequency, ω_b :

$$\psi = \omega_b \lambda.$$

The Simulink blocks to perform these calculations are not easily interpreted, instead the simplified block diagrams for the stator equations are shown in Figure 8 and the rotor equations are shown in Figure 9.

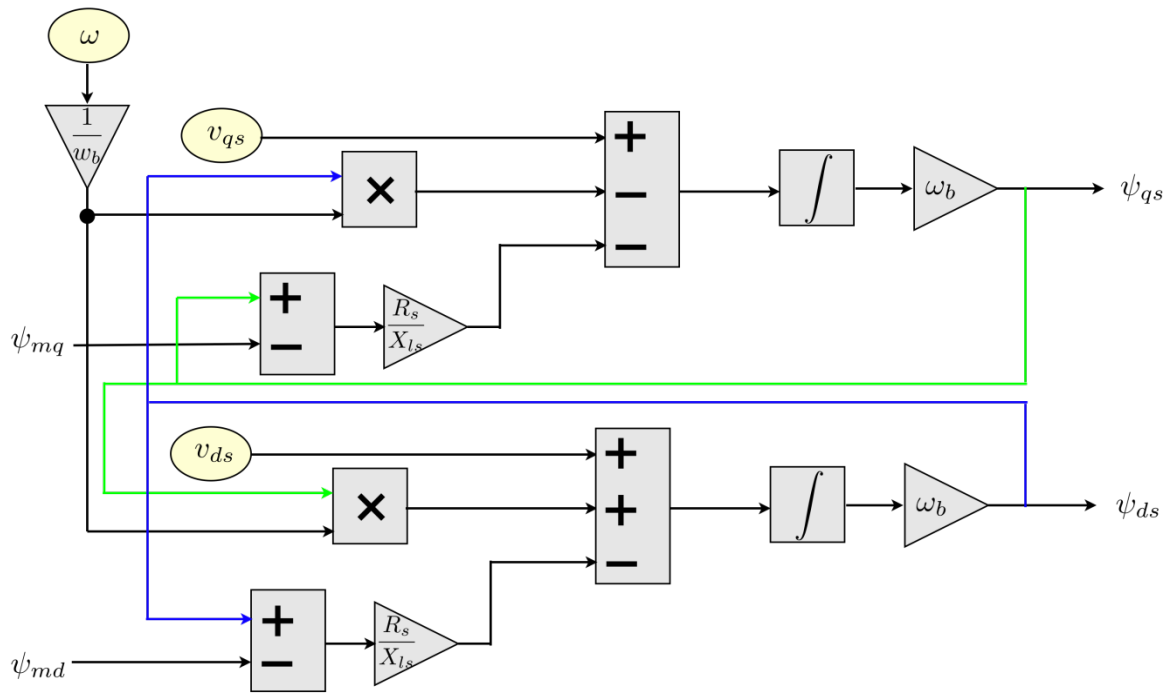


Figure 8: Block Diagram of the Induction Motor Stator Flux Linkage per Second Calculations

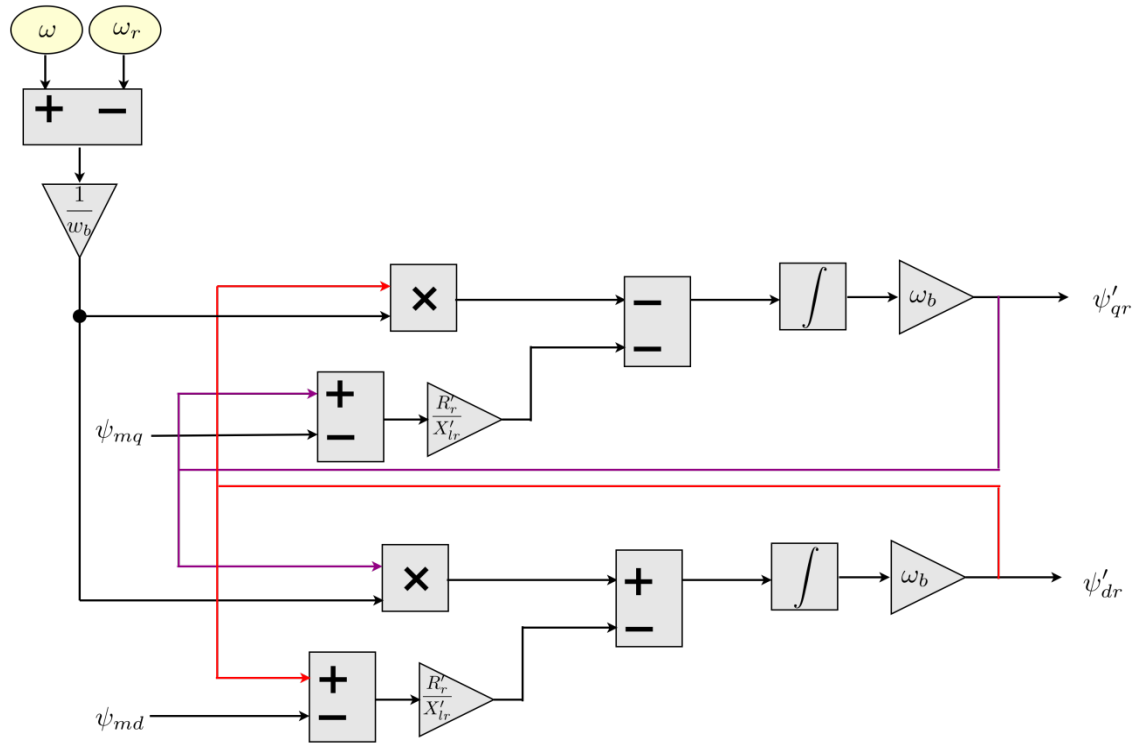


Figure 9: Block Diagram of the Induction Motor Rotor Flux Linkage per Second Calculations

The mutual flux linkages incorporate saturation, therefore modifications of the Equations (VII-10), and are described in Subsection 3.2. The block diagrams describing the calculation of the currents from the flux linkages with Equations (VII-11) are shown in Figures 10 and 11, for the stator and rotor respectively.

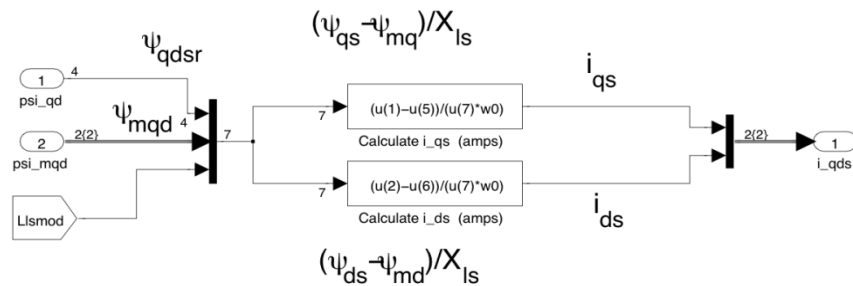


Figure 10: Simulink Block of the Induction Motor Stator Current Calculations

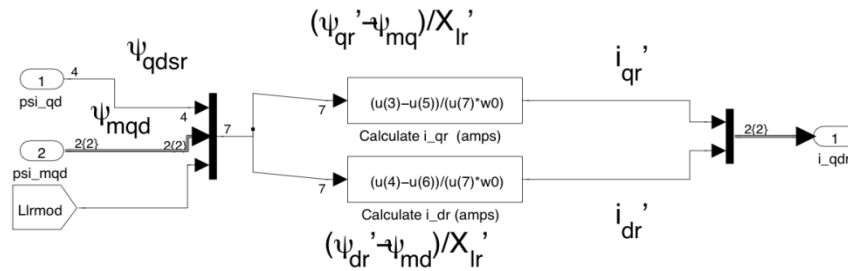


Figure 11: Simulink Block of the Induction Motor Rotor Current Calculation

The electromagnetic torque produced by the induction motor, $T_{em,motor}$, is calculated using the following equation (Krause, Wasynczuk, & Sudhoff, 2002), (Ong, 1998):

$$T_{em,motor} = \frac{3}{2} N_{P,motor} (\lambda_{ds} i_{qs} - \lambda_{qs} i_{ds}) \quad (\text{N-m}), \quad (\text{VII-13})$$

$N_{P,motor}$ is the number pole pairs of the motor.

The motor's rotational speed is calculated from the mechanical equation of motion based on the rotational torques and the machine inertia. For the motor the difference between the electromagnetic torque and the load torque plus frictional losses based on the speed of the rotor and load, $\omega_{load} = \omega_r / N_{P,motor}$, determines the acceleration of the motor. The equation of the motor motion solving for the motor electrical speed is (Krause, Wasynczuk, & Sudhoff, 2002), (Ong, 1998):

$$\omega_r = \frac{1}{J} \int (T_{em,motor} - T_{load} - D_f \omega_{load}) dt \quad (\text{rad/sec}), \quad (\text{VII-14})$$

where, D_f is the friction coefficient that simulates the frictional losses. The Simulink block of Equation (VII-14) is shown in Figure 12.

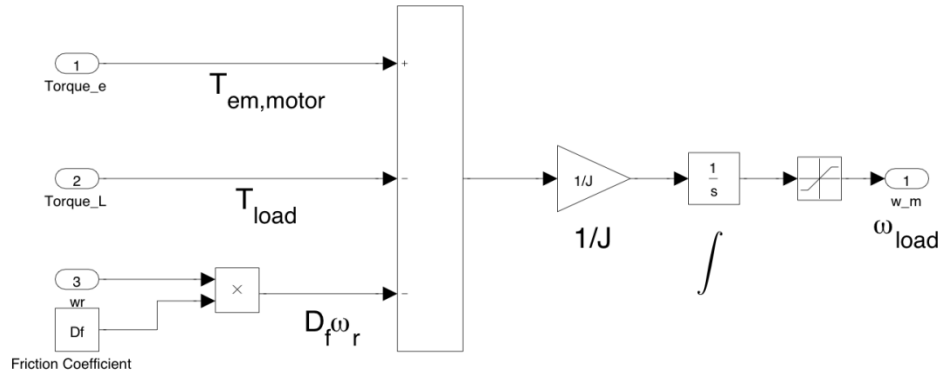


Figure 12: Simulink Block of the Motor Rotational Speed Calculation

3.2. Modeling the Magnetic Core Saturation

Inclusion of the magnetic core saturation in the induction motor is performed with the flux-correction method described in (Krause, Wasynczuk, & Sudhoff, 2002), (Ong, 1998). (The saturation of the leakage inductance is neglected.) The method uses the no load test of the RMS terminal voltage and peak stator current to determine the relationship of the flux linkage correction factor that displaces the unsaturated or air gap line to the saturation curve as in Figure 13. Therefore, the previous Equation (VII-10) for the mutual magnetizing fluxes becomes:

$$\begin{aligned}\psi_{md} &= L_M \left(\frac{\psi_{ds}}{L_{ls}} + \frac{\psi'_{dr}}{L'_{lr}} \right) - \frac{L_M}{L_m} f(\psi_{md}) \\ \psi_{mq} &= L_M \left(\frac{\psi_{qs}}{L_{ls}} + \frac{\psi'_{qr}}{L'_{lr}} \right) - \frac{L_M}{L_m} f(\psi_{mq})\end{aligned}\tag{VII-15}$$

(Wb-turns/sec),

where,

$$L_M = \left(\frac{1}{L_{ls}} + \frac{1}{L'_{lr}} + \frac{1}{L_m} \right)^{-1}\tag{H).}\tag{VII-16}$$

And, the proportional values for each axis are calculated based on the ratio of the mutual flux linkage magnitude φ_m in equations:

$$\begin{aligned} f(\psi_{md}) &= \frac{\psi_{md}}{\psi_m} f(\psi_m) \\ f(\psi_{mq}) &= \frac{\psi_{mq}}{\psi_m} f(\psi_m) \end{aligned} \quad (\text{VII-17})$$

where,

$$\psi_m = \sqrt{\psi_{mq}^2 + \psi_{md}^2} \quad (\text{Wb-turns/sec}). \quad (\text{VII-18})$$

A Matlab function is written to convert the RMS terminal voltage and peak stator current to the instantaneous mutual magnetizing flux linkage and current following the linearized piecewise method found in (Prusty & Rao, 1980), and the code is found in Appendix F. The converted values are used as the parameters for lookup tables. These are used to subtract the saturation curve from the air gap line to produce the correction factor used in Equation (VII-15). The block diagram equivalent of the flux linkage saturation calculation is shown in Figure 14.

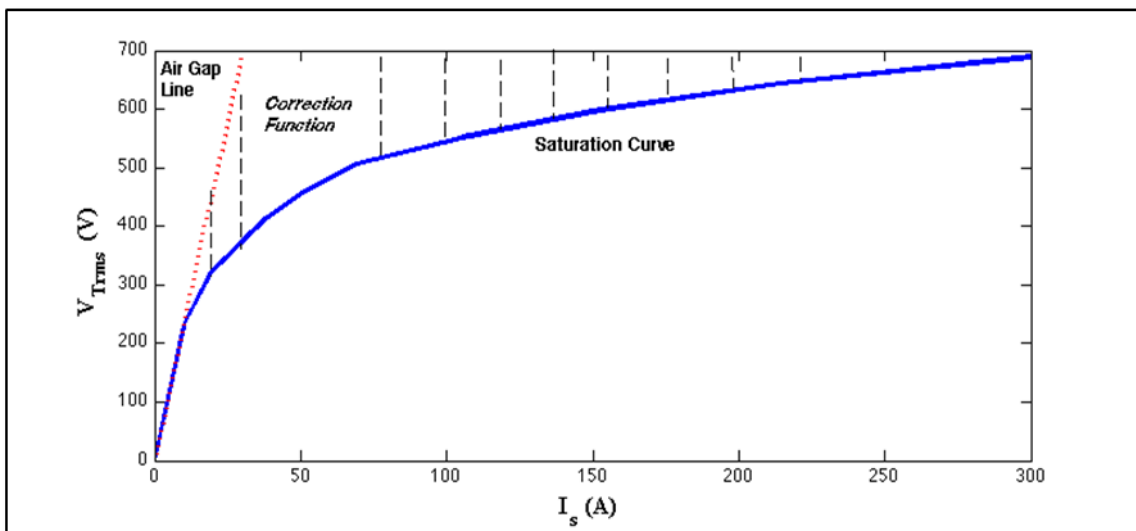


Figure 13: No Load Saturation Curve of Stator Current and Terminal Voltage

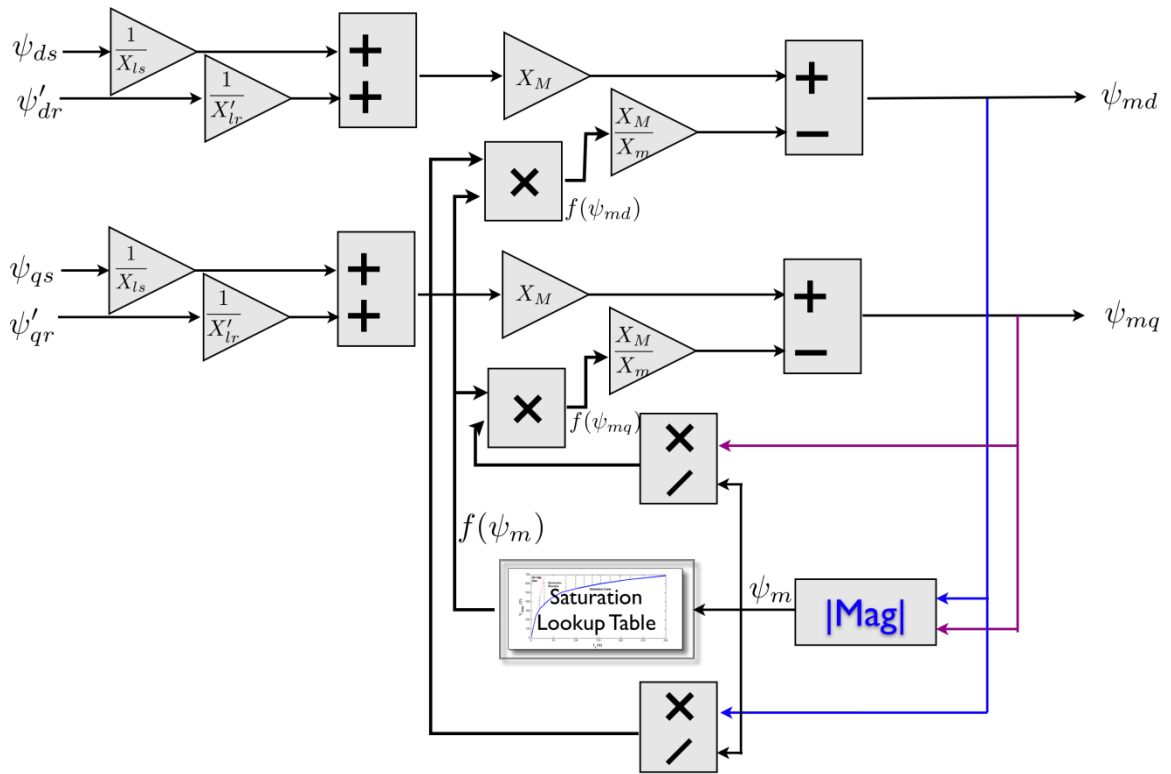


Figure 14: Simulink Block to Calculate Mutual Magnetic Flux Linkage with Saturation

Putting all the equations together for the induction motor model, the block diagram is described in Figure 15. The feedbacks are highlighted with blue, purple, and green arrows.

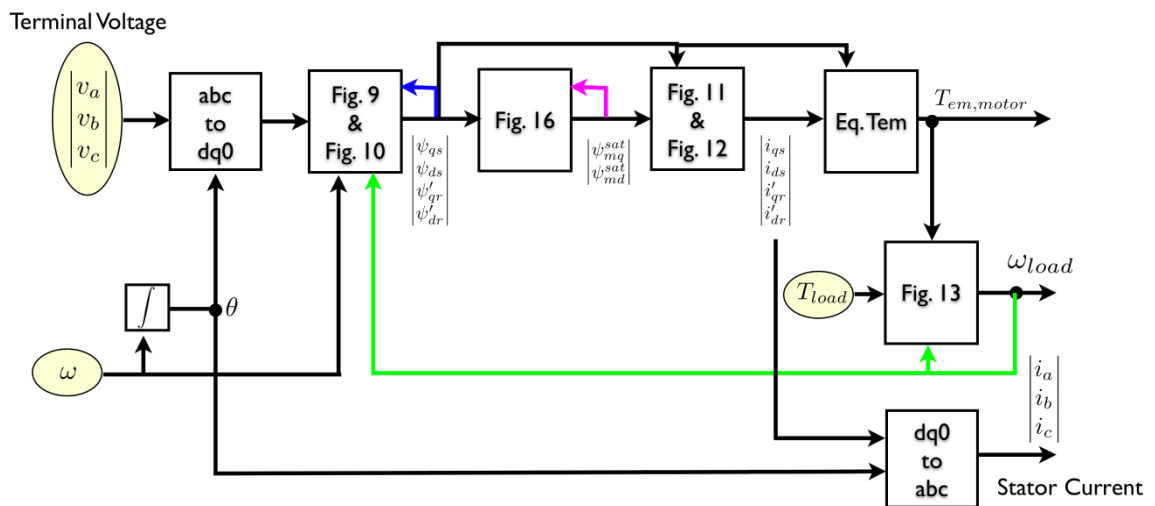


Figure 15: Block Diagram of the Overall Induction Motor

4. Diesel Engine and Speed Governor

Caterpillar Inc. provided the diesel engine and speed governor models and they are described in reference (Dilimot & Algrain, 2006). Only slight modifications are necessary to incorporate the provided model into the overall system model. The model is proprietary and must be described only in general. The general system of the diesel engine and speed-governor is shown in Figure 16. This model connected to the following voltage regulator and synchronous generator has been validated against measured data (Dilimot & Algrain, 2006).

The mechanical power, P_{mech} , of the system can be calculated by multiplying the mechanical torque and speed of the engine:

$$P_{mech} = T_{mech}\omega_{eng} \quad (\text{W}). \quad (\text{VII-19})$$

The torque balance equation is:

$$T_{eng} = T_{em} + J_{eng}\alpha + T_{losses} \quad (\text{N-m}). \quad (\text{VII-20})$$

The angle, α , of the engine shaft can be calculated from the torque differential between the mechanical torque and the torque of the electrical system, T_{em} , as well as any losses due to friction, T_{losses} , divided by the system inertia, J_{sys} . Since the engine speed is the integral of the angle it can be calculated as:

$$\omega_{eng} = \frac{1}{J_{sys}} \int (T_{eng} - T_{em} - T_{losses}) dt \quad (\text{rad/sec}), \quad (\text{VII-21})$$

where it is assumed the inertia is not changing. This operation is performed in the “Torque Balance” block of Figure 16. Other models that have been built are described in Appendix B.

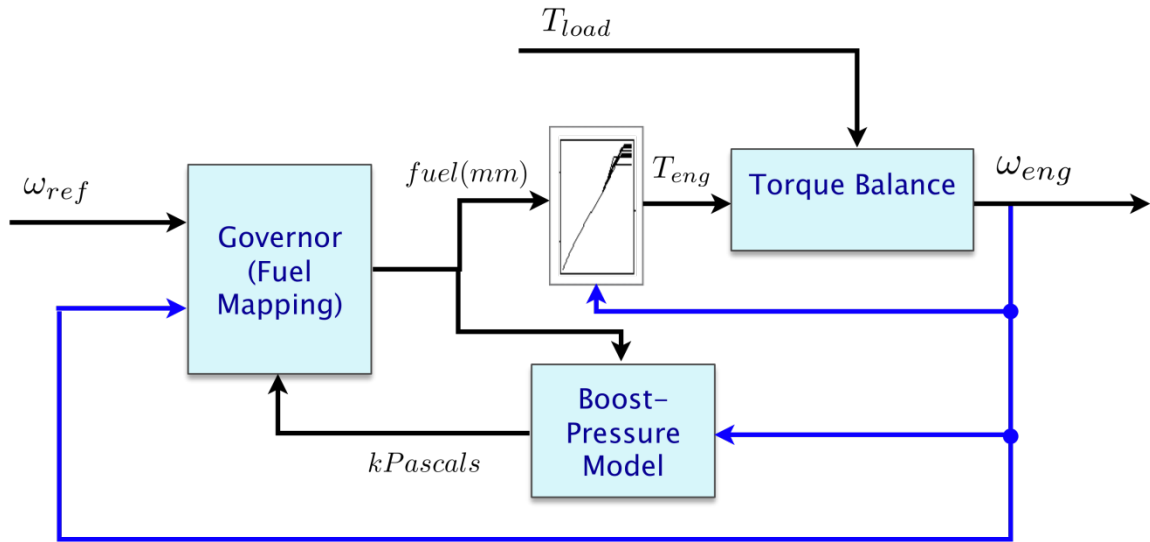


Figure 16: General Model of the Diesel Engine and Governor Controller

5. Excitation System

The model of the excitation system is based on model AC8B in (IEEE Std 421.5-2005, 2006). This excitation system is for an AC alternator with a digital PID (proportional-integral-derivative) automatic voltage regulator feeding a dc rotating exciter. The mathematical functional control block is shown in Figure 17 and the Simulink equivalent block in Figure 18. In Figure 17 the K_C and K_D parameters are zero, because only a digital voltage regulator based system is considered (IEEE Std 421.5-2005, 2006). The saturation of the exciter is modeled as a proportional value based on the full-load test. The inputs to the excitation system are the reference voltage, RMS terminal voltage as measured, and a stabilizer voltage, denoted V_{ref} , V_T , and V_{stab} , respectively. The difference is used to regulate the excitation voltage E_{FD} applied to the synchronous generator. The stability voltage is usually set to zero unless a Power System Stabilizer (PSS) is used. This model connected to the engine and governor and synchronous generator has been validated against measured data (Dilimot & Algrain, 2006).

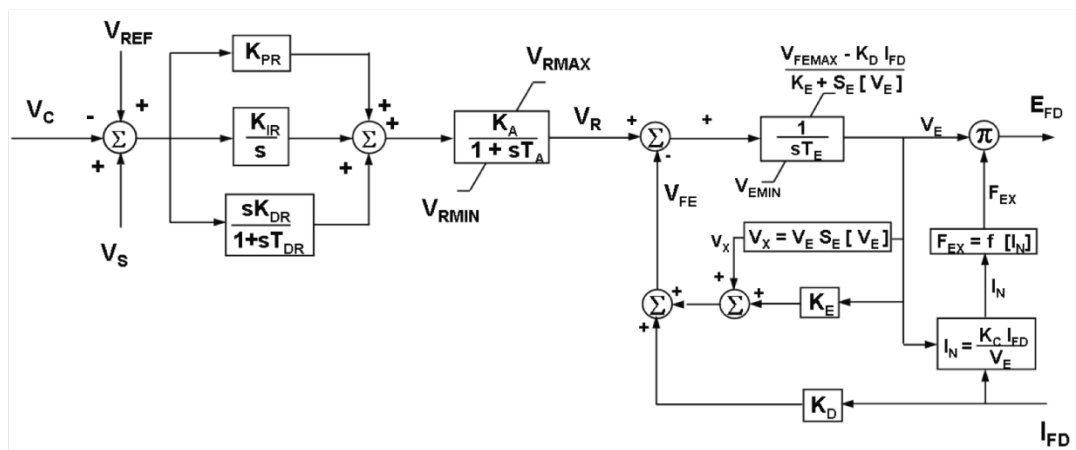


Figure 17: Functional Block Model of the AC8B Alternator-Rectifier Excitation System
 Reproduced from IEEE Standard 421.5 (2005) Figure 6-8, p. 15

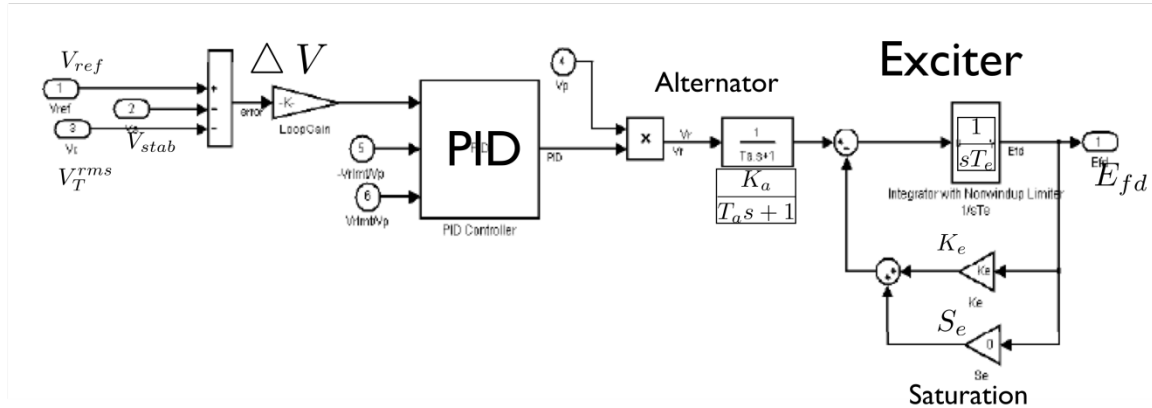


Figure 18: Simulink Block of the Automatic Voltage Regulator

5.1. Reference Voltage Setpoint

To achieve a volts per hertz regulator added to the PID regulator, a lookup table has been implemented that takes the engine speed as input and then interpolates the reference voltage. Figure 19 shows the trace of the lookup table. The under-frequency setpoint and the minimum voltage thresholds are shown for reference. The slope between the minimum voltage threshold and the reference voltage is a linear interpolation that keeps the volts per hertz of under frequency constant which helps the generator and engine recover from large load sets (Dilimot & Algrain, 2006).

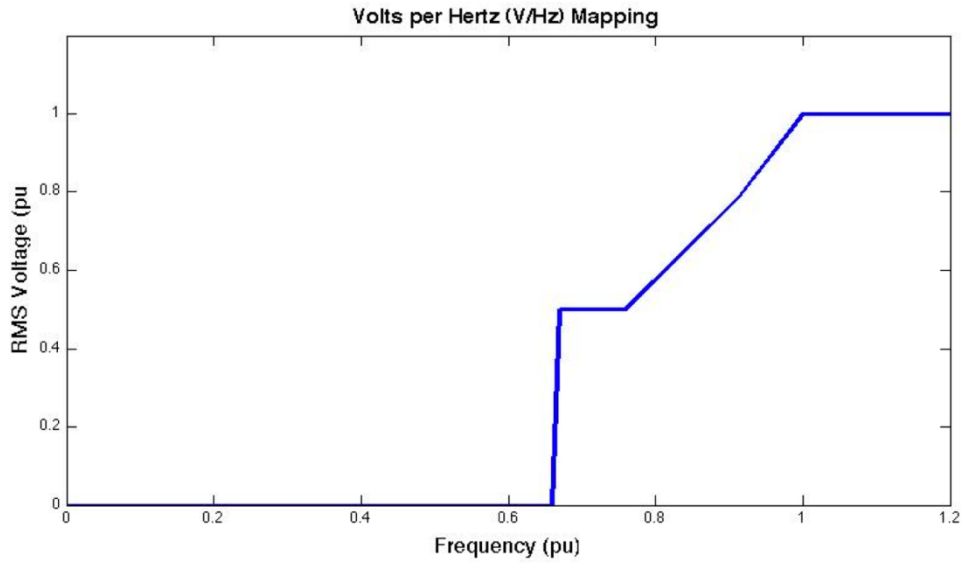


Figure 19: The Volts per Hertz Curve of the Reference Voltage Regulator

5.2. Power System Stabilizer

A power system stabilizer (PSS) is built based on the PSS1A model of (IEEE Std 421.5-2005, 2006), but it is not used in the resulting simulations. In general PSS are used to damp low frequency oscillations that are not the focus of the dynamic simulations of this thesis. The Simulink block of the PSS model is found in Figure 20. In the simulation presented the PSS has not been used.

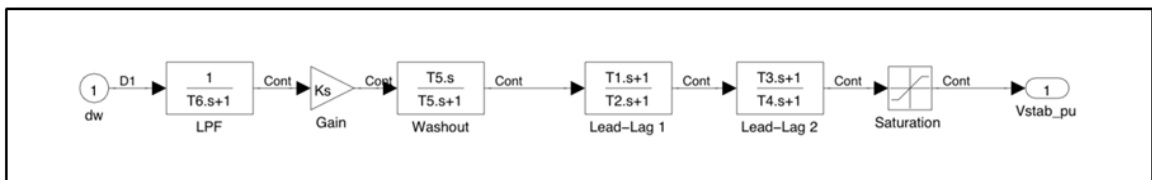


Figure 20: Power System Stabilizer (PSS1A)

6. Mechanical Load

The mechanical loads applied to the induction motor are simple models of fan and pump loads. The output speed of the induction motor, ω_{load} , is used as the input to calculate the applied torque. The first model is based on simply the square of the motor speed and a constant initial torque, T_{const} :

$$T_{load} = T_{const} + K\omega_{load}^2 \quad (\text{N-m}), \quad (\text{VII-22})$$

where, the coefficient K is calculated specifically to reach the rated torque of the mechanical load. Figure 21 displays the speed-torque curve associated with the first mechanical load of Equation (VII-22). The second model is based calculated using the equation:

$$T_{load} = T_0(1 - \omega_{load})^5 + T_{rated}\omega_{load}^2 \quad (\text{N-m}). \quad (\text{VII-23})$$

T_0 is the initial torque and T_{rated} is the rated torque of the attached mechanical load. The mechanical load of Equation (VII-23) should be more realistic for most mechanical loads and thus is the model used in the simulations and is to be assumed when referring to the mechanical load. Figure 22 displays the speed-torque curve associated with the mechanical load of Equations (VII-23). More mechanical loads have the dip characteristic shown as the 5th order term dominates at low speeds.

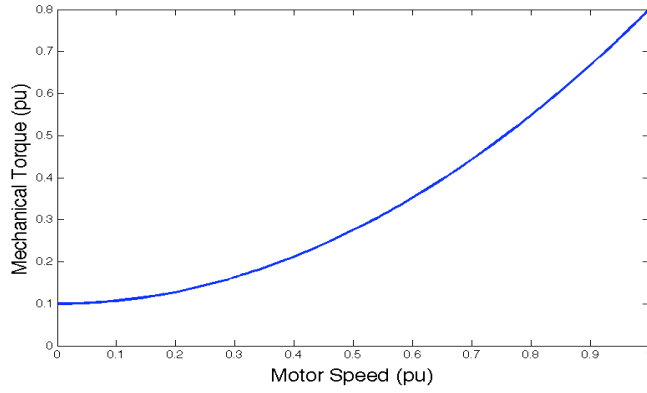


Figure 21: Speed-Torque Curve of Equation (VII-22)

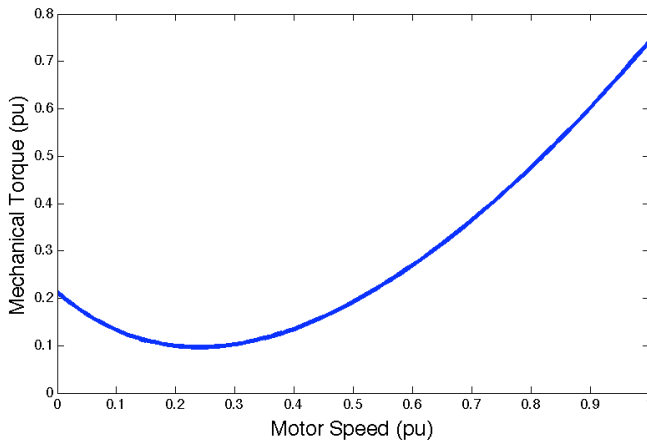


Figure 22: Speed-Torque Curve of Equation (VII-23)

7. Electrical System

It is appropriate to test the starters when connected to constant source, or infinite bus test, for baselining the starter performance as well as verifying the simulation. Figure 23 shows the Simulink model of this system with the major components labeled. Accordingly, the genset and induction motor coupled system is shown in Figure 24. In the next few sections we consider how to couple the generator and the induction motor electrical system together.

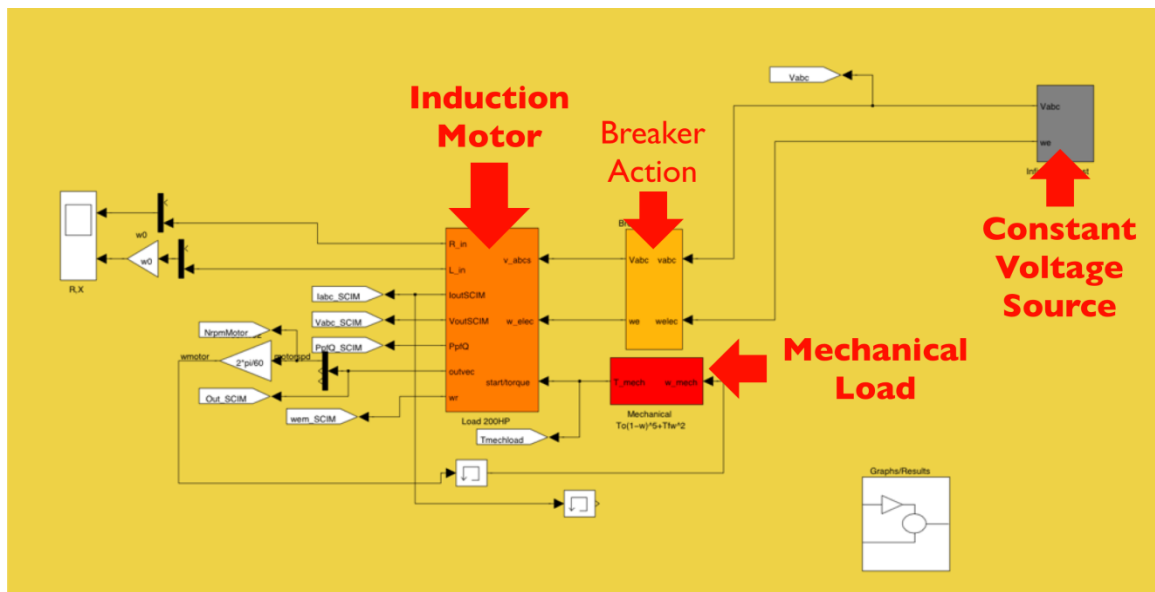


Figure 23: Simulink Infinite Source Test System Overview

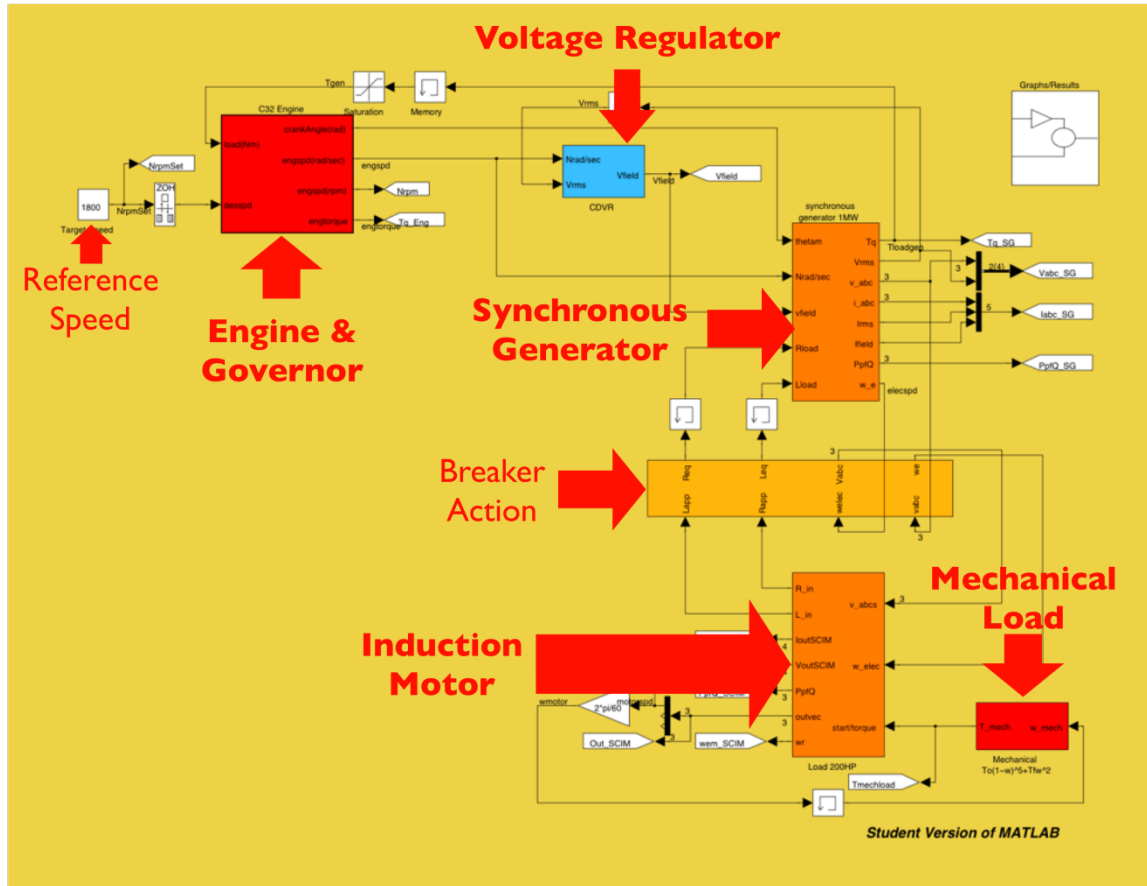


Figure 24: Simulink Genset System Overview

7.1. Calculating Equivalent Impedance

The common method of simulating an electrical system is to use the Jacobean matrix and perform a power flow analysis. The method taken in this system is to measure the voltage and current phasors at the point of connection to calculate the equivalent, apparent impedance as seen by the generator. The phasors used in the calculation are the voltage calculated from the generator model and the current calculated from the motor model. Since only balanced conditions are considered, the equation for calculating the impedance is:

$$\begin{aligned}
R_{app}^e &= \operatorname{Re} \left(\frac{\tilde{V}}{\tilde{I}} \right) = \frac{P}{|I_s|^2} = \frac{v_d^e i_d^e + v_q^e i_q^e}{\sqrt{(i_d^e)^2 + (i_q^e)^2}} \\
X_{app}^e &= \operatorname{Im} \left(\frac{\tilde{V}}{\tilde{I}} \right) = \frac{Q}{|I_s|^2} = \frac{v_q^e i_d^e - v_d^e i_q^e}{\sqrt{(i_d^e)^2 + (i_q^e)^2}}
\end{aligned} \tag{VII-24}$$

(Ω),

and

$$Z_{app}^e = R_{app}^e - j\omega_b L_{app}^e \tag{VII-25}$$

where the $|I_s|$ is the magnitude of the stator current. It is assumed here that the synchronous generator is performed in the synchronous reference frame, thus using the superscript e to denote the synchronous reference frame parameters. This direct measurement of the load impedance has been used in other types of applications including voltage stability analysis methods for load points and in relays (Vu & Novosel, 2001). This approach can be applied to this system because its apparent impedance can be used as feedback into the generator block calculation by adding the appropriate parameter to the stator equivalent circuit. However, it is necessary to take the RMS of values of the apparent impedance values to ensure stability when connected to the generator set model. This in turn causes the synchronous generator calculated stator response to lag the induction motor by about two cycles. However, this method allows the motor and generator internal parameters to be separate, so that different blocks can be used interchangeably. The equivalent dq circuit for the system as seen by the generator is shown in Figure 25. Future work will be to address the lag between the models with power balancing or other similar methods.

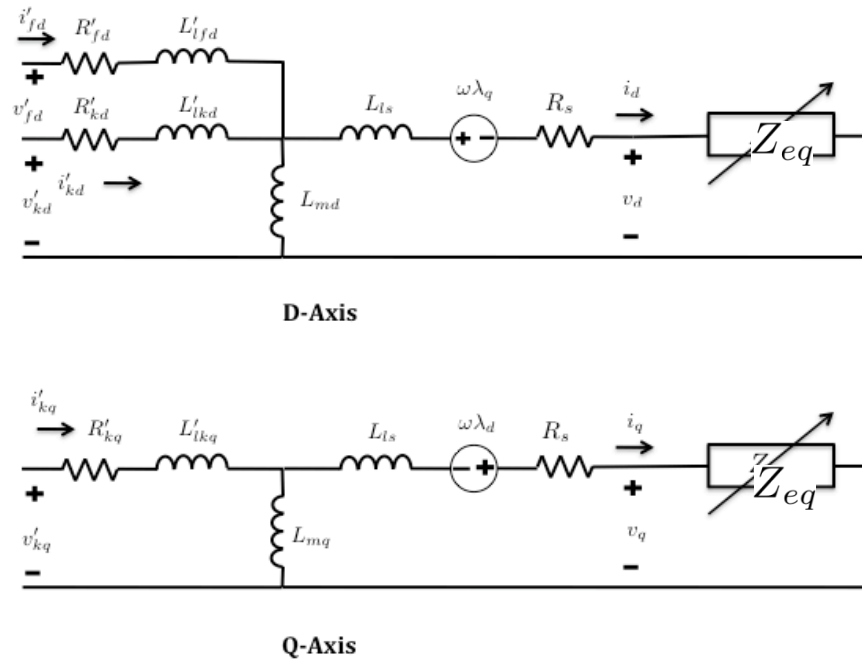


Figure 25: Equivalent Circuit of the Generator and Apparent Impedance

7.2. Equivalent Impedance Feedback to the Generator

To include the equivalent impedance of the network, the dynamic load, in the synchronous generator model the equivalent impedance must be added to the stator circuit. The equivalent impedance will depend on the network design. For example the equivalent impedance is the apparent impedance calculated at the motor for the DOL starting method, $Z_{eq} = Z_{app}$. Therefore, the calculation of the synchronous generator flux linkage derivatives must add the apparent impedances, and Equation (VII-5) of the synchronous generator model becomes:

$$\begin{aligned}
\begin{bmatrix} \frac{d}{dt} \lambda_q \\ \frac{d}{dt} \lambda_d \\ \frac{d}{dt} \lambda'_{fd} \\ \frac{d}{dt} \lambda'_{kd} \\ \frac{d}{dt} \lambda'_{kq} \end{bmatrix} &= \begin{bmatrix} v_q \\ v_d \\ v'_{fd} \\ 0 \\ 0 \end{bmatrix} - \begin{bmatrix} -(R_s + R_{eq}) & 0 & 0 & 0 & 0 \\ 0 & -(R_s + R_{eq}) & 0 & 0 & 0 \\ 0 & 0 & R_{fd} & 0 & 0 \\ 0 & 0 & 0 & R_{kd} & 0 \\ 0 & 0 & 0 & 0 & R_{kq} \end{bmatrix} \begin{bmatrix} i_q \\ i_d \\ i'_{fd} \\ i'_{kd} \\ i'_{kq} \end{bmatrix} \\
- \omega_r & \begin{bmatrix} 0 & -(L_d + L_{eq}) & L_{md} & L_{md} & 0 \\ (L_q + L_{eq}) & 0 & 0 & 0 & -L_{mq} \\ 0 & 0 & 0 & 0 & 0 \\ 0 & 0 & 0 & 0 & 0 \\ 0 & 0 & 0 & 0 & 0 \end{bmatrix} \begin{bmatrix} i_q \\ i_d \\ i'_{fd} \\ i'_{kd} \\ i'_{kq} \end{bmatrix} \quad (V).
\end{aligned} \tag{VII-26}$$

Also, the inductance matrix must include the apparent load stator impedance as well.

Thus, Equation (VII-6) of the synchronous generator model becomes:

$$\begin{bmatrix} \lambda_q \\ \lambda_d \\ \lambda'_{fd} \\ \lambda'_{kd} \\ \lambda'_{kq} \end{bmatrix} = \begin{bmatrix} -(L_q + L_{eq}) & 0 & 0 & 0 & L_{mq} \\ 0 & -(L_d + L_{eq}) & L_{md} & L_{md} & 0 \\ 0 & -L_{md} & L'_{fd} & L_{md} & 0 \\ 0 & -L_{md} & L_{md} & L'_{kd} & 0 \\ -L_{mq} & 0 & 0 & 0 & L'_{kq} \end{bmatrix} \begin{bmatrix} i_q \\ i_d \\ i'_{fd} \\ i'_{kd} \\ i'_{kq} \end{bmatrix} \quad (A). \tag{VII-27}$$

It is important to point out that if the values of effective stator inductances are near zero, which may occur for short transients, the currents are extremely large. This would mean that the load inductance and the source inductance are approximately equal and system is reaching instability because the power is not being balanced.

The functional calculation model of the synchronous generator model with the apparent impedance from the equivalent network load is the same as in Figure 5 except for the added apparent impedances to the stator resistance and inductance.

7.3. Cable Impedance

The cable impedance is modeled as a simple series resistance and reactance between the synchronous generator and the starter and induction motor. However, it is not used in

simulation tests. To calculate the AC voltage drop across the cable the loop equation is formulated as:

$$V_{gen} = Z_{line}I_s + V_{terminal} \quad (\text{V}), \quad (\text{VII-29})$$

where V_{gen} is the complex voltage from the generator source, Z_{line} is the line impedance, I_s , is the loop current, and $V_{terminal}$ is the voltage at the motor terminal (prior to any starting device). Solving for the $V_{terminal}$

$$V_{terminal} = V_{gen} - Z_{line}I_s \quad (\text{V}). \quad (\text{VII-30})$$

To perform this calculation the abc parameters are converted to the dq0 synchronous reference frame. It is assumed that there is no mutual resistance between the lines. Therefore, the conversion of the line impedance to the dq0 reference can be performed as is given for the resistive and inductive element change of variables from reference (Krause, Wasynczuk, & Sudhoff, 2002). For the line resistive element, the equivalent equation for the voltage drop, $R_{line}I_s$, from the line resistance in dq0 reference frame is:

$$\begin{bmatrix} v_d^R \\ v_q^R \\ v_0^R \end{bmatrix} = \begin{bmatrix} R_{line} & 0 & 0 \\ 0 & R_{line} & 0 \\ 0 & 0 & R_{line} \end{bmatrix} \begin{bmatrix} i_d \\ i_q \\ i_0 \end{bmatrix} \quad (\text{V}). \quad (\text{VII-31})$$

The R superscript denotes it is the resistance associated voltage drop. The line inductive element dq0 equation for the voltage drop, $jX_{line}I_s$, is calculated as:

$$\begin{bmatrix} v_d^L \\ v_q^L \\ v_0^L \end{bmatrix} = \omega \begin{bmatrix} 0 & -L_{line} & 0 \\ L_{line} & 0 & 0 \\ 0 & 0 & 0 \end{bmatrix} \begin{bmatrix} i_d \\ i_q \\ i_0 \end{bmatrix} + \frac{d}{dt} \begin{bmatrix} L_{line} & 0 & 0 \\ 0 & L_{line} & 0 \\ 0 & 0 & L_{line} \end{bmatrix} \begin{bmatrix} i_d \\ i_q \\ i_0 \end{bmatrix} \quad (\text{V}). \quad (\text{VII-32})$$

The L superscript denotes that the voltage is the reactance associated voltage drop. Adding these voltage drops produces the voltage drop across the line, $(R_{line}+jX_{line})I_s$, that

can then be subtracted from V_{gen} to produce $V_{terminal}$. The Simulink block implementing the line voltage drop effect is shown in Figure 26. The calculated voltage drop is then subtracted from the input voltage for the output voltage.

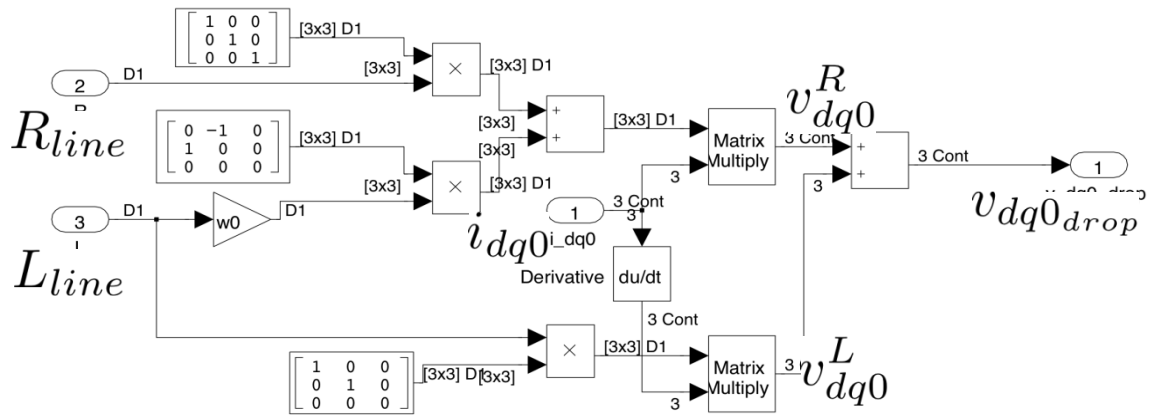


Figure 26: Line Equivalent dq0 Reference Frame Calculation of the Voltage Drop Across the Line

VIII. Motor Starter Simulation and Results

1. Starting Methods Implementation

All the starting methods are implemented in the synchronous reference frame so that the parameters can be directly implemented in the synchronous generator model. This will be assumed for all the equations in this section, and therefore the superscript symbol to denote each parameter in the synchronous reference frame is left off. The methods are all simulated in their ideal scenarios, in which no transients are seen during switching and the switching is instantaneous.

1.1. Direct-On-Line (DOL) Start

The DOL starting method does not add any additional components and can be implemented with a direct connection of the generator to the motor terminals as shown in Figure 27. The equivalent impedance is equal to the apparent impedance:

$$Z_{eq} = Z_{app} \quad (\Omega). \quad (\text{VIII-1})$$

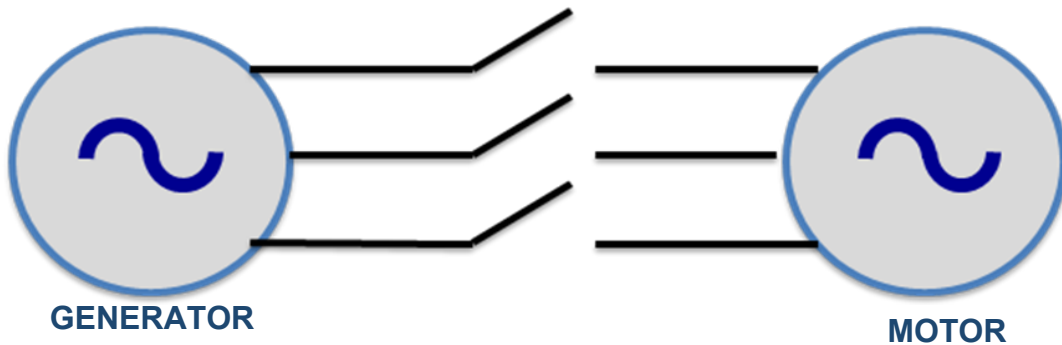


Figure 27: DOL Start Scheme

1.2. Shunt Capacitance

The shunt capacitor method can be used as a sole additional component or in conjunction with other starting methods. To implement the affect of the capacitor starting the equivalent impedance of the load is calculated as the apparent induction motor impedance in parallel with the capacitance, $Z_c = -jX_c$. The equivalent impedance is calculated:

$$Z_{eq} = Z_c // Z_{app} = \frac{Z_c Z_{app}}{Z_c + Z_{app}} \quad (\Omega). \quad (\text{VIII-2})$$

The implementation allows for the capacitors to be disconnected once a specified speed of the motor is reached. Figure 28 shows the method application on the electrical system.

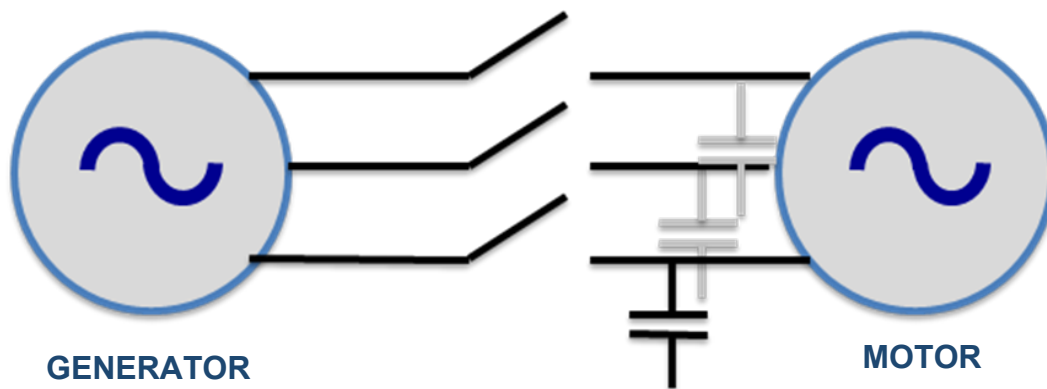


Figure 28: Shunt Capacitor Start Scheme

1.3. Star-Delta

To implement the star-delta starting method it is assumed that the terminals are connected in the star pattern initially and that the rated voltage is applied when in delta connection. For all other methods it is assumed that the rated voltage is applied regardless of the terminal connection pattern. A delta connected terminal voltage is approximately a

factor of the square root of three of the star connected voltage. In other words the star connected voltage is about 57% of the delta connected voltage or:

$$V_Y = V_{\Delta} / \sqrt{3} \quad (\text{V}). \quad (\text{VIII-3})$$

The implementation allows for the transition from star to delta connection to occur at a specified motor speed. Also, the application is performed simply as a scaling of the applied voltage. Figure 29 shows the method as applied to the electrical system.

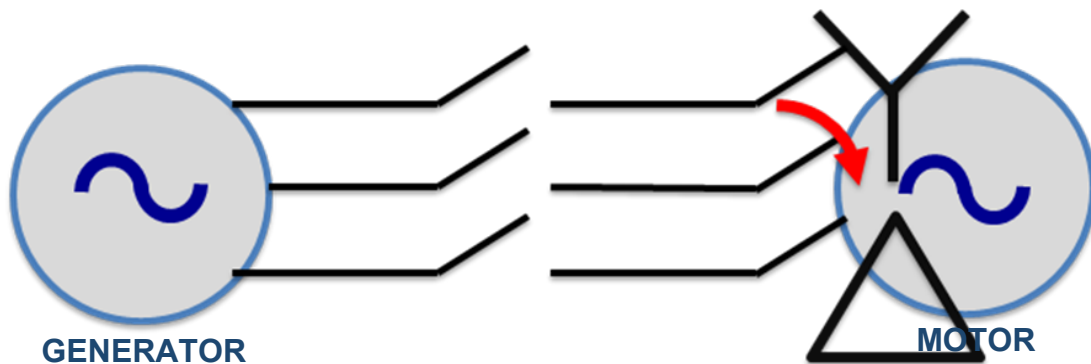


Figure 29: Wye-Delta Start Scheme

1.4. Autotransformer

The autotransformer is implemented in simulation by simply scaling the voltage according to the tap ratio. The voltage at the motor terminal V_T is a factor of the input source voltage V_{in} :

$$V_T = \eta_{tap\%} V_{in} \quad (\text{V}), \quad (\text{VIII-4})$$

where $\eta_{tap\%}$ is the tap ratio and is less than one. The implementation is performed in a manner that multiple taps can occur. The transitions of the taps are based on the motor speed.

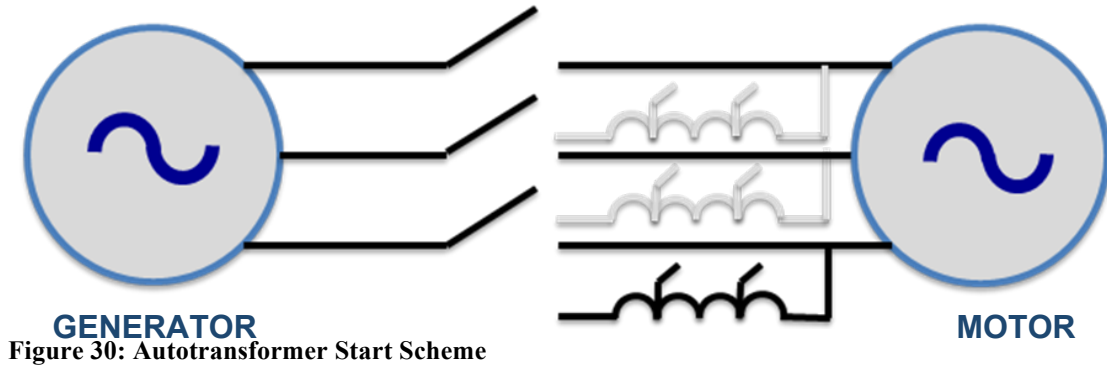


Figure 30: Autotransformer Start Scheme

1.5. Primary Resistance and Reactance

The series resistance or reactance, Z_p , can be added to the apparent motor impedance to simulate the primary resistance or reactance starting method. The equivalent impedance is therefore:

$$Z_{eq} = Z_p + Z_{app} \quad (\Omega). \quad (\text{VIII-5})$$

Also, the voltage drop or lag must be accounted for in the model by subtracting the impedance voltage drop across the series component from the supply voltage. The stator voltage at the motor side is calculated as:

$$V_{motor} = V_{supply} - Z_p I_{loop} \quad (\text{V}). \quad (\text{VIII-6})$$

Where, I_{loop} is the current in the generator and motor stator loop, as calculated at the motor. It can be noticed this is equivalent to the cable impedance calculation of section VII, and the implementation is the same as shown in Figure 26. Figure 31 shows the primary resistor or reactance starter scheme.

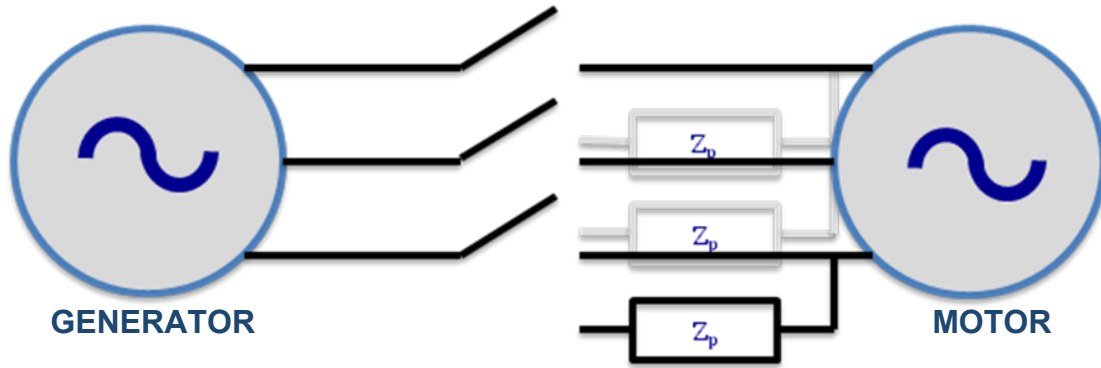


Figure 31: Primary Impedance Start Scheme

1. Studied Cases

The synchronous generator, diesel engine and speed-governor, and excitation system are all held constant for the system study. The synchronous generator is rated for 480 volts (line-to-line), 60 hertz, and a size of 1 MW. The associated parameters of the 200 HP and 500 HP induction motor can be found in Appendix D. The study focused on varying the size of the induction motor and the performance of the various starting methods that can be applied. The simulation characteristics of Simulink that the study is performed on are given in Appendix E. These characteristics include the time-step, solver, and so on. The induction motor models are based on parameters found in the literature, including (Krause, Wasynczuk, & Sudhoff, 2002) and (TransÉnergie Technologies Inc., 2003). The metrics gathered from the data for comparison are described in Table 2.

Table 2: Comparative Analysis Metric Descriptions

Metric	Description	Constant Source	Genset Source
Max Voltage Dip	Maximum voltage dip over the entire starting period.		✓
Max Inrush Current	Maximum instantaneous inrush current before 50% of rated speed is reached.	✓	✓
Average Inrush Current	Mean inrush current until full motor rated speed is reached.	✓	✓
Max Starting Torque	Maximum instantaneous electromagnetic motor torque before 50% of rated speed is reached.	✓	✓
Average Starting Torque	Mean starting torque until full motor rated speed is reached.	✓	✓
Max Frequency Dip	Maximum frequency dip over the entire starting period.		✓
Start Time	Time in seconds it takes to reach full motor rated speed.	✓	✓
Min Generator PF	Generator minimum power factor until full rated motor speed is reached.		✓

2. 200 HP Simulation Results

The first figure in this section, Figure 32, presents the DOL results of the constant source compared to the diesel-generator source. As can be seen from Figure 32 the results are comparable and verify the diesel-generator source application. Therefore, for the sake of brevity the other constant source connected starter results are not presented. Figures 33-37 show the results of the different implementations of the shunt capacitor, star-delta, autotransformer, primary resistance, and primary reactance starters, respectively. Each figure displays the voltage responses, current response, speed responses, motor torque response, real power responses, and reactive power responses, in six different traces. The traces start at 9 seconds into the simulation (after the generator is stable with no-load) and the traces stop at 20 seconds. The RMS currents, real and reactive powers are shown on two scales for the motor rating (left hand side) and the generator rating (right hand side of the traces). The simulated starter parameters used for the 200 HP induction motor are as follows:

- *Shunt Capacitor*: (A) 200 kVar and (B) 300 kVar; switched to direct at 0.97 rated motor speed
- *Star-Delta*: switched to direct at 0.97 rated motor speed
- *Autotransformer*:
 - (A) 50% voltage up to 0.3; 65% voltage up to 0.6; 80% voltage up to 0.97 rated motor speed, full voltage after 0.97 rated motor speed
 - (B) 50% voltage up to 0.5; 65% voltage up to 0.9; 80% voltage up to 0.97 rated motor speed, full voltage after 0.97 rated motor speed

(C) 65% voltage up to 0.9; 80% voltage up to 0.97 rated motor speed, full voltage after 0.97 rated motor speed

- *Primary Resistance:* (A) 0.20Ω and (B) 0.05Ω up to 0.97 rated motor speed, full voltage after 0.97 rated motor speed
- *Primary Reactance:* (A) $j0.20 \Omega$ and (B) $j0.05 \Omega$ up to 0.97 rated motor speed, full voltage after 0.97 rated motor speed.

1.6. 200 HP Genset Source Results

1.6.1. Direct-On-Line (DOL) Start

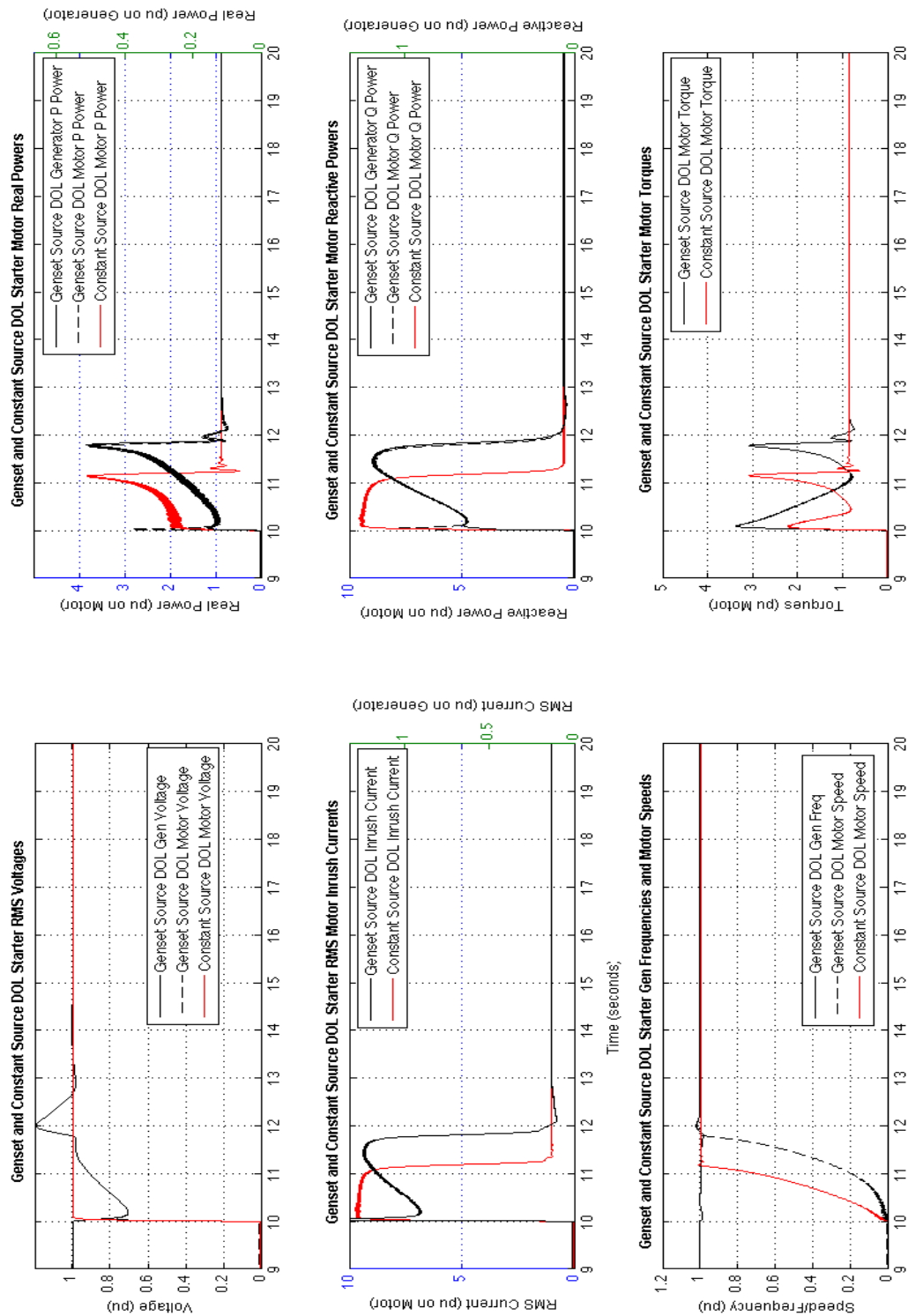


Figure 32: Genset and Constant DOL Starter Results for the 200 hp Motor

1.6.2. Shunt Capacitor Start

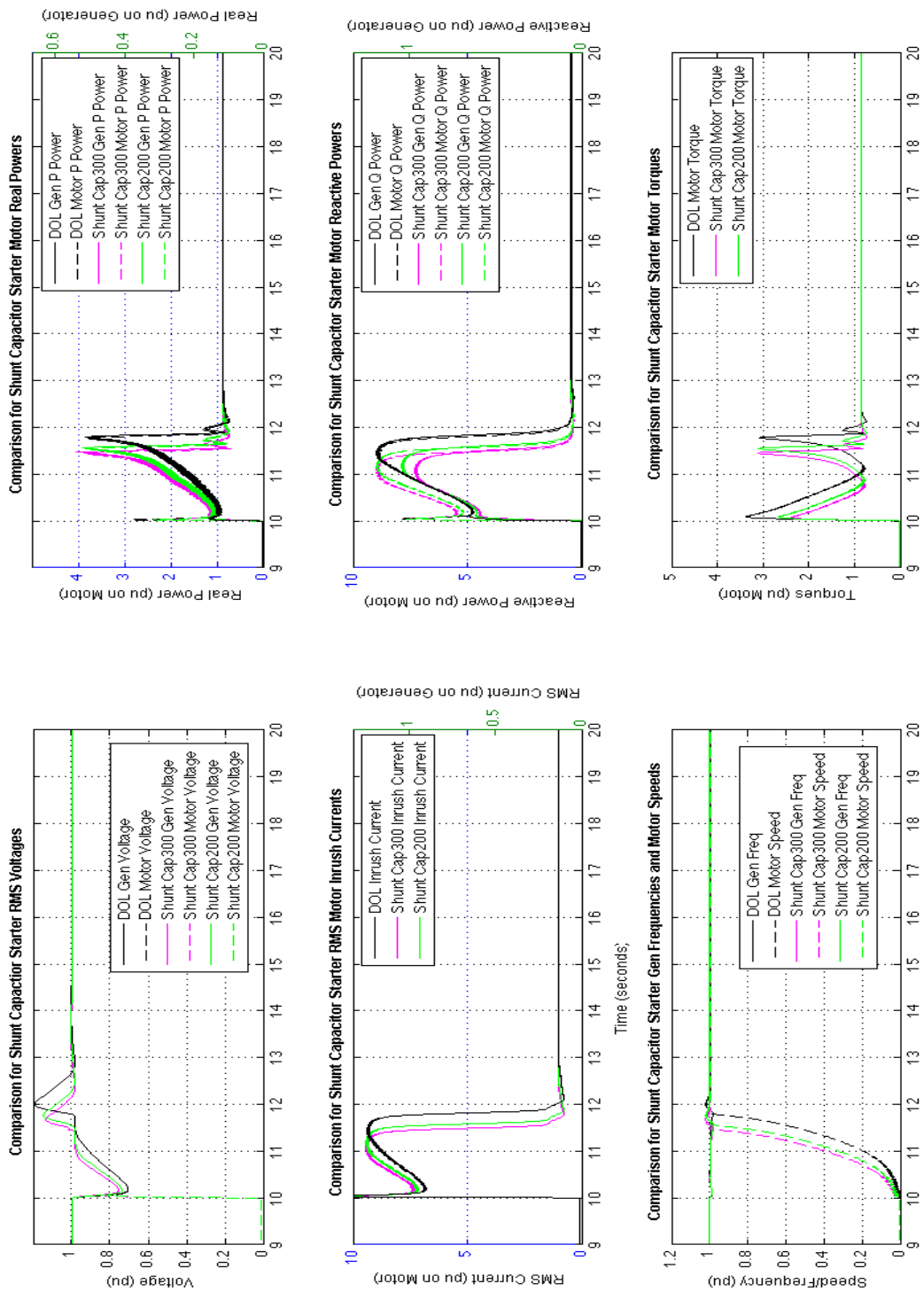


Figure 33: Genset Shunt Capacitor Starter Results for the 200 HP Motor

1.6.3. Star-Delta Start

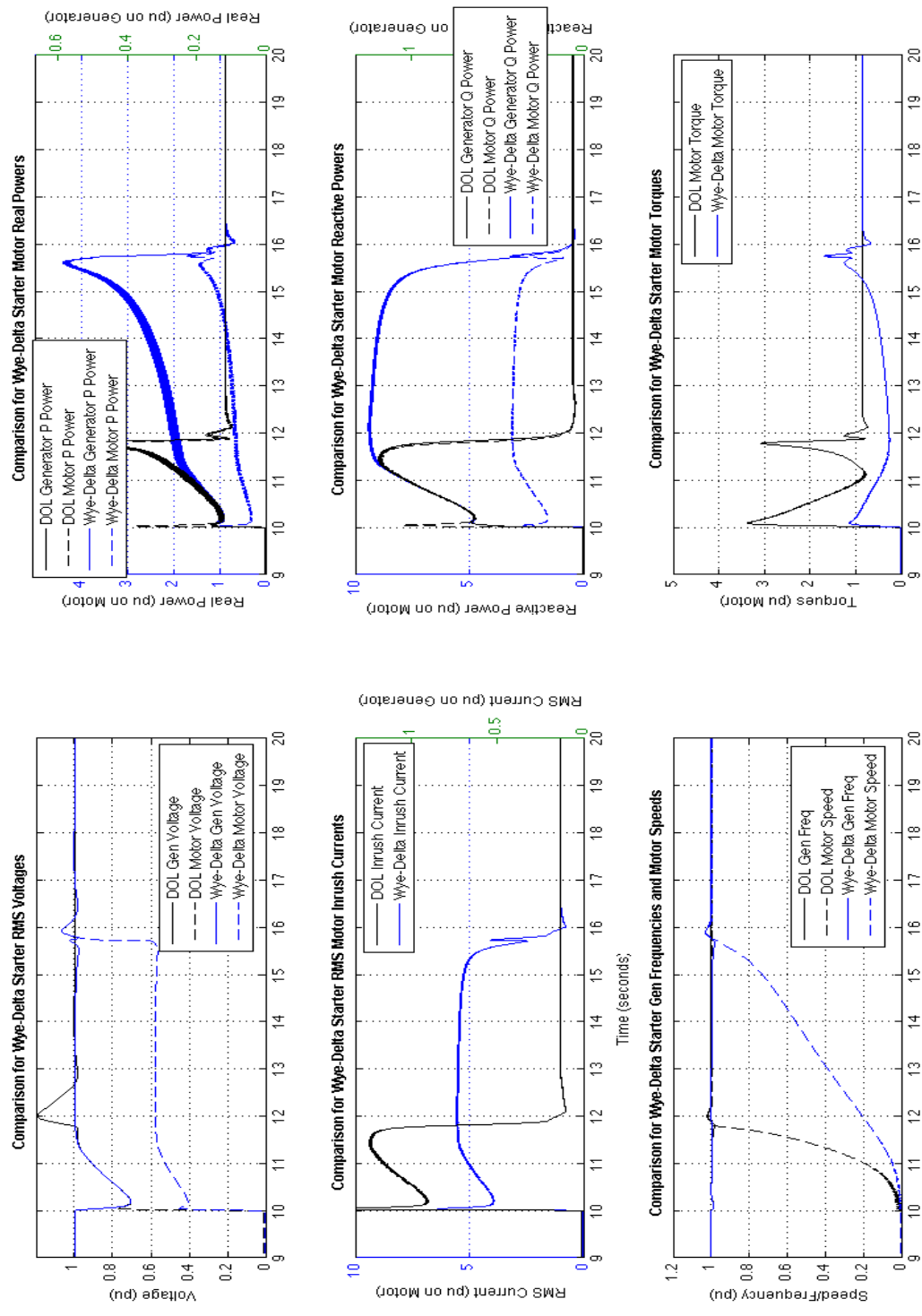


Figure 34: Genset Star-Delta Starter Results for the 200 HP Motor

1.6.4. Autotransformer Start

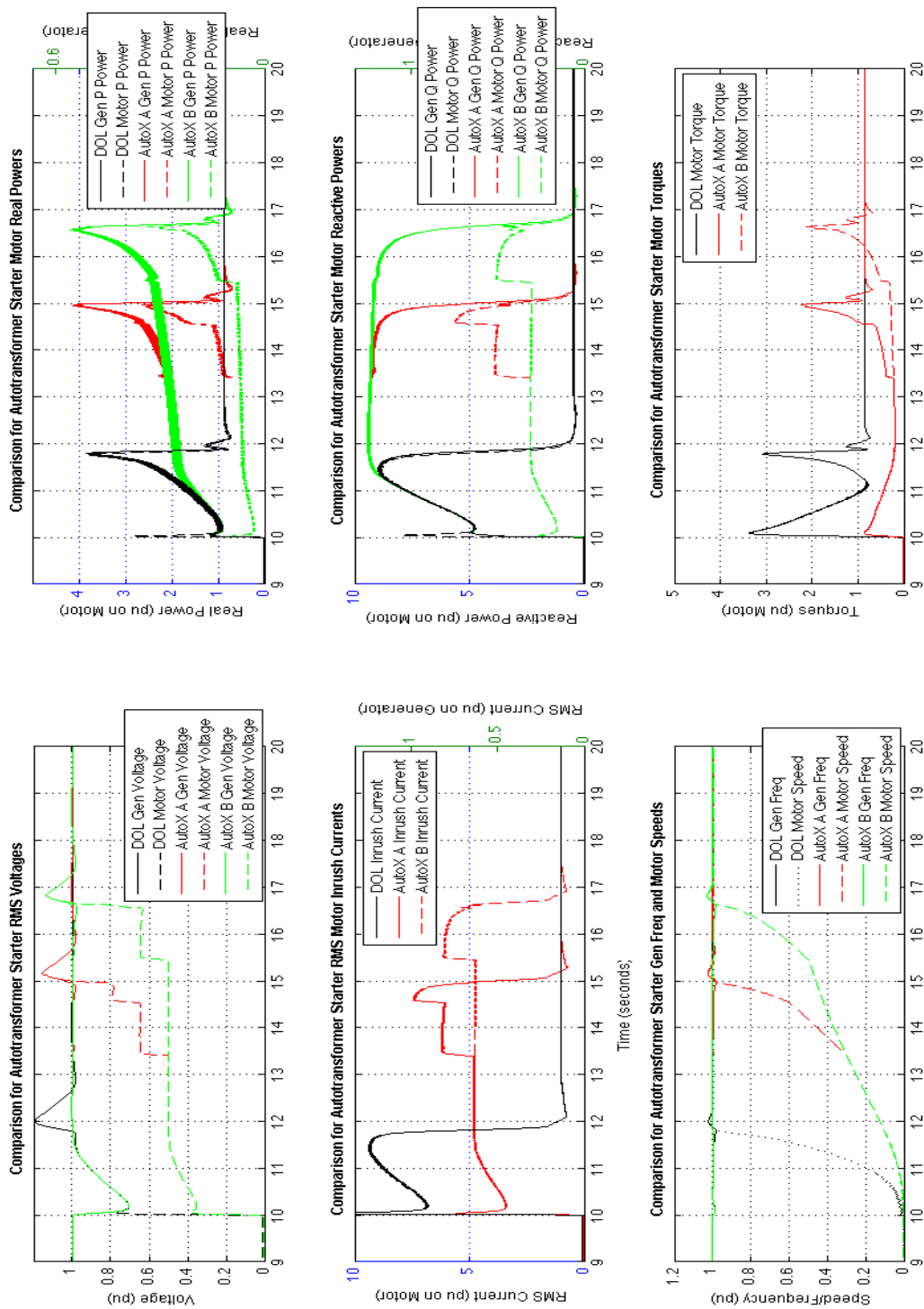


Figure 35: Genset Autotransformer Starter Results for the 200 HP Motor

1.6.5. Primary Resistance Start

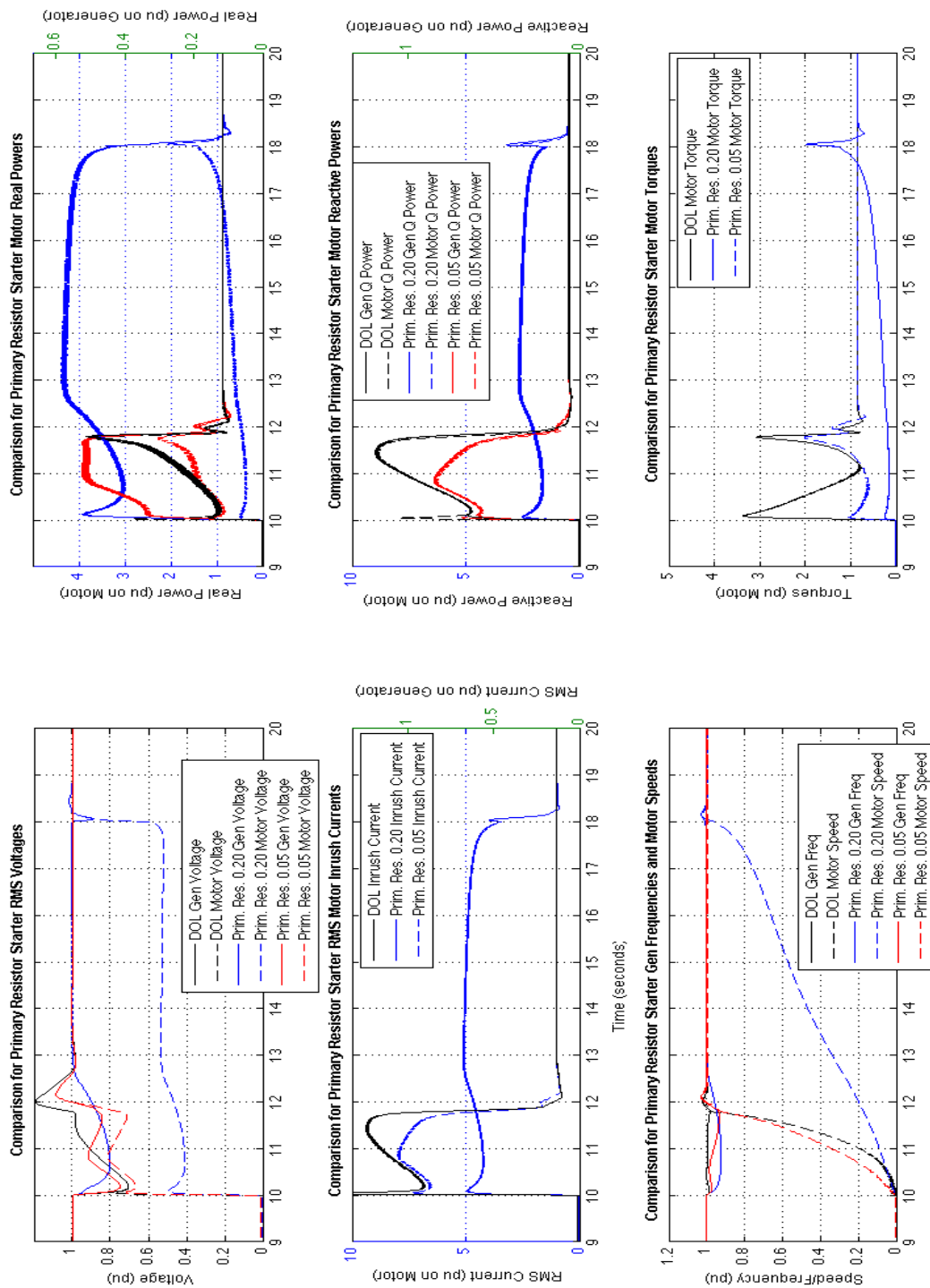


Figure 36: Genset Primary Resistance Starter Results for the 200 HP Motor

1.6.6. Primary Reactance Start

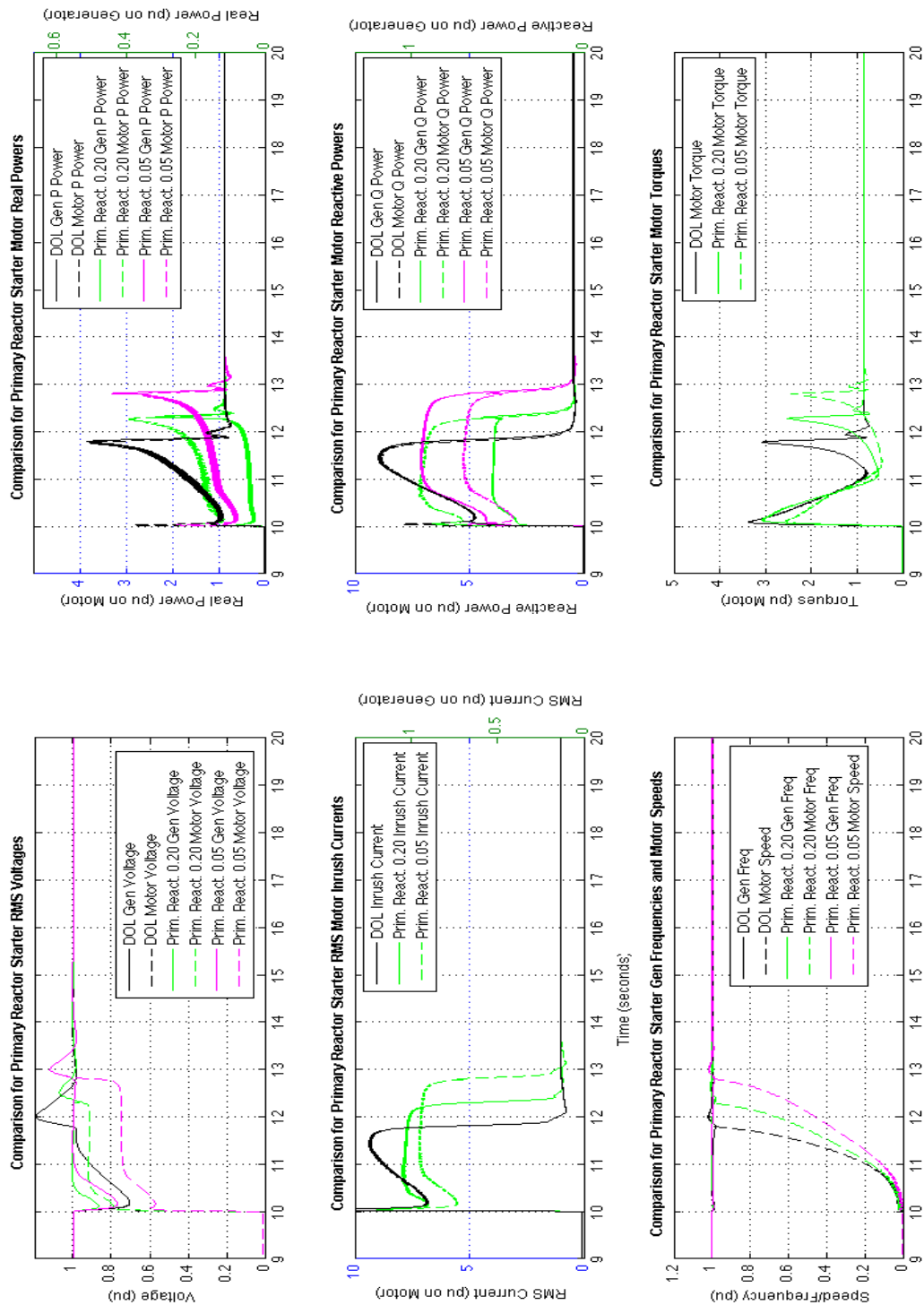


Figure 37: Genset Primary Reactance Starter Results for the 200 HP Motor

1.7. 200 HP Performance Summary

The constant and genset sources are compared in Figure 32. The voltage (top left) and current (middle left) both decrease initially for the genset start, which indicates that power during this initial startup is decreased. Comparing the real and reactive powers in the top right and middle right, respectively, they confirm that the powers dip for the genset start. Due to the real power and torque (bottom right) for the genset start the time to rated speed is decreased as can be seen in the bottom left. Also, we can see that the genset controls respond to the dip after approximately 1.5 seconds. At this point the voltage is approximately nominal and the current peaks at the same value it did for the constant source. These results correspond well to the information gathered in the literature review. Therefore, they provide some verification, and the rest of the constant source results are not shown.

The shunt capacitor start is shown in Figure 33. As can be expected, the voltage dip and time recovery (top left) as well as the decreasing of the reactive power (middle right) are improved. Also, note that since the recovery is improved the time to rated speed (bottom left) is faster than for the DOL start. The star-delta and autotransformer results are shown in Figures 34 and 35. These direct proportional voltage reduction methods, as discussed previously, reduce both the current (middle left) and torque (bottom right) with the voltage (top left). The real and reactive powers (top and middle right) are reduced significantly from the generation to the motor. The time to reach rated speed (bottom left) is significantly increased. It does not appear that the voltage reduction performs better for multiple tap changes. A possible approach to using an autotransformer would be to

determine either the highest rated current or the minimum torque that can be applied and determine the voltage level accordingly.

The primary resistance and reactance starters are shown in Figures 36 and 37, respectively. For the primary resistance the voltage applied to the motor (top left) is decreased for both the high and low resistances. However, the high resistance causes a significant decrease much similar to the star-delta or autotransformer starters, but one important difference is that the real power supplied by the generator is much larger because of the power loss to the resistance. The primary reactance moderately improves the voltage support (top left), the inrush current (middle left), and the efficiency through decreasing the reactive power support (middle right) for both the higher and lower reactances.

Figures 38, 39, and 40 compare the responses of the starter results discussed. The inrush currents, generator voltages, and generator frequency are shown in Figure 38, while motor speed, generator electromagnetic torque, and motor inrush electromagnetic torque are shown in Figure 39. The mechanical load, motor, and generator torques are shown in Figure 40.

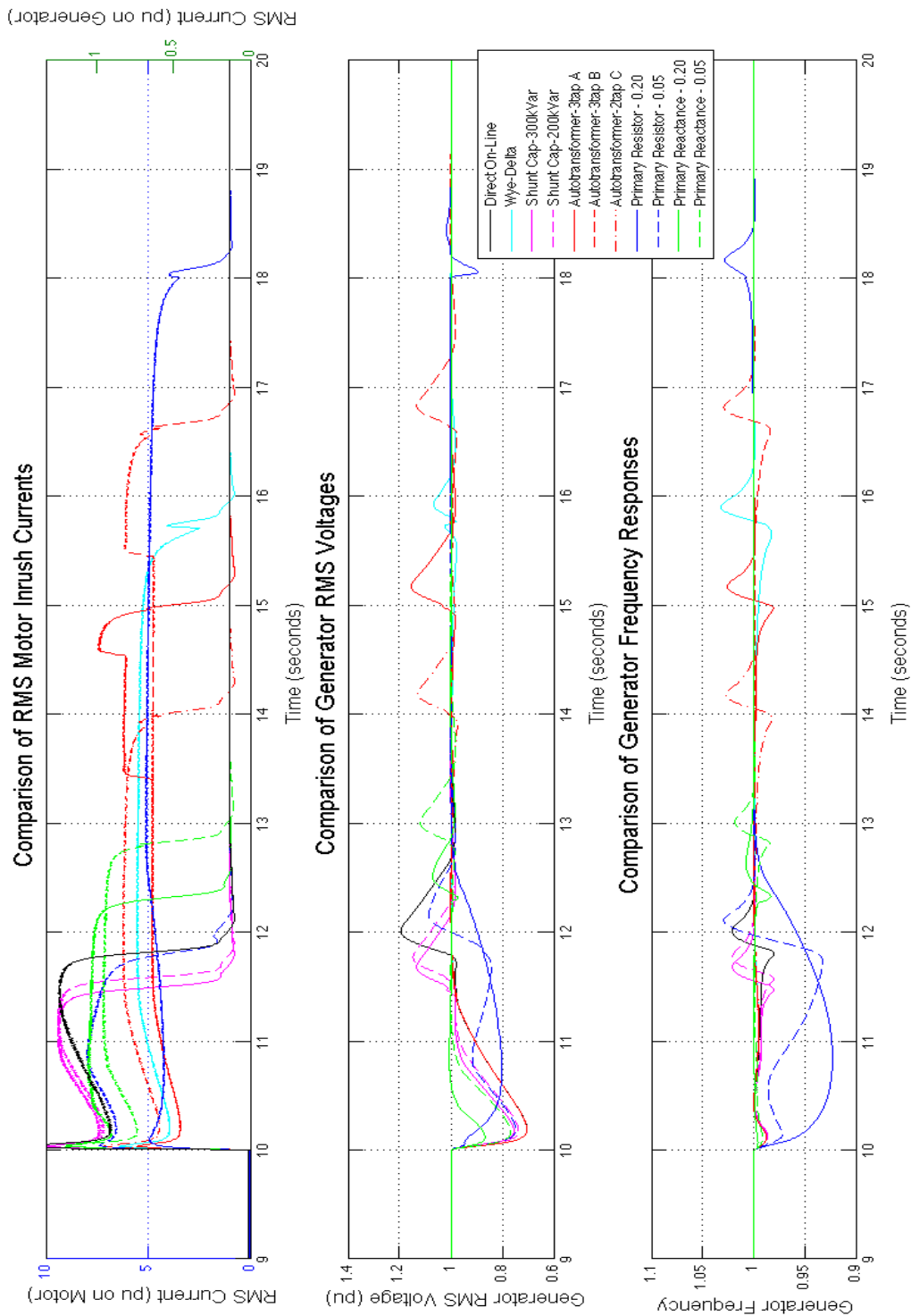


Figure 38: Comparison of All Genset Source Results for Inrush Current, Generator Voltage, and Generator Frequency for the 200 HP Motor

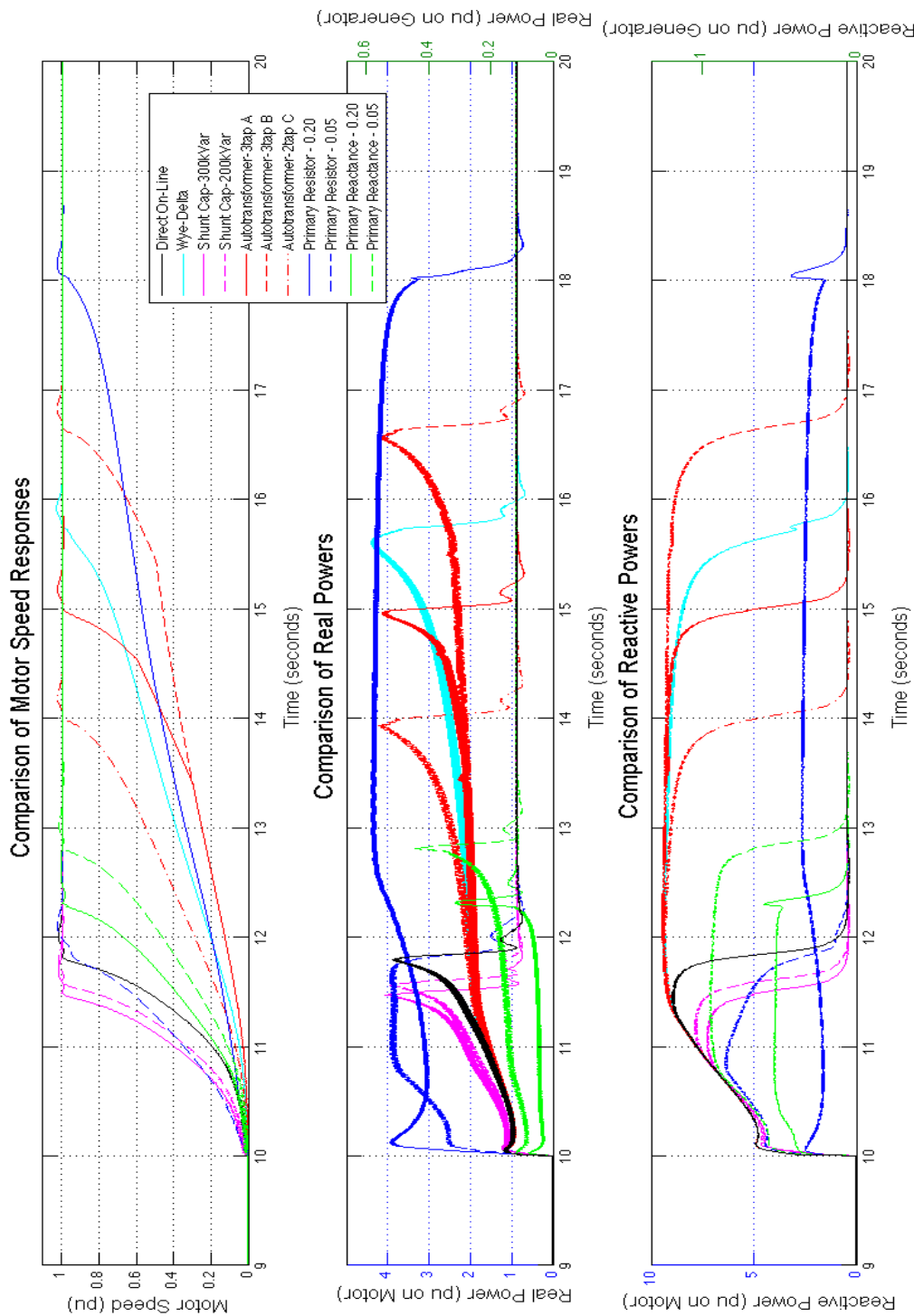


Figure 39: Comparison of All Genset Source Results for Motor Speed, Generator Real and Reactive Powers for the 200 HP Motor

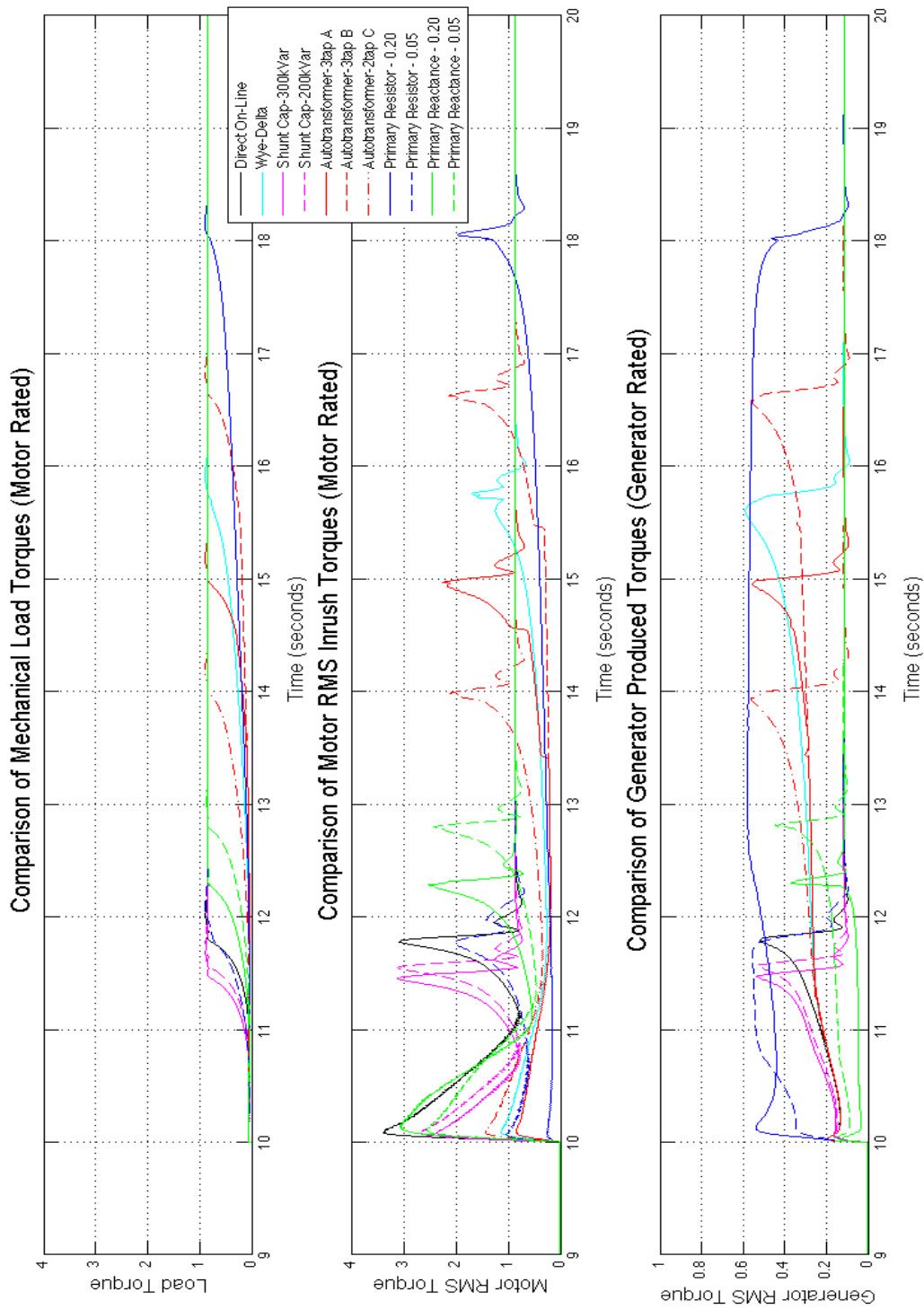


Figure 40: Comparison of All Genset Source Results for Load Mechanical Torque, Inrush Torques, and Generator Torques for the 200 HP Motor

The Figures 38, 39 and 40 can be used to compare the responses of the motor and generator to conclude general trends that each of the starter produces. Most of the results have been discussed from the results shown in Figures 33-37. The metrics from Table 2 column 2 for each of the starter methods is listed in Table 3. A general analysis of the results is given in the Summary and Conclusion section IX, but in general the results agree with the discussion in the Literature Review section VI. All the voltage reduction methods are able to have achieved current reduction as shown in Figure 38 (top). The shunt capacitor and primary reactance starters can be used to improve voltage and reactive power support in Figure 38 (middle) and Figure 39 (bottom), respectively. However, the shunt capacitor starter continues to consume more real power versus the primary reactance starter in as shown in Figure 39 (middle). The primary resistance starter consumes significantly more real power as shown in Figure 39 (middle). It also significantly increases the voltage dip as shown in Figure 38 (bottom), which is a very negative impact. This is related to the longer time it takes for voltage recovery as shown in Figure 38 (middle), although the voltage does not experience as significant decrease as in the DOL start.

The sizing of the shunt capacitor, primary resistance, and primary reactance starters are important to take into consideration to achieve the best benefit and tradeoffs of each method. The shunt capacitor should also be able to be used in conjunction with other methods to improve voltage support. The voltage reduction methods can be used to achieve current reduction as long as the acceleration time can last longer and therefore, although at a decreased level, the current is still exceeding the rated current but now for a longer period of time.

Table 3: Starter Metrics for 200 HP Induction Motor Results

Starter Method	Max Voltage Dip	Max Freq. Dip	Max Inrush Current	Average Inrush Current	Max Starting Torque	Average Starting Torque	Start Time	Min Gen PF
DOL	-29.7%	-2.0%	1111.0%	831.0%	375.0%	191.0%	1.80	0.18
Y-Delta	-29.6%	-1.8%	641.5%	516.0%	126.4%	60.2%	5.74	0.18
Cap 200 kVar	-26.3%	-2.0%	1021.1%	848.2%	296.8%	169.2%	1.56	0.21
Cap 300 kVar	-24.6%	-2.0%	986.9%	856.2%	263.4%	160.4%	1.47	0.23
AutoX A	-29.6%	-1.9%	621.0%	507.4%	94.9%	52.9%	4.98	0.18
AutoX B	-29.6%	-1.6%	555.6%	481.5%	94.9%	46.0%	6.64	0.18
AutoX C	-29.6%	-1.7%	722.2%	577.6%	159.9%	76.5%	4.00	0.18
Prim Resist .20	-19.9%	-7.7%	512.4%	474.9%	38.1%	43.0%	8.04	0.37
Prim Resist .05	-25.1%	-6.7%	799.0%	675.8%	116.0%	103.4%	1.96	0.32
Prim React.20	-13.3%	-1.7%	906.2%	760.4%	341.5%	154.8%	2.30	0.69
Prim React.05	-23.1%	-1.6%	906.9%	682.0%	284.9%	125.6%	2.80	0.14

2. 500 HP Simulation Results

The first figure in this section, Figure 41, presents the DOL results of the constant source compared to the diesel-generator source. As can be seen from Figure 41 the results are comparable and verify the diesel-generator source application. Therefore, for the sake of brevity the other constant source connected starter results are not presented. Figures 42-46 show the results of the different implementations of the shunt capacitor, star-delta, autotransformer, primary resistance, and primary reactance starters, respectively. Each figure displays the voltage responses, current response, speed responses, real power responses, reactive power, and motor torque responses, in six different traces. As can be expected, the simulation of the 500 HP induction motor required different implementations of the starters to meet the greater supplied torque for the same nominal voltage. Note that the figures have an additional 10 seconds (the traces start at 9 seconds and the traces stop at 30 seconds). The RMS currents, real and reactive powers are shown on two scales for the motor rating (left hand side) and the generator rating (right hand side of the traces). The simulated starter parameters used the 500 HP induction motor are as follows:

- *Shunt Capacitor*: (A) 200 kVar and (B) 400 kVar; switched to direct at 0.9 rated motor speed
- *Star-Delta*: switched to direct at 0.9 rated motor speed
- *Autotransformer*:
 - (A) 50% voltage up to 0.1; 65% voltage up to 0.2; 80% voltage up to 0.5 rated motor speed, full voltage after 0.5 rated motor speed
 - (B) 65% voltage up to 0.1; 65% voltage up to 0.2; 80% voltage up to 0.5 rated

motor speed, full voltage after 0.5 rated motor speed

(C) 65% voltage up to 0.1; 80% voltage up to 0.5 rated motor speed, full voltage after 0.5 rated motor speed

- *Primary Resistance:* (A) 0.05Ω and (B) 0.01Ω up to 0.9 rated motor speed, full voltage after 0.9 rated motor speed
- *Primary Reactance:* (A) $j0.05 \Omega$ and (B) $j0.01\Omega$ up to 0.9 rated motor speed, full voltage after 0.9 rated motor speed.

2.1. 500 HP Genset Source Results

2.1.1. Direct-On-Line (DOL) Start

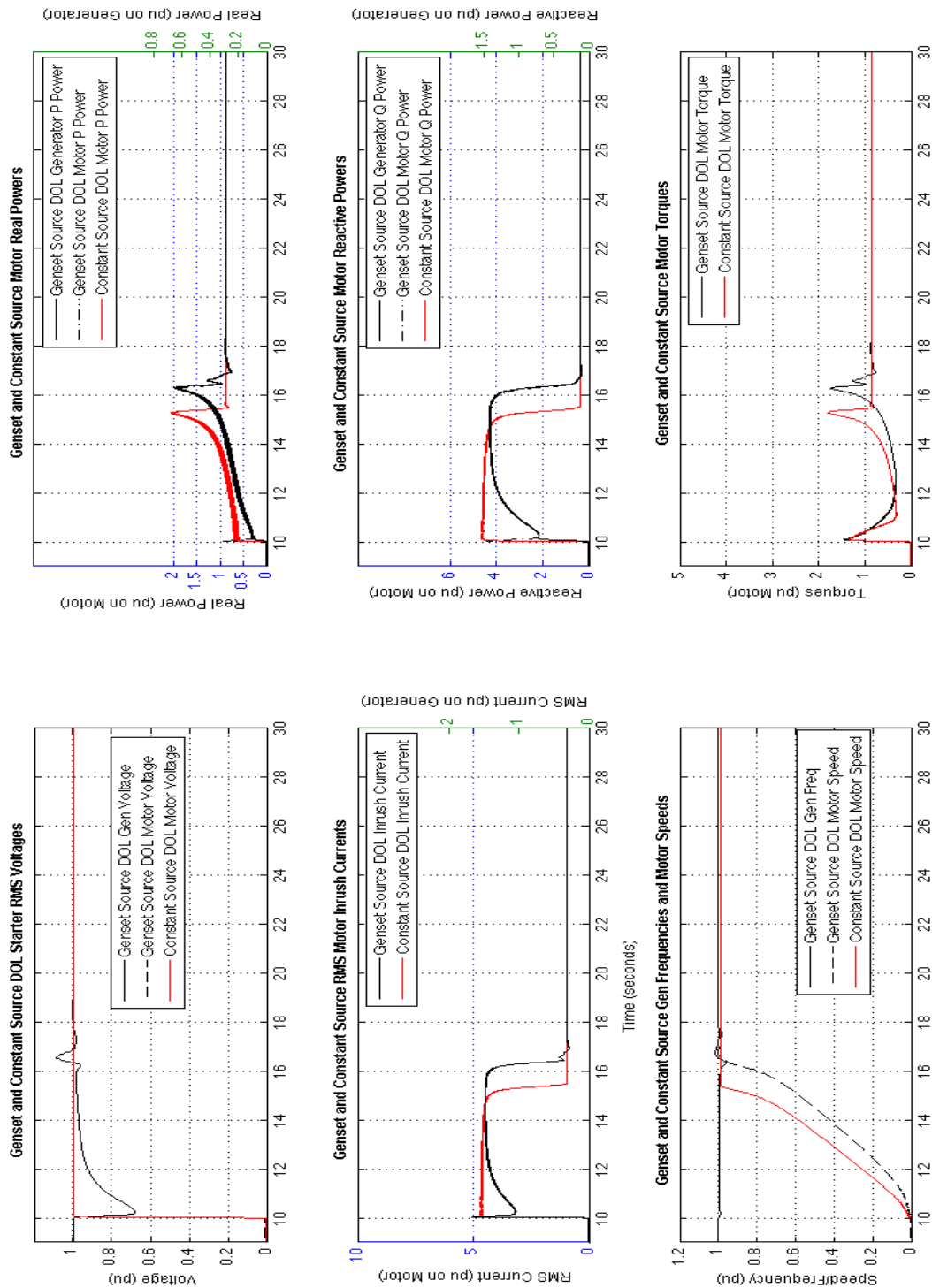


Figure 41: Genset and Constant DOL Starter Results for the 500 HP Motor

2.1.2. Shunt Capacitor Start

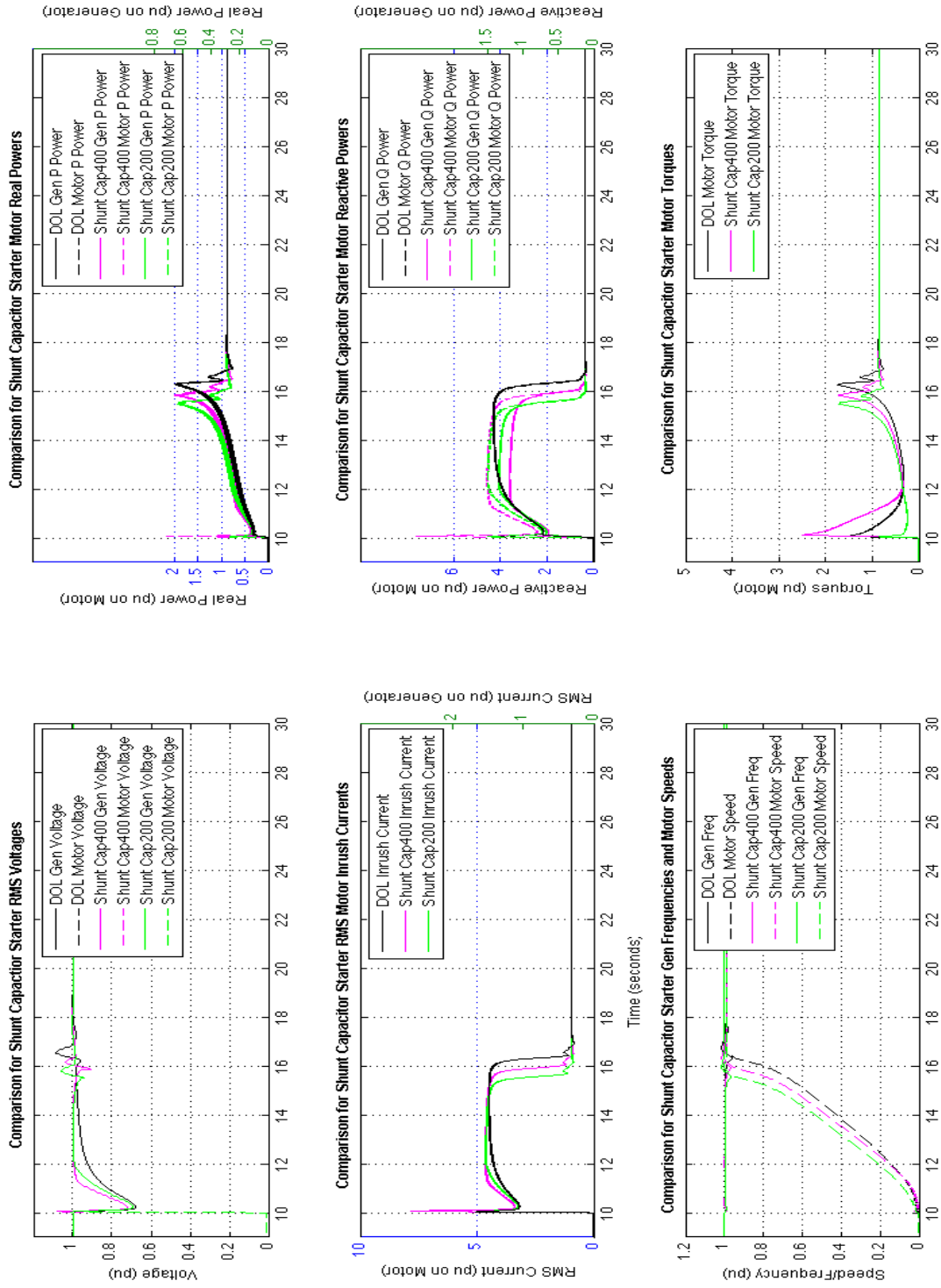


Figure 42: Genset Shunt Capacitor Starter Results for the 500 HP Motor

2.1.3. Star-Delta Start

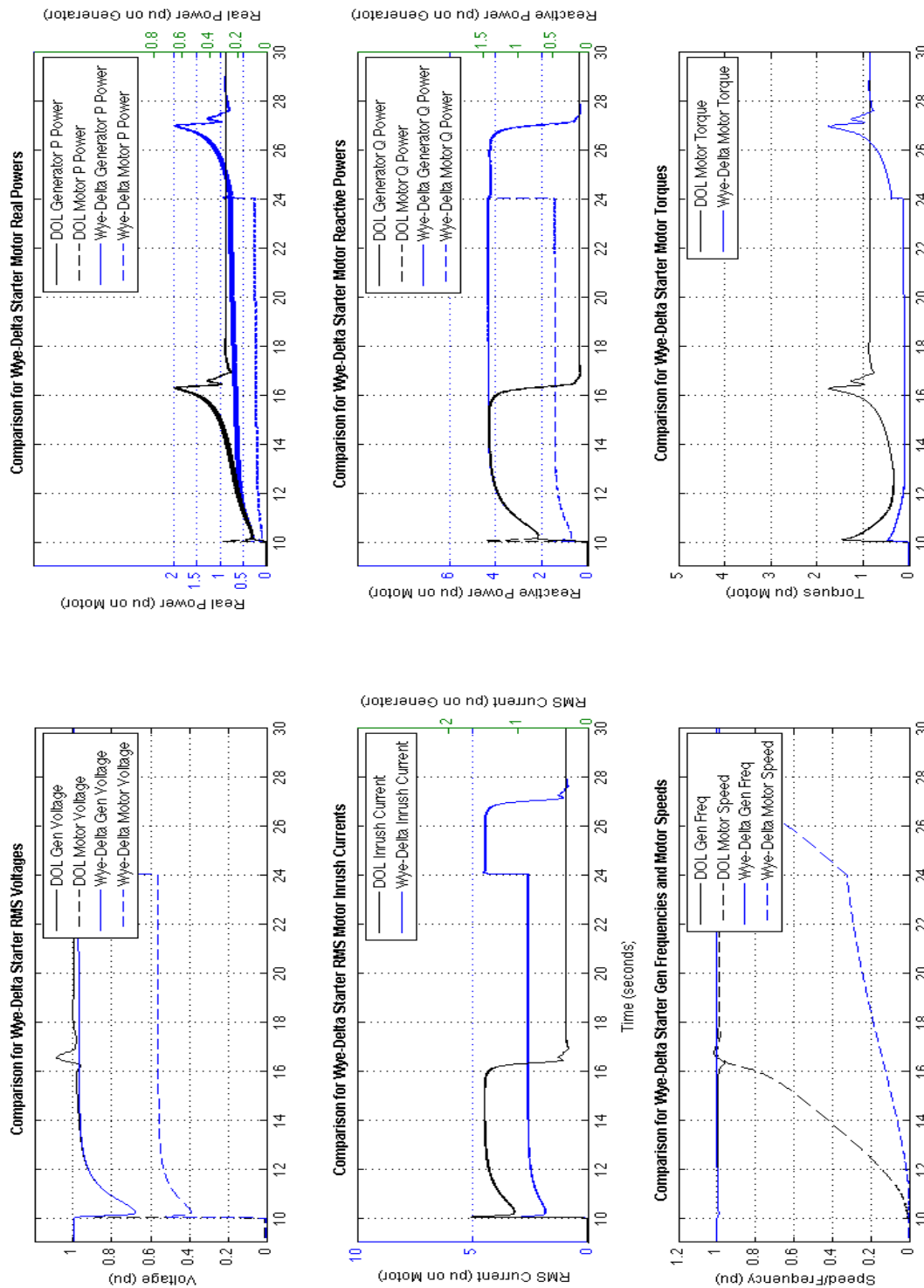


Figure 43: Genset Star-Delta Starter Results for the 500 HP Motor

2.1.4. Autotransformer Start

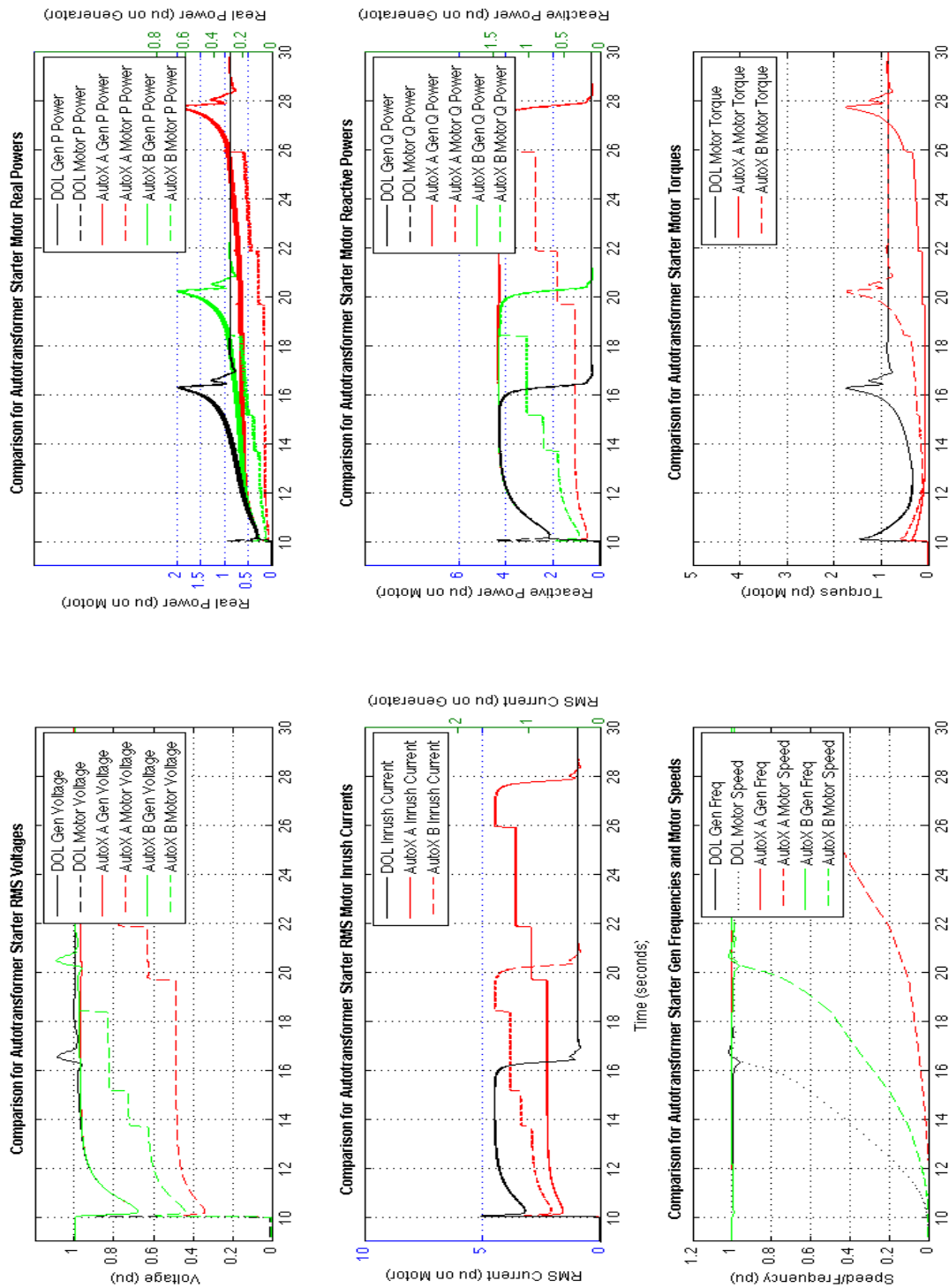


Figure 44: Genset Autotransformer Starter Results for the 500 HP Motor

2.1.5. Primary Resistance Start

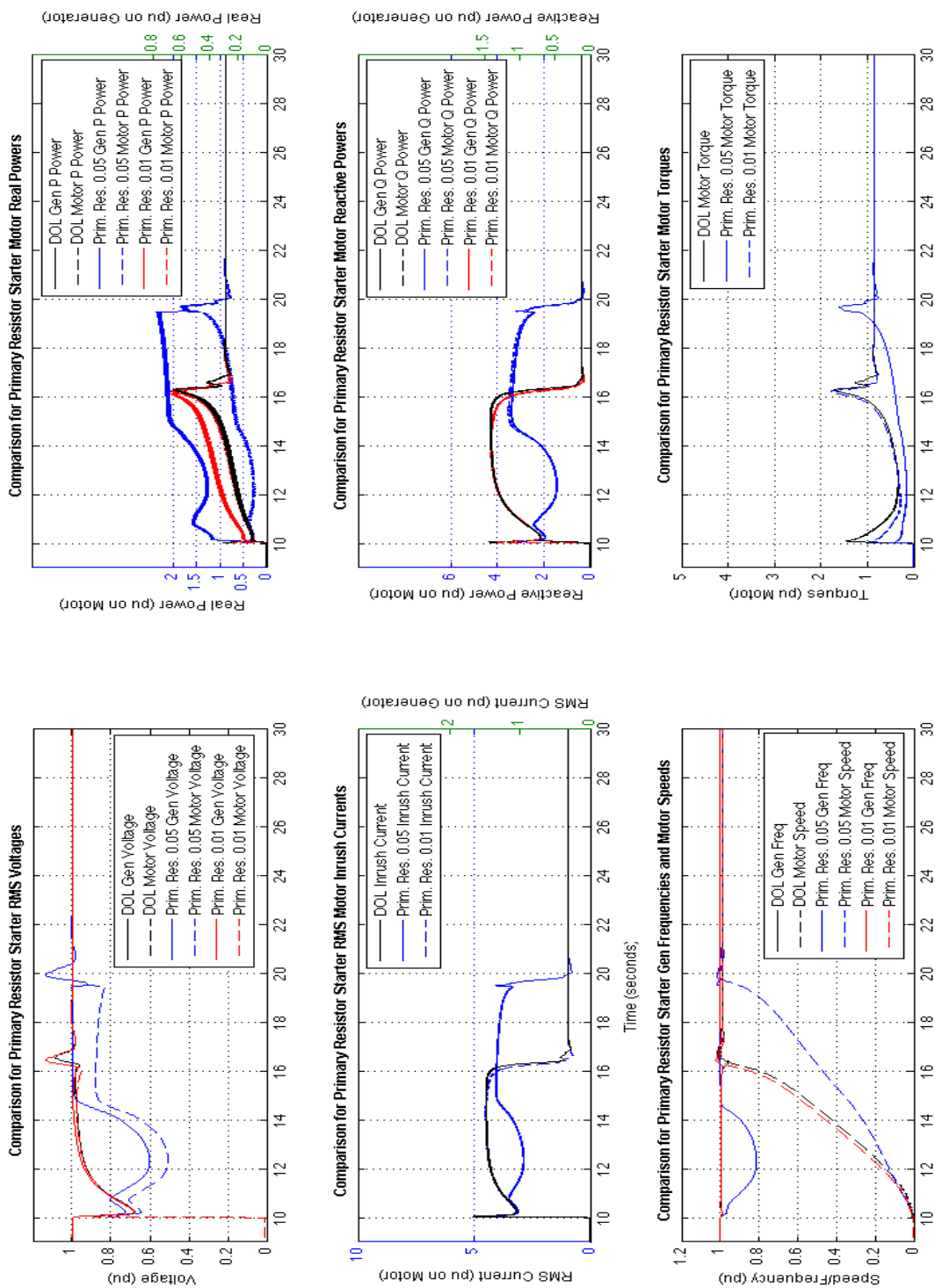


Figure 45: Genset Primary Resistance Starter Results for the 500 HP Motor

2.1.6. Primary Reactance Start

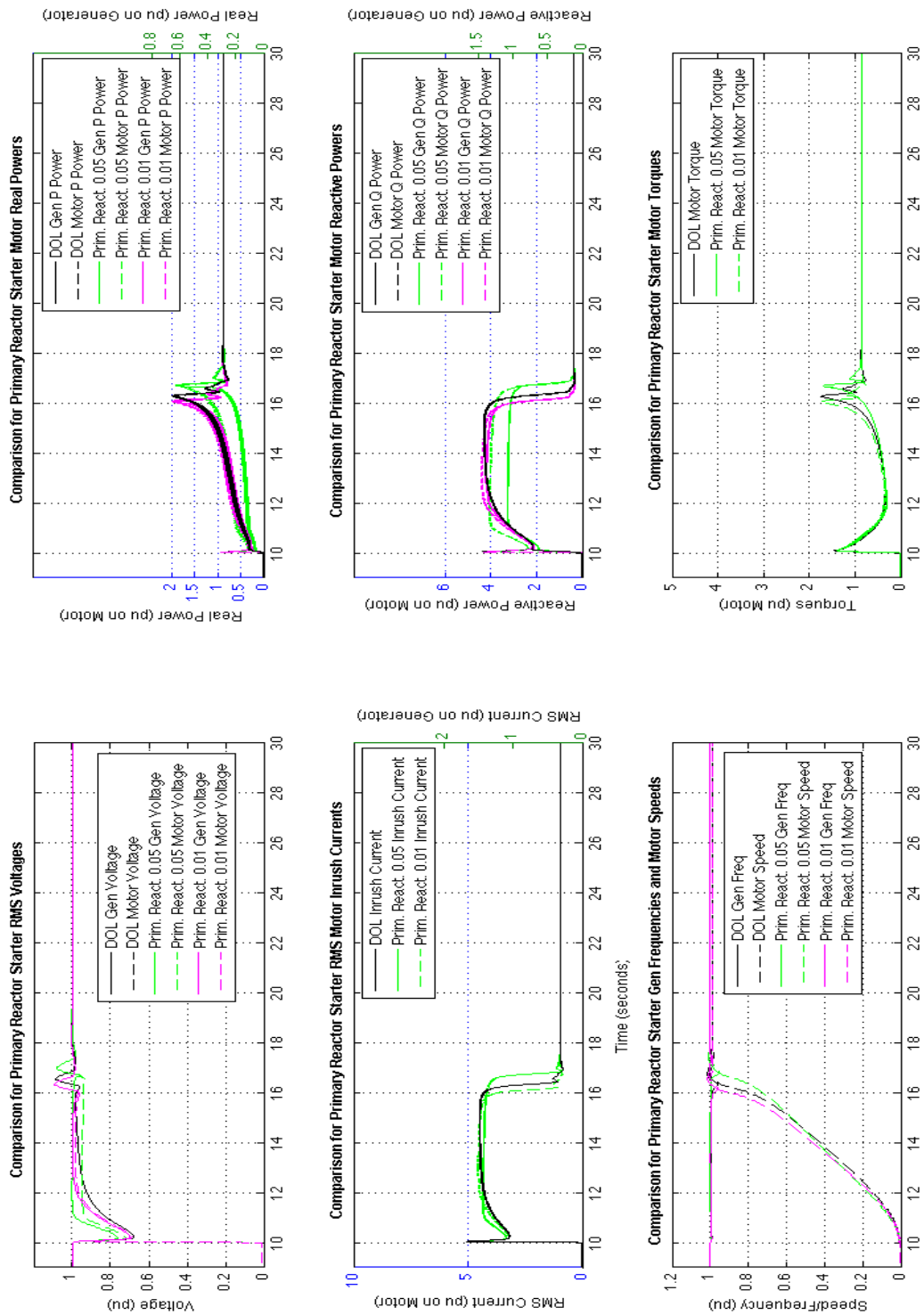


Figure 46: Genset Primary Reactance Starter Results for the 500 HP Motor

2.2. 500 HP Motor Performance Summary

In general the 500 HP motor results are similar to the 200 HP motor results. Many of the takeaways are very similar. The constant and genset sources are compared in Figure 41. The voltage dip (top left) and current dip (middle left) for the genset source is seen, as well as the corresponding power reduction (top and middle right).

The shunt capacitor starter is shown in Figure 42. As can be expected, the voltage dip and time recovery (top left) as well as the decreasing of the reactive power (middle right) are slightly improved. Also, note that since the recovery is improved the time to rated speed (bottom left) is slightly faster than for the DOL start. The star-delta and autotransformer results are shown in Figures 34 and 35. These direct proportional voltage reduction methods reduce both the current (middle left) and torque (bottom right), according to the supplied voltage. The real and reactive powers (top and middle right) are reduced significantly from the generation to the motor. The time to reach rated speed (bottom left) is significantly increased. One important point is that to reach rated speed within the set time frame the full-voltage (starter removed) needed to occur before approximately reaching rated speed. Thus, the maximum inrush current is still reached.

The primary resistance and reactance starters are shown in Figures 36 and 37, respectively. For the primary resistance the voltage applied to the motor (top left) is decreased for both the high and low resistances. As for the 200 HP motor the larger resistance causes a significant voltage and frequency dip well past most standards. However, the low resistance performance characteristics do not differ too much from the DOL start. The primary reactance moderately improves the voltage support (top left), but

little effect on the inrush current (middle left), and the efficiency through decreasing the reactive power support (middle right) for both the higher and lower reactances.

Figures 47, 48, and 49 compare the responses of the starter results discussed. The inrush currents, generator voltages, and generator frequency are shown in Figure 47, while motor speed, generator electromagnetic torque, and motor inrush electromagnetic torque are shown in Figure 48. The mechanical load, motor, and generator torques are shown in Figure 49.

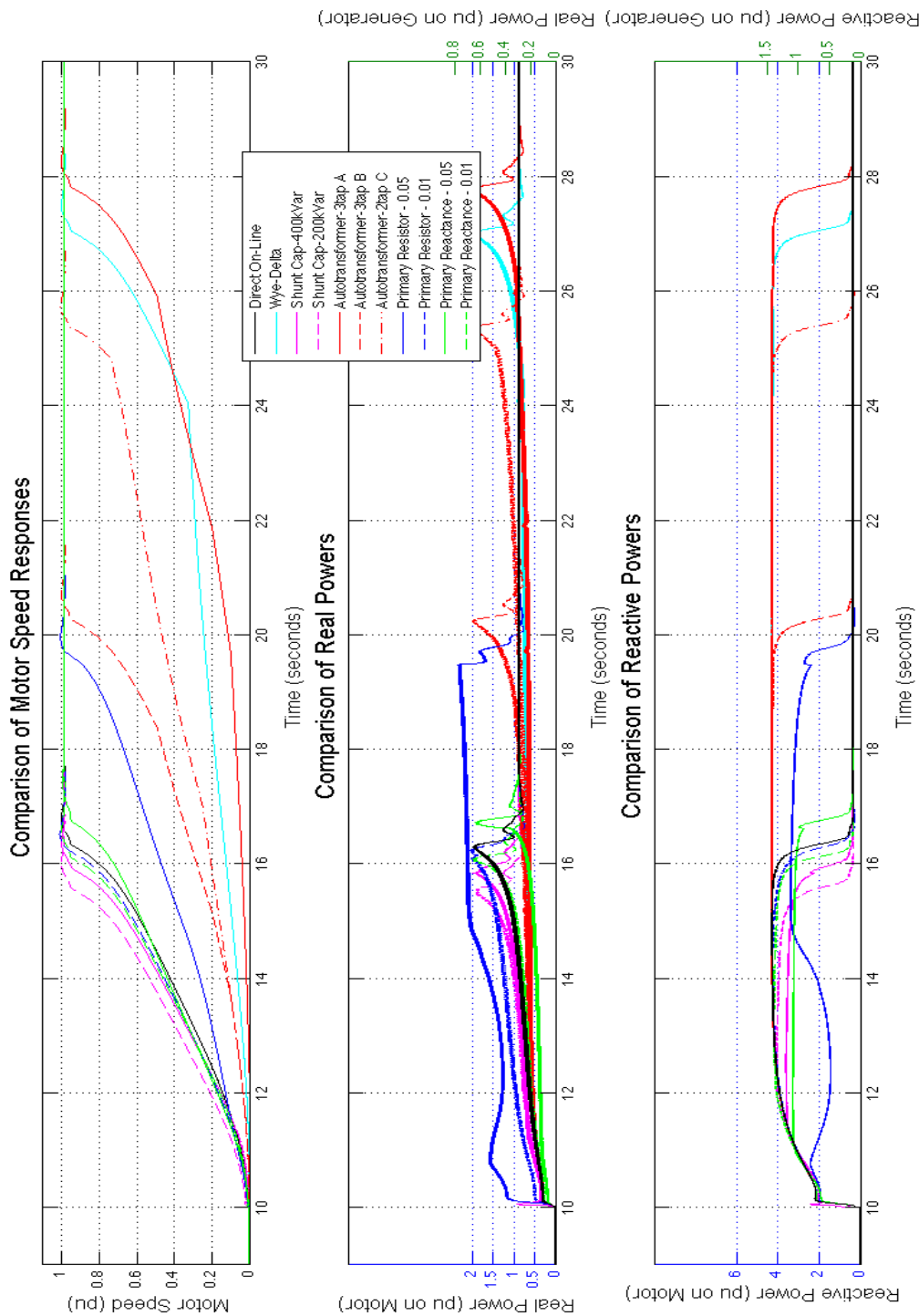


Figure 47: Comparison of All Genset Source Results for Inrush Current, Generator Voltage, and Generator Frequency for the 500 HP Motor

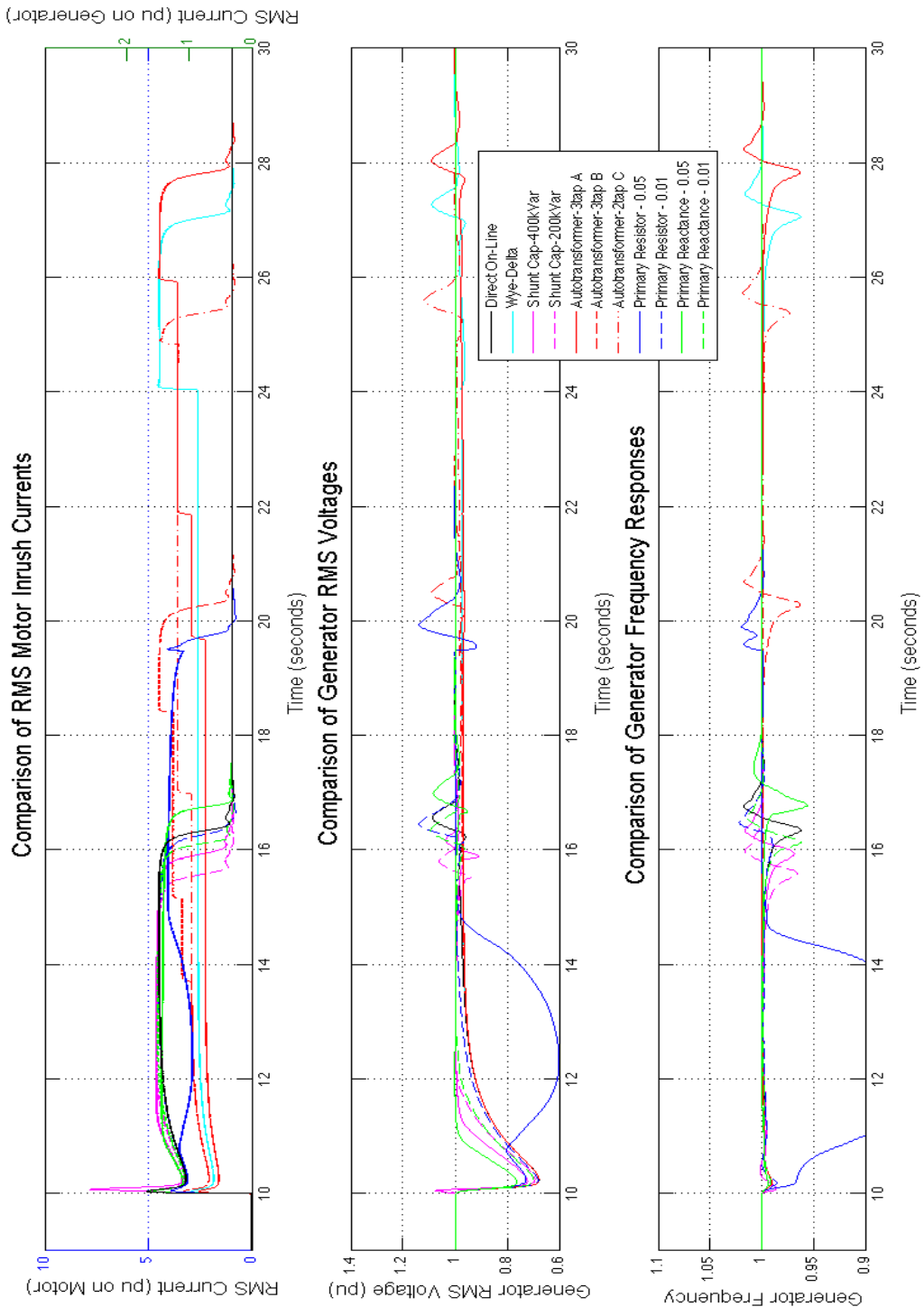


Figure 48: Comparison of All Genset Source Results for Motor Speed, Generator Real and Reactive Power for the 500 HP Motor

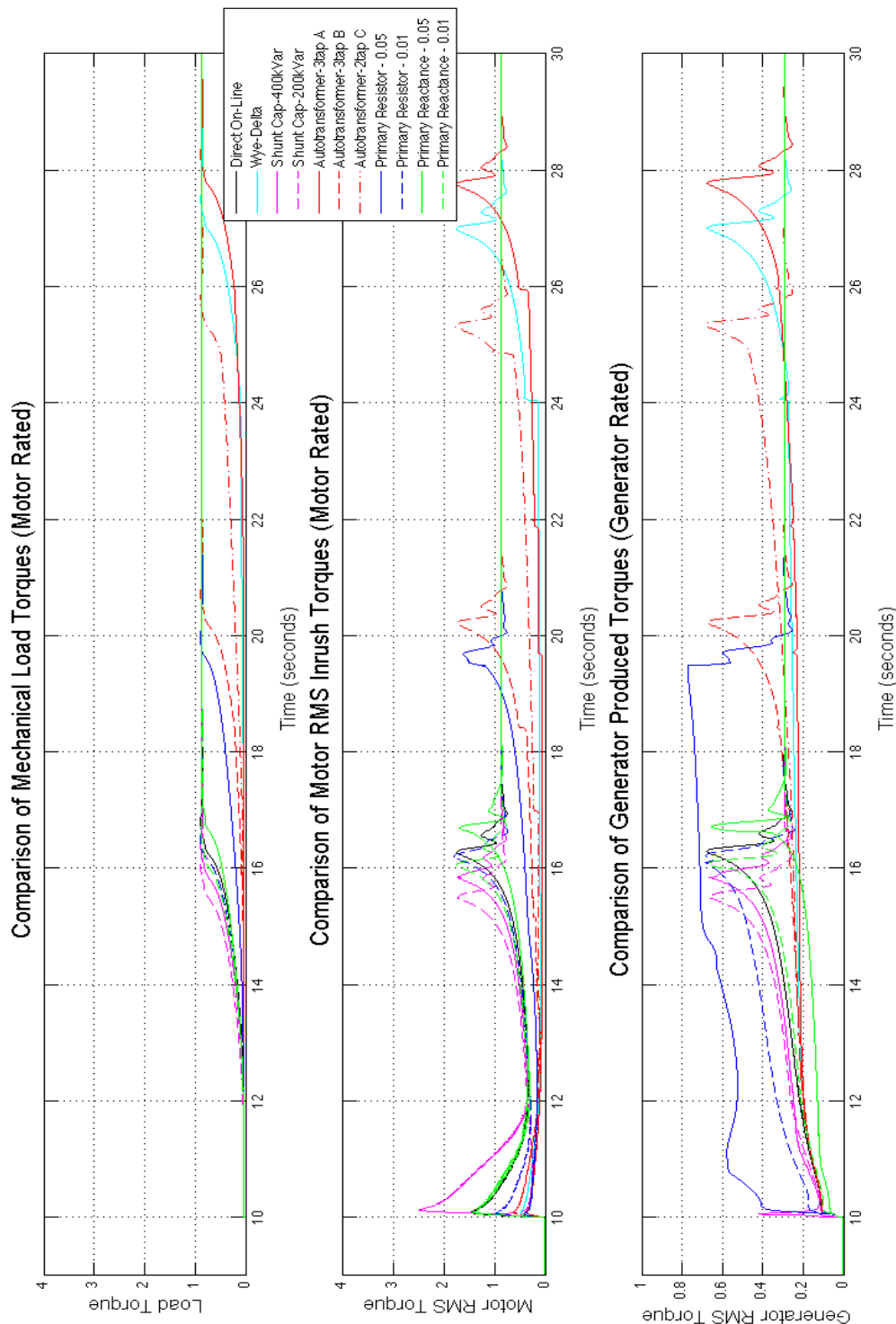


Figure 49: Comparison of All Genset Source Results for Load Torques, Motor Inrush Torques, and Generator Torques for the 500 HP Motor

The Figures 47, 48 and 49 can be used to compare the responses of the motor and generator to conclude general trends that each of the starter produces. Most of the results have been discussed from the results shown in Figures 42-46, and are very similar to the results of the 200 HP motor. The metrics from Table 2 column 2 for each of the starter methods is listed in Table 4 for the 500 HP induction motor. A general analysis of the results is given in the Summary and Conclusion section IX, but in general the results agree with the discussion in the Literature Review section VI. In general many of the same conclusions can be drawn for the 200 HP motor and the 500 HP motor. However, it is more difficult for adequate torque to be achieved for the voltage reduction methods and proper sizing becomes a more critical task. Many of the starters require to be removed well before rated speed, which means that the maximum inrush current is still reached and seemingly only delayed.

Table 4: Starter Metrics for 500 HP Induction Motor Results

Starter Method	Max Voltage Dip	Max Freq. Dip	Max Inrush Current	Average Inrush Current	Max Starting Torque	Average Starting Torque	Start Time	Min Gen. PF
DOL	-32.2%	-3.8%	505.5%	410.1%	160.9%	70.7%	6.57	0.08
Y-Delta	-32.2%	-3.8%	454.6%	283.8%	55.9%	27.0%	17.28	0.08
Cap 200 kVar	-30.7%	-3.4%	487.4%	419.4%	93.8%	61.8%	5.81	-0.28
Cap 400 kVar	-27.8%	-3.2%	785.0%	430.8%	276.3%	90.0%	6.17	-0.26
AutoX A	-32.2%	-3.7%	361.5%	279.4%	40.5%	25.8%	18.05	0.08
AutoX B	-32.2%	-3.7%	384.2%	338.1%	68.3%	41.6%	10.50	0.08
AutoX C	-32.2%	-2.7%	361.6%	321.8%	68.3%	36.4%	15.55	0.08
Prim Resist .05	-40.0%	-18.7%	408.6%	355.3%	45.7%	45.1%	9.72	0.10
Prim Resist.01	-31.8%	-1.5%	458.1%	416.8%	106.9%	63.1%	6.30	0.09
Prim React .05	-23.8%	-4.4%	475.5%	400.2%	151.0%	69.6%	7.16	0.08
Prim React.01	-30.1%	-3.8%	499.2%	415.1%	158.5%	73.1%	6.37	0.08

IX. Summary and Conclusion

It cannot be said with certainty that one starter is better than any other until the particulars of the implementation are known. However, the results from this thesis show that through the applied simulation method the system responses can be studied and compared across multiple starters. Computer simulations provide a cost effective manner to test the different starters. This simulation software is not a substitute to practical knowledge and common sense; instead it is to aid in the decision making of the best starting method to apply as well as testing new starter control designs. Several measures not particularly analyzed in this thesis, such as actual cost and equipment lifetime, also need to be taken into consideration. Special attention should be given to the assumptions made in the system, such as neglecting switching transients and induction motor leakage flux saturation.

From the tests performed in this thesis some general conclusions can be drawn. The shunt capacitor can have a significant impact on the starting power factor, but has sizing limitations based on the parameters of the induction motor. It is also able to slightly decrease the voltage dip and therefore slightly increase the inrush torque and current, and therefore slightly reduce the starting time. The star-delta (wye-delta) and autotransformer approaches can be grouped together because of their similar effects through proportional reduction of the terminal voltage. The important tradeoff among these methods is the reduced inrush current to the reduced starting torque. Ensuring sufficient starting torque and the starting time are important considerations. The primary resistance and primary reactance starters also have the same tradeoff between the inrush current and torque. But,

if the primary impedance size is too large they will make the voltage and frequency dip worse. The size of the induction motor and the motor design characteristics (parameters) as compared to the size of the generator also must be taken into consideration when choosing the starter. The larger the size of the motor the more susceptible the starter is to possibly reducing the starting torque below the requirement. It is important to note that the starters were not optimized with any particular objective in mind. Instead the characteristics of each of the starters as well as the system have been displayed.

The developed simulation tools are meant to be a helpful aid in choosing a starting method and not a definitive methodology. Therefore further value optimization for the starter is not covered in this thesis. Future work can focus on particular value attributes, such as ensuring reliability of the electrical system. It can also be utilized as an aid to optimizing the performance of a starter.

Further work should be done to improve the dynamic load impedance. Conservation of energy and power balancing are likely candidates to improve upon the instantaneous phasor-based calculation. Power balancing would also be important if multiple generators or motors are to be implemented. Additional work could be done to implement other starting methods, or to make more specific types of the starters already implemented.

The main contribution of this thesis has been in the method of calculating the dynamic apparent impedance and using it to simulate the response of the isolated system. The simulation tool can be easily applied to test a variety of starters and the system response. It provides a cost effective, safe, and timely manner that provides insight into the advantages of the various starting methods. The simulation tool provides a solid

foundation for comparatively analyzing the starting methods, so that the starter choices can be narrowed down based on the user's specific desired value.

V. Bibliography

- Ansari, A., & Deshpande, D. (2009). Investigation of Performance of 3-Phase Asynchronous Machine under Voltage Unbalance. *Journal of Theoretical and Applied Information Technology*, 6 (1), 21-26.
- Badr, M., Alolah, A., & Abdel-Halim, M. (1995). A capacitor start three phase induction motor. *IEEE Transactions on Energy Conversion*, 10 (4), 675 - 680.
- Bellarmino, G., Suri, N., Robinette, M., & Dreadin, M. (1994). Motor start program. *Proceedings of the IEEE Southeastcon* (pp. 35-39). Miami, FL: IEEE.
- Cabanas, M., Gondlez, I., Sampayo, I., Melerot, M., Rojas, C., Pedrayes, F., et al. (2003). Analysis of the fatigue causes on the rotor bars of squirrel cage asynchronous motors: experimental analysis and modelling of medium voltage motors. *Symposium on Diagnostics for Electric Machines, Power Electronics and Drives* (pp. 247-252). Atlanta: IEEE.
- Chapman, S. J. (2005). *Electric Machinery Fundamentals* (4th Edition ed.). New York, NY: McGraw-Hill.
- Charles, S., & Bhuvameswari, G. (2009). Power Quality Studies on a Soft-Start for an Induction Motor. *International Journal of Recent Trends in Engineering*, 1 (3), 261-265.
- Cohen, V. (1995). Induction motors-protection and starting. *Elektron Journal-South African Institute of Electrical Engineers.12*, pp. 5-10. Citeseer.
- da Silveira, E.-e., Pires, R., de Almeida, A., Jose, A., & Rezek, J. (2009). Direct on line starting induction motor with Thyristor Switched Capacitor based voltage regulation. *Brazilian Power Electronics Conference* (pp. 1124 - 1129). Bonito-Mato Grosso do Sul : IEEE.
- Dilimot, M., & Algrain, M. (2006). *C32 Transient Response Analysis Tool*. Caterpillar, Inc. Internal Document.
- EDSA Corporation, Inc. (2009). *Paladin® DesignBase - Power Systems Design and Simulation Platform*. Retrieved February 2010 from EDSA Products: <http://www.edsa.com/designbase/main.php>
- Electric Machines Committee of the IEEE Power Engineering Society. (2003, November). IEEE Guide for Synchronous Generator Modeling Practices and Applications in Power System Stability Analyses.
- Erdogan, N., Heno, H., & Grisel, R. (2004). The Analysis of Saturation Effects on Transient Behavior of Induction Machine Direct Starting. *International Symposium on Industrial Electronics.2*, pp. 975-979. IEEE.
- Gobbi, R., Sa'diah, J., & Siang, T. (2003). Industrial problems in design, selection and installation of an adjustable speed drives (ASD) for asynchronous motor. *National Power Engineering Conference Proceedings* (pp. 139 - 143). Bangi, Malaysia: IEEE.

- Hadidi, R., Mazhari, I., & Kazemi, A. (2007). Simulation of Induction Motor Starting With SVC. *IEEE Conference on Industrial Electronics and Applications* (pp. 1135-1140). Harbin: IEEE.
- IEEE Committee Report. (1968). Computer Representation of Excitation Systems. *IEEE Transactions on Power Apparatus and Systems*, 87 (6), 1460-1464.
- IEEE Committee Report. (1973). Dynamic Models for Steam and Hydro Turbines in Power System Studies. *IEEE Transactions on Power Apparatus and Systems*, 92 (6), 1904-1915.
- IEEE Std 1110-2002. (2003, November 11). IEEE Guide for Synchronous Generator Moeling Practices and Applications in Power System Stability Analyses. New York, NY: The Institute of Electrical and Electronics Engineers, Inc.
- IEEE Std 1566-2005. (2006, June 7). IEEE Standard for Performance of Adjustable Speed AC Drives Rated 375 kW and Larger. New York, NY: The Institute of Electrical and Electronics Engineers, Inc.
- IEEE Std 399-1997. (1998, August). IEEE Recommended Practice for Industrial and Commercial Power Systems Analysis. New York, NY: The Institute of Electrical and Electronics Engineers, Inc.
- IEEE Std 421.5-2005. (2006, April 21). IEEE Recommended Practice for Excitation System Models for Power System Stability Studies. New York, NY: Institute of Electrical and Electronics Engineers, Inc.
- Jabr, H., & Kar, N. (2007). Starting Performance of Saturated Induction Motors. *Power Engineering Society General Meeting* (pp. 1-7). Tampa, FL: IEEE.
- Kay, J., Paes, R., Seggewiss, J., & Ellis, R. (1999). Methods for the control of large medium-voltage motors: application considerations and guidelines. *IEEE Transactions on Industry Applications*, 36 (6), 1688--1696.
- Kerkman, R., Thunes, J., Rowan, T., & Schlegel, D. (1995). A frequency based determination of the transient inductance and rotor resistance for field commissioning purposes. *Industry Applications Conference. I*, pp. 359-366. Orlando, FL: IEEE.
- Kjellberg, M., & Kling, S. (2003, February). Softstarter Handbook. 2. Västerås,, Sweden: ABB Automation Technology Products AB.
- Krause, P., & Thomas, C. (1965). Simulation of Symmetrical Induction Machinery. *IEEE Transactions on Power Apparatus and Systems*, 76, 1038-1053.
- Krause, P., Wasynczuk, O., & Sudhoff, S. (2002). *Analysis of Electric Machinery and Drive Systems* (2 ed.). (M. El-Hawary, Ed.) Piscataway, NJ, USA: IEEE Press; John Wiley & Sons, Inc.
- Larabee, J., Pellegrino, B., & Flick, B. (2005). Induction motor starting methods and issues. *Petroleum and Chemical Industry Conference, 2005. Industry Applications Society 52nd Annual* , 217--222.
- Lewis, H. L., & Woodbury, F. A. (1978). Large Motors on Limited Capacity Transmission Lines. *IEEE Transactions on Industry Applications*, 14 (3), 198-208.

- Li, S., & Liu, Z. (2009). Constant-Current Soft Starting of Induction Motor Based on Fuzzy Control. *Proceedings of the 2009 International Conference on Computer Engineering and Technology*.2, pp. 358--361. Singapore: IEEE.
- Li, X., Zhao, Y., Yang, F., & Zhang, H. (2009). The Study of Full-voltage Starting Method of Highpower Asynchronous Motors with Dynamic Reactive Power Compensation. *Asia-Pacific Power and Energy Engineering Conference* (pp. 1-5). Wuhan: IEEE.
- Liang, X., Laughy, R., & Liu, J. (2007). Investigation of Induction Motors Starting and Operation with Variable Frequency Drives. *Conference on Electrical and Computer Engineering* (pp. 556 - 561). Vancouver, BC : IEEE.
- Lipo, T., & Krause, P. (1969 , January). Stability Analysis of a Rectifier-Inverter Induction Motor Drive. *IEEE Transaction on Power Apparatus and Systems* , 55 - 66 .
- Liu, H., Jiang, Q., Hu, Q., & Zhou, E. (1997). Modeling and Simulation of the Capacitor Starting System of Large and Medium Squirrel Cage Motors On Limited Capacity Transmission Lines. *Electric Machines and Drives Conference* (pp. 1-3). Milwaukee, WI: IEEE.
- McElveen, R., Toney, M., Autom, R., & Mountain, K. (2001). Starting high-inertia loads. *IEEE Transactions on Industry Applications*, 37 (1), 137-144.
- Medrea, N., & Demean, A. (2008). Induction Motor Starting in a Power System Using EDSA Paladin Designbase Software. *Annals of the University of Craiova, Electrical Engineering series*, 32 , 138-141. University of Craiova.
- Mirosevic, M., Maljkovic, Z., & Milkovic, M. (2005). Diesel-Generator-Units Dynamic Analysis During the Start-Up of Induction Motors Drives. *European Conference on Power Electronics and Applications* (pp. 1-7). Dresden: IEEE.
- Mirosevic, M., Maljkovic, Z., & Milkovic, M. (2009). Dynamics of Diesel-Generator-Units during Direct-on-Line Starting of Induction Motors. *13th European Conference on Power Electonics and Applications* (pp. 1-8). IEEE.
- Mirosevic, M., Maljkovic, Z., & Milkovic, M. (2007). Torsional dynamics of generator-units during autonomous operation. *European Conference on Power Electronics and Applications* (pp. 1-7). IEEE.
- Munoz-Garcia, A., Lipo, T., & Novotny, D. (1997). A new induction motor open-loop speed control capable of low frequency operation. *Industry Applications Conference.1*, pp. 579 - 586. New Orleans, LA : IEEE.
- NEMA. (2009). *NEMA Standards MG 1 -2009*. Rosslyn, VA: National Electrical Manufacturers Association.
- NEMA. (2007). *NEMA Standards Publication Condensed MG 1-2007*. Rosslyn, VA: National Electrical Manufacturers Association.
- Ogata, K. (2002). *Modern Control Engineering* (4th Edition ed.). Upper Saddle River, NJ: Pearson Education Inc.

- Okoro, O., Weidemann, B., & Oswald, B. (2006). Dynamic Modelling and Simulation of Squirrel-Cage Asynchronous Machine with Non-Linear Effects. *Revista Ciências Exatas*, 12 (1), 71-77.
- Ong, C.-M. (1998). *Dynamic Simulation Electric Machinery Using Matlab(R)/Simulink*. Upper Saddle River, NJ, USA: Prentice Hall.
- Ozpineci, B., & Tolbert, L. (2003). Simulink implementation of induction machine model-a modular approach. 2, pp. 728-734. IEEE.
- Park, R. (1929). Two-Reaction Theory of Synchronous Machines-Generalized Method of Analysis, Part I. *AIEEE Transactions*, 48, 716-727.
- Patil, P., & Porate, K. (2009). Starting Analysis of Induction Motor: A Computer Simulation by Etap Power Station. *International Conference on Emerging Trends in Engineering and Technology* (pp. 494 - 499). Nagpur : IEEE.
- Pillay, K., Nour, M., Yang, K., Datu Harun, D., & Haw, L. (2009). Assessment and Comparison of Conventional Motor Starters and Modern Power Electronic Drives for Induction Motor Starting Characteristics. *Symposium on Industrial Electronics and Applications (ISIEA)* (pp. 584-589). Kuala Lumpur: IEEE.
- Pillay, P., Harley, R., & Odendal, E. (1984). A Comparison between Star and Delta Connected Induction Motors when Supplied by Current Source Inverters. *Electric Power Systems Research*, 8, 41-51.
- Portos, J., King, R., & Gaynor, P. (2007). The Influence of Magnetic Retaining Rings on AC Motors for Boosting Torque and Reducing Starting Current. *Petroleum and Chemical Industry Technical Conference* (pp. 1-8). Calgary: IEEE.
- Prusty, S., & Rao, M. (1980). A Direct Piecewise Linearized Approach to Convert rms Saturation Characteristic to Instantaneous Saturation Curve. *IEEE Transactions on Magnetics*, 16 (1), 156-160.
- Rajaji, L., Kumar, C., & Vasudevan, M. (2008). Fuzzy and ANFIS based Soft Starter Fed Induction Motor Drive for High Performance Applications. *ARPJN Journal of Engineering and Applied Sciences*, 3 (4), 12-24.
- Sauer, B., & Brady, P. (2009). Application of AC Induction Motors with Variable Frequency Drives. *Cement Industry Technical Conference Record* (pp. 1 - 10). Palm Springs, CA: IEEE.
- Seman, S., Saitz, J., & Arkkio, A. (2004). Dynamic Model of Cage Induction Motor Considering Saturation and Skin Effect. *International Conference on Electrical Machines and Systems.2*, pp. 710-713. IEEE.
- Solveson, M., Mirafzal, B., & Demerdash, N. (2006). Soft-Started Induction Motor Modeling and Heating Issues for Different Starting Profiles Using a Flux Linkage ABC Frame of Reference. *IEEE Transactions on Industry Applications*, 42 (4), 973--982.
- Stout, J. H. (1978). Capacitor Starting of Large Motors. *IEEE Transactions on Industry Applications*, 14 (3), 209-212.

TransÉnergie Technologies Inc.; Hydro-Québec. (2003). *SimPowerSystems User's Guide* (3 ed.). Natick, MA: The MathWorks, Inc.

Trzynadlowski, A. M. (2001). *Control of Induction Motors*. San Diego, CA, USA: Academic Press.

Tuinman, E., Piers, P., & De Weerd, R. (1998). Simulation of a 'Direct On Line' Start of a Large Induction Motor Connected to a Salient Pole Synchronous Generator. *International Conference on Simulation* (pp. 362-367). York: IEEE.

Vu, K., & Novosel, D. (2001). *Patent No. 6,219,591*. US.

Williams, A., & Griffith, M. (1978). Evaluating the effects of motor starting on industrial and commercial power systems. *IEEE Trans. Ind. Appl.*, 14 (4), 292-299.

Working Group on Prime Mover and Energy Supply Models for System Dynamic Performance Studies. (1991). Dynamic models for fossil fueled steam units in power system studies. *IEEE Transactions on Power Systems*, 6 (2), 753-761.

Yeager, K., & Willis, J. (1993). Modeling of emergency diesel generators in an 800 megawatt nuclear power plant. *IEEE Transaction on Energy Conversion*, 8 (3), 433-441.

Youxin, Y., Zehong, X., Yalan, W., Peigang, Y., & Wanquan, P. (2007). A Soft Starter of Three Phase Asynchronous Motor. *IEEE Power Electronics Specialists Conference* (pp. 563-567). Orlando, FL: IEEE.

Appendix A: Reference Frame Transformations

Reference frame transformations can be found in references (Krause, Wasynczuk, & Sudhoff, 2002), (Ong, 1998), (Trzynadlowski, 2001). It is common practice to transform the AC three phase variables into DC phases because of their advantageous analysis characteristics of the flux patterns. Here we use f is an arbitrary variable that can be flux linkage, voltage, or current (notation λ , v , and i , respectively). The conversion from the abc to stationary reference frame is performed with Clarke's transformation, where the s superscript denotes stationary reference frame:

$$\begin{bmatrix} f_q^s \\ f_d^s \\ f_0^s \end{bmatrix} = \frac{2}{3} \begin{bmatrix} 1 & -1/2 & -1/2 \\ 0 & -\sqrt{3}/2 & \sqrt{3}/2 \\ 1/2 & 1/2 & 1/2 \end{bmatrix} \begin{bmatrix} f_a \\ f_b \\ f_c \end{bmatrix}, \quad (\text{A-1})$$

where f is an arbitrary variable that can be flux linkage, voltage, or current (notation λ , v , and i , respectively). Balanced conditions are only considered in this work, thus the 0, zero-sequence, variables are negligible. The inverse transformation, the dq0 variables transformed into the abc variables is:

$$\begin{bmatrix} f_a \\ f_b \\ f_c \end{bmatrix} = \begin{bmatrix} 1 & 0 & 1 \\ -1/2 & -\sqrt{3}/2 & 1 \\ -1/2 & \sqrt{3}/2 & 1 \end{bmatrix} \begin{bmatrix} f_q^s \\ f_d^s \\ f_0^s \end{bmatrix}. \quad (\text{A-2})$$

Transforming to a rotating reference frame from a stationary reference can be done using the following transformation:

$$\begin{bmatrix} f_q \\ f_d \\ f_0 \end{bmatrix} = \begin{bmatrix} \cos \theta & -\sin \theta & 0 \\ \sin \theta & \cos \theta & 0 \\ 0 & 0 & 1 \end{bmatrix} \begin{bmatrix} f_q^s \\ f_d^s \\ f_0^s \end{bmatrix}. \quad (\text{A-3})$$

And the inverse transformation from the rotating to the stationary reference frame is:

$$\begin{bmatrix} f_q^s \\ f_d^s \\ f_0^s \end{bmatrix} = \begin{bmatrix} \cos \theta & \sin \theta & 0 \\ -\sin \theta & \cos \theta & 0 \\ 0 & 0 & 1 \end{bmatrix} \begin{bmatrix} f_q \\ f_d \\ f_0 \end{bmatrix} \quad (\text{A-4})$$

θ is the angle of rotation, and is calculated as the integral of the rotational speed ω :

$$\theta = \int \omega dt + \theta_0 \quad (\text{rad}), \quad (\text{A-5})$$

where θ_0 is the initial angle offset.

The common reference frames used are the stationary, synchronous, and rotor reference frames. The associated speeds used for each are:

Stationary: $\omega = 0$

Synchronous: $\omega = \omega_e$

Rotating: $\omega = \omega_r$

These values can be used to determine the angle of rotation to use in equations (A-3) and (A-4).

Appendix B: Additional Engine Models

1. Simple Genset Model

The combined diesel engine and speed governor model described by (Yeager & Willis, 1993) was built as a simple engine model. The speed governor consists of a control box described by a second order transfer function and an actuator described by a third order transfer function. A deadband was added to the model to prevent further dynamics when within an acceptable speed range. The diesel engine itself is modeled by a transfer delay and outputs the mechanical torque, T_{mech} . The block diagram model in Figure 50, which is used in the simulations, shows the linear approximate control system of the diesel engine and speed governor.

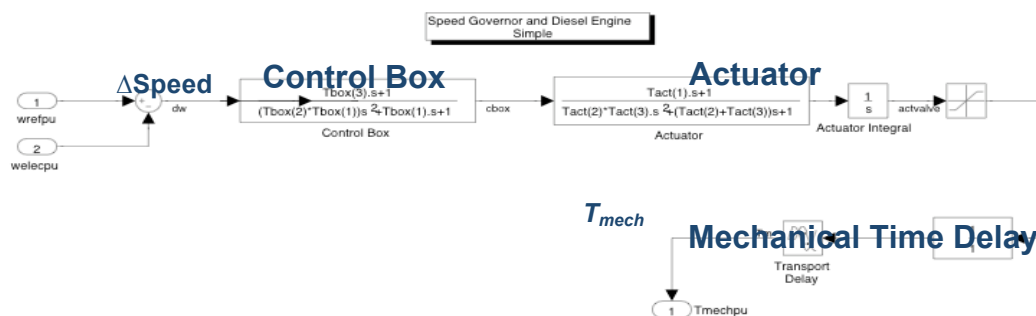


Figure 50: The Simplified Diesel-Generator Set Model
As presented by Yeager and Willis (1993)

2. Steam Engine and Governor

Two engine models are built. Both are based on models from the IEEE Committee Report “Dynamic Models for Steam and Hydro Turbines in Power System Studies” (IEEE Committee Report, 1973). They are both models for steam turbines with speed-governors. The steam turbine is modeled with the first-order transfer function, which is

the linear model of the steam chest shown in Figure 51 being the first block on the far left. The associated steam system modeled is the tandem compound with double-reheat. The approximated linear functional block model is shown in Figure 51 (reproduced from Figure 7.C in reference (IEEE Committee Report, 1973)), and the Simulink equivalent block is shown in Figure 52. The steam system structure is the same for both models. The difference in the models comes from the two different types of speed-governor models. One is based on a general speed-governor, and the other is based on an electro-hydraulic speed-governor based on a General Electric system (IEEE Committee Report, 1973). In all the simulations performed, the steam system (reheaters and condensers) is ignored, and only the linear system model is used. Thus it is a simple generic model that has a slower response than modern diesel engines.

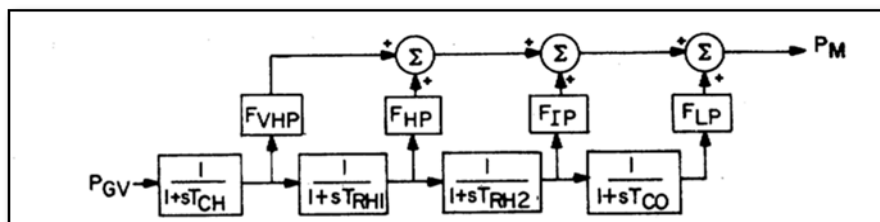


Figure 51: Linear Approximate Functional Block Model of the Tandem Compound Steam Turbine Engine with Double Reheat

Reproduced from "Dynamic Models for Steam and Hydro Turbines in Power System Studies" (1973)
Figure 7 C, p. 1908

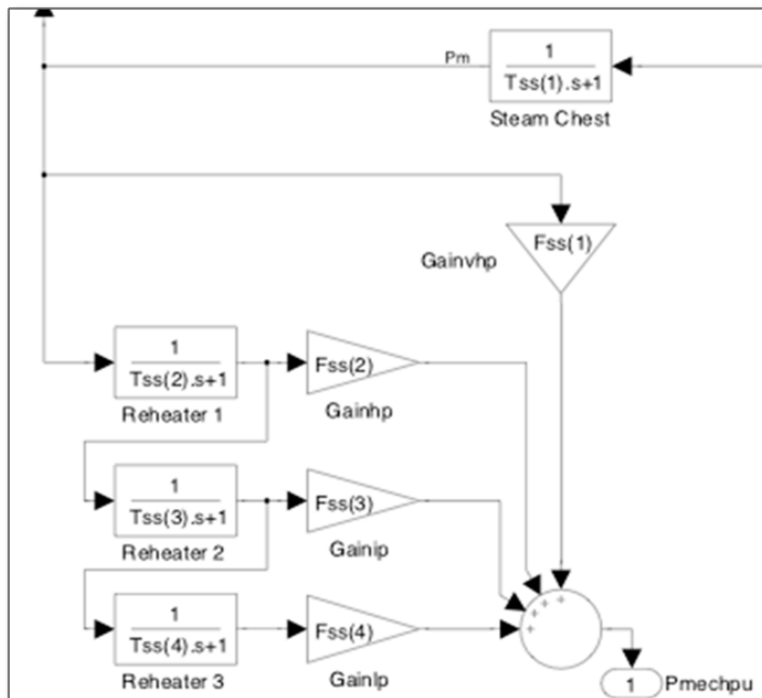


Figure 52: Simulink Block of the Tandem Compound Steam Turbine Engine with Double Reheat

2.1. Electro-Hydraulic Speed-Governing Model

The electro-hydraulic model presented in (IEEE Committee Report, 1973) is reproduced here in Figure 53. The Simulink block built is shown with the steam system in Figure 54.

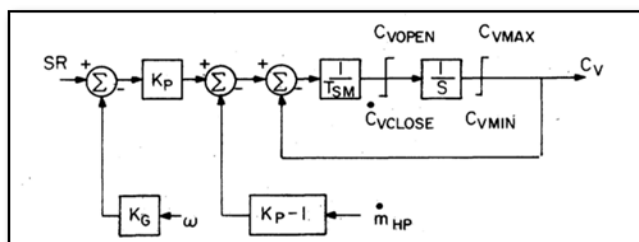


Figure 53: Electro-Hydraulic Speed-Governor Model for a Steam Turbine

Reproduced from "Dynamic Models for Steam and Hydro Turbines in Power System Studies" (1973) Figure 3 B, p. 1905

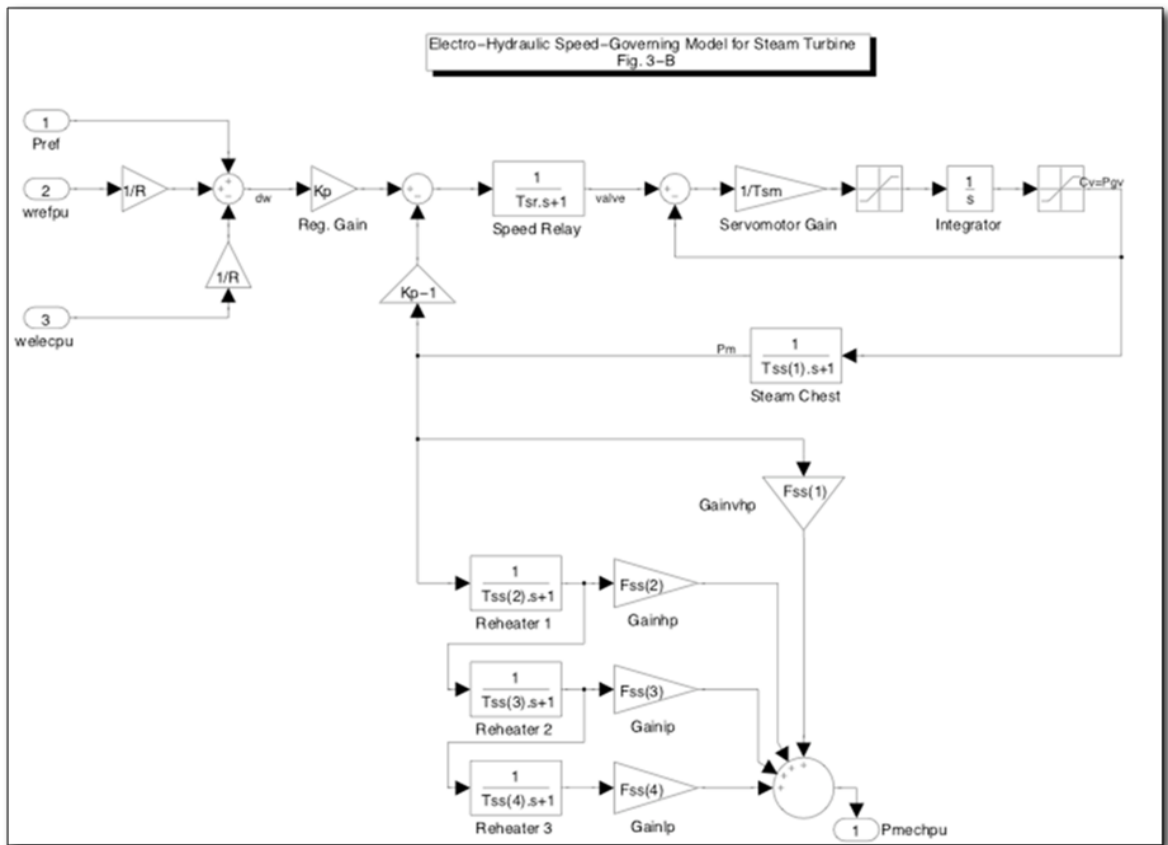


Figure 54: Simulink Block of the Electro-Hydraulic (GE) Speed-Governor and Steam Turbine

2.2. General Model for Steam Turbine Speed-Governor

The general functional block model from (IEEE Committee Report, 1973) is shown in Figure 55. This is the general speed-governor model of a steam turbine; therefore it can model both electro-hydraulic and mechanical hydraulic governors. The Simulink block of this model is shown in Figure 56 with the steam system.

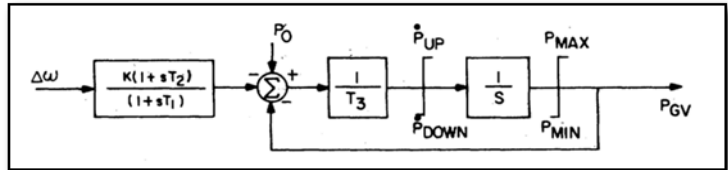


Figure 55: Functional Block Model of a General Speed-Governor
 Reproduced from "Dynamic Models for Steam and Hydro Turbines in Power System Studies" (1973)
 Figure 4 A, p. 1906

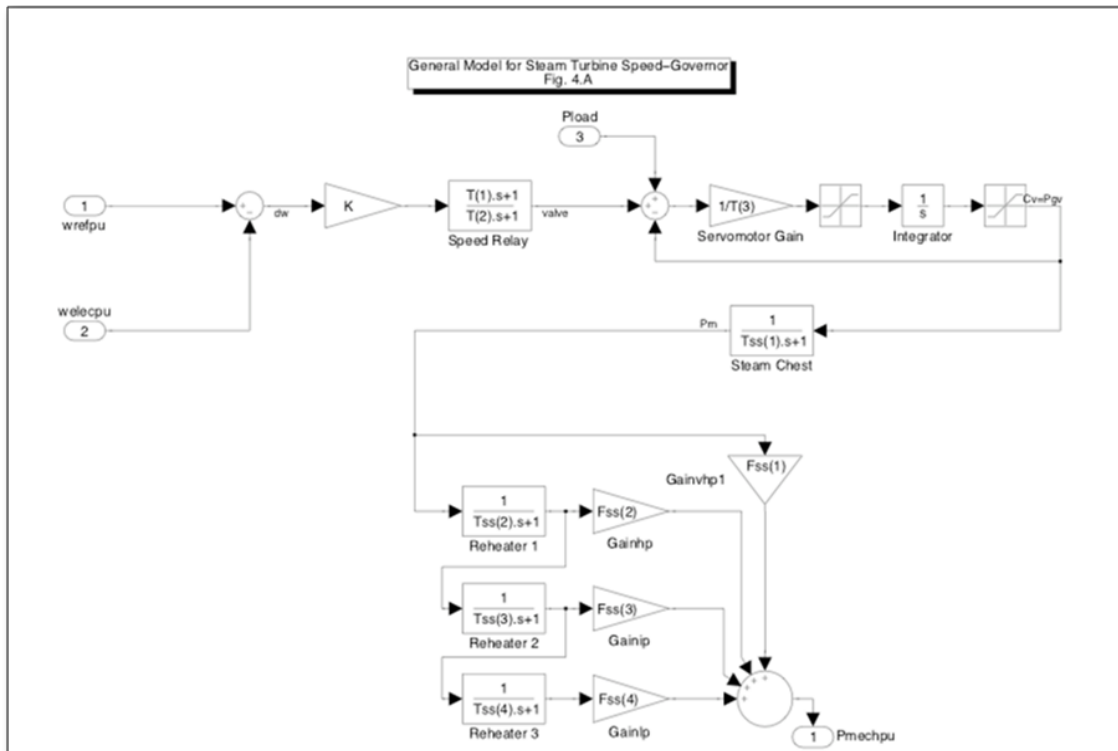


Figure 56: Simulink Block of General Speed-Governor and Steam Turbine

Appendix C: NEMA Letter Codes

The NEMA Codes by letter grade are reproduced here for convenience from (NEMA, 2007) and (NEMA, 2009) in Tables 5 and 6.

Table 5: NEMA Letter Code Typical Characteristics (NEMA Standards Publication Condensed MG 1-2007)

Table 11
TYPICAL CHARACTERISTICS AND APPLICATIONS
OF FIXED FREQUENCY SMALL AND MEDIUM AC SQUIRREL-CAGE INDUCTION MOTORS

Polyphase Characteristics	Locked Rotor Torque (Percent Rated Load Torque)	Pull-Up Torque (Percent Rated Load Torque)	Breakdown Torque (Percent Rated Load Torque)	Locked Rotor Current (Percent Rated Load Current)	Slip	Typical Applications	Relative Efficiency
Design A High locked rotor torque and high locked rotor current	70-275 [*]	65-190	175-300 [*]	Not defined	0.5-5%	Fans, blowers, centrifugal pumps and compressors, motor-generator sets, etc., where starting torque requirements are relatively low	Medium or high
Design B Normal locked rotor torque and normal locked rotor current	70-275 [*]	65-190	175-300 [*]	600-700	0.5-5%	Fans, blowers, centrifugal pumps and compressors, motor-generator sets, etc., where starting torque requirements are relatively low	Medium or high
Design C High locked rotor torque and normal locked rotor current	200-285	140-195	190-225 [*]	600-700	1-5%	Conveyors, crushers, stirring motors, agitators, reciprocating pumps and compressors, etc., where starting under load is required	Medium
Design D High locked rotor torque and high slip	275	NA	275	600-700	5-8%	High peak loads with or without flywheels such as punch presses, shears, elevators, extractors, winches, hoists, oil-well pumping and wire-drawing motors	Low
Design N Small motor	—	NA	—	—	NA	Centrifugal loads where starting torque requirements are relatively low	Low
Design O Small motor	—	NA	—	—	NA		
Design L Medium motor	—	100%	—	—	NA	Fans, blowers, centrifugal pumps and compressors, motor-generator sets, etc., where starting torque requirements are relatively low	Medium or Low
Design M Medium motor	—	100%	—	—	NA	Fans, blowers, centrifugal pumps and compressors, motor-generator sets, etc., where starting torque requirements are relatively low	Medium or high

^{*}Higher values are for motors having lower horsepower ratings.

Table 6: NEMA Code Letter Locked-Rotor kVA (NEMA, 2009)

NEMA Code Letter	Locked Rotor kVA per HP
A	0.0 - 3.15
B	3.15 - 3.55
C	3.55 - 4.0
D	4.0 - 4.5
E	4.5 - 5.0
F	5.0 - 5.6
G	5.6 - 6.3
H	6.3 - 7.1
J	7.1 - 8.0
K	8.0 - 9.0
L	9.0 - 10.0
M	10.0 - 11.2

Appendix D: Model Parameters

The parameters used in the simulation system models are listed in Tables 7 and 8 for the 200 HP and 500 HP induction motors, respectively. The mechanical load parameters are listed in Table 9. The engine, speed governor, voltage regulator, and synchronous generator parameters are proprietary, but have been verified against measured data.

Table 7: 200 HP Induction Motor Simulation Parameter Values

Parameter Name	Symbol	Simulation Value
Rated Horsepower	-	200 HP
Rated Power Factor	pf	0.9
Rated Power	$P_{rated,motor}$	149.2 kW
Pole Pairs	$N_{p,motor}$	2
Rated RPM	-	1780 RPM
Stator Resistance	R_s	0.018181 Ω
Rotor Resistance	R_r	0.009956 Ω
Mutual Inductance	L_m	0.00945H
Stator Leakage Inductance	L_{ls}	0.00019H
Rotor Leakage Inductance	L_{lr}	0.00019H
Rotational Inertia	J	2.6 kg-m ²
Frictional Coefficient	D_f	0.1 N-m-s

Table 8: 500 HP Induction Motor Simulation Parameter Values

Parameter Name	Symbol	Simulation Value
Rated Horsepower	-	500 HP
Rated Power Factor	pf	0.9
Rated Power	$P_{rated,motor}$	372.8kW
Pole Pairs	$N_{p,motor}$	2
Rated RPM	-	1773 RPM
Stator Resistance	R_s	0.0095 Ω
Rotor Resistance	R_r	0.0075 Ω
Mutual Inductance	L_m	0.0072 H
Stator Leakage Inductance	L_{ls}	0.00016 H

Rotor Leakage Inductance	L_r	0.00016 H
Rotational Inertia	J	11.06 kg-m ²
Frictional Coefficient	D_f	0.05 N-m-s

Table 9: Mechanical Load Parameters

Parameter Name	Symbol	Simulation Value 200 HP	Simulation Value 500 HP
Nominal Mechanical Power	$P_{rated,load}$	140 kW	360 kW
Initial Mechanical Power	$P_{0,load}$	10 kW	20 kW
Rated RPM	RPM	1780 RPM	1773 RPM

Appendix E: Simulation Settings

MATLAB(R)/Simulink Settings used for the simulation parameters are listed in Table 10. The version of MATLAB used is 2009. Special note should be given to the solver and the time-step used. For consistent well performing simulations it was found that the Euler solver 'ode1' is insufficient for this model because at the time of connection the initial values of the flux calculated are unrealistic.

Table 10: The Simulink Setting Parameters

Setting Parameter	Value Simulated
Solver Type	Fixed-Step
Solver	Runge-Kutta (ode4)
Fundamental Sample Time	0.0001
Engine Controls Sample Time	0.0075
Automatic Voltage Regulator Sample Time	0.0010

Appendix F: Linear Piecewise Conversion Code

```

function [psi_m, i_m] = satconvert(Vrms, Ipk)
%   Adam Wigington, April 2010
%   Master's Thesis Work
%   University of Nebraska - Lincoln
% This function converts the no-load curve of the terminal
rms
%   voltage and current and converts it the mutual flux
linkage and
%   current, as presented in Ong, "Dynamic Simulation of
Electric
%   Machinery," 1998, equations 4.60, 4.63, 4.65, and 4.71-
4.73
%   Orinally from
%   "A Direct Piecewise Linearized Approach to Convert rms
%   Saturation Characteristic to Instantaneous Saturation
Curve"
%   S. PRUSTY M. V. S. RAO (1975)
% INPUT: (first points should be the origin, 0)
%   Vector of Terminal voltage LL rms (V)
%   Vector of Stator (for induction machine) or Field
Current (for synchronous machine) peak (A)
% OUPUT:
%   Vector of Mutual flux linkage (Wb-turns, Vs)
%   Vector of Mutual current (A)

% Check lengths
if (length(Vrms) ~= length(Ipk))
error('ERROR: Lengths of Vrms and Ipk are not equal.');
```

```

end
% insert zeros if not there already
if(Vrms(1) ~= 0)
    Vrms = [0 Vrms];
end
if(Ipk(1) ~= 0)
    Ipk = [0 Ipk];
end
n = length(Vrms);
% Convert current from pk to rms
Irms = Ipk/sqrt(2);

% The slopes at each linear portion are Ks
% Simplified polynomial  $AK^2+B*K+C=0$ 

```

```

K = zeros(1,n);
A = K; B = K; C = K; psi_m = K; i_m = K;
d = K; t = K; theta = K; s = K; g = K;

% Convert from RMS voltage to mutual flux
psi_m = Vrms*sqrt(2);

% Convert from RMS stator or field current to total mutual
current
%initial case
i_m(1) = 0;
theta(1) = 0;
% should be 0
%initial condition
K(1) = (Irms(2)*sqrt(2))/psi_m(2);    %No sqrt(2) b/c
already peak
%i_m(2) = K(2)*psi_m(2)*sin(theta(2))
%main loops Equations 10-13 in Prusty & Rao
for k=2:n
%    summation = 0;
for j=2:k
% solve in reverse order as presented in Prusty & Rao
theta(j) = asin(psi_m(j)/psi_m(k));
g(j) = cos(theta(j)) - cos(theta(j-1)); %Wrong in Ong
s(j) = 0.5*(sin(2*theta(j)) - sin(2*theta(j-1)));
t(j) = theta(j) - theta(j-1);
d(j) = i_m(j-1)^2*t(j);
B(j) = -2*i_m(j-1)*(psi_m(k)*g(j)+psi_m(j-1)*t(j));
A(j) = 0.5*psi_m(k)^2*(t(j)-s(j))+2*psi_m(k)*psi_m(j-
1)*g(j)+psi_m(j-1)^2*t(j);
%    summation = summation + K(j)^2*A(j) + K(j)*B(j) +
d(j);
end
%    theta(k) = asin(1);
%    t(k) = theta(k) - theta(k-1);
%    d(k) = i_m(k-1)^2*t(k);
summation = 0;
for l=1:k-1
summation = summation + K(l)^2*A(l) + K(l)*B(l) + d(l);
end
C(k) = d(k) + summation - 0.5*pi*Irms(k)^2;
%Solve the 1st order polynomial
r = roots([A(k) B(k) C(k)]);
if r(1) > 0
K(k) = r(1);
elseif r(2) > 0
K(k) = r(2);
else

```

```
K(k) = 0;
end
for l=2:k
%error in equation 10 of Prusty &Rao is assumed (two
lambda_ns in
%the first group of terms
i_m(k) = i_m(k) + K(l)*(psi_m(l)-psi_m(l-1));
end
end
```